ISTANBUL TECHNICAL UNIVERSITY ★ GRADUATE SCHOOL OF SCIENCE ENGINEERING AND TECHNOLOGY

SEMI-CRYSTALLINE HYDROGELS WITH SHAPE-MEMORY AND SELF-HEALING FUNCTIONS

Ph.D. THESIS

Çiğdem BİLİCİ

Department of Chemistry

Chemistry Programme

NOVEMBER 2018

ISTANBUL TECHNICAL UNIVERSITY ★ GRADUATE SCHOOL OF SCIENCE ENGINEERING AND TECHNOLOGY

SEMI-CRYSTALLINE HYDROGELS WITH SHAPE-MEMORY AND SELF-HEALING FUNCTIONS

Ph. D. THESIS

Çiğdem BİLİCİ
(509132015)

Department of Chemistry

Chemistry Programme

Thesis Advisor: Prof. Dr. Oğuz OKAY

NOVEMBER 2018

<u>İSTANBUL TEKNİK ÜNİVERSİTESİ ★ FEN BİLİMLERİ ENSTİTÜSÜ</u>

ŞEKİL-HAFIZALI VE KENDİ-KENDİNİ ONARABİLEN SEMİ-KRİSTALİN HİDROJELLER

DOKTORA TEZİ

Çiğdem BİLİCİ
(509132015)

Kimya Anabilim Dalı

Kimya Programı

Tez Danışmanı: Prof. Dr. Oğuz OKAY

KASIM 2018

Çiğdem Bilici, a Ph.D. student of ITU Graduate School of Science Engineering and Technology, student ID 509132015, successfully defended the thesis entitled "SEMI-CRYSTALLINE HYDROGELS WITH SHAPE-MEMORY AND SELF-HEALING FUNCTIONS", which she prepared after fulfilling the requirements specified in the associated legislations, before the jury whose signatures are below.

Thesis Advisor : **Prof. Dr. Oğuz OKAY** ....
Istanbul Technical University

Jury Members : **Prof. Dr. H. Yıldırım ERBİL** ....
Gebze Technical University

Prof. Dr. Nermin ORAKDÖĞEN ....
Istanbul Technical University

Prof. Dr. Orhan GÜNEY ....
Istanbul Technical University

Assoc. Prof. Dr. Deniz TUNCABOYLU ....
Bezmialem Vakıf University

Teslim Tarihi : **18 September 2018**
Savunma Tarihi : **29 November 2018**

To myself,

FOREWORD

I am thankful to my supervisor, Prof. Dr. Oğuz OKAY for allowing me to perform my BSc, MSc and PhD studies in his research group. I would like to express my sincere gratitude to my advisor for his motivation, patience, enthusias and deep knowledge. His guidance helped me in all the time of research of my studies.

I would like to express my thanks to the members of the thesis committee Prof. Dr. H. Yıldırım ERBİL, Prof. Dr. Nermin ORAKDÖĞEN, Assoc. Prof. Dr. Deniz TUNCABOYLU for their help.

I would like to thank all the past and present member of "Okay Research Group" for their help. I would especially like to express my deep appreciation to Aslıhan ARGUN, Merve ÇAĞLI, Sevil MÜSLÜMOVA for their friendship, goodwill and support inside and outside the laboratory.

Finally, I'm grateful to my mother Hubrişah, my father Yaşar and my sister Burçin BİLİCİ for their encouragement, understanding, patience and support during all my life and education.

September 2018 Çiğdem BİLİCİ
(M.Sc. Chemist)

TABLE OF CONTENTS

ABBREVIATIONS

DMA	: N,N-Dimethylacrylamide
AAc	: Acrylic acid
APS	: Ammonium persulfate
C18A	: Octadecyl acrylate
C12M	: Lauryl methacrylate
NaCl	: Sodium chloride
$Na_2S_2O_5$	: Sodium pyrosulfite
PDMA	: Polydimethylacrylamide
PAAc	: Polyacrylic acid
DN	: Double Network
SDS	: Sodium dodecyl sulfate
XRD	: X-ray Diffraction
SAXS	: Small angle X-ray Scattering
WAXS	: Wide angle X-ray Scattering
DSC	: Differantial Scanning Calorimetry

SYMBOLS

T_m	: Melting temperature of crystalline domains
T_{cry}	: Crystalization temperature of crystalline domains
m	: Swollen masses of the gel sample
m_{dry}	: Dry masses of the gel sample
C_o	: Total monomer concentration
ω	: Angular frequency
R_r	: Strain recovery rate
R_f	: Strain fixing rate
R_θ	: Recovered angle
θ_d	: Deformation angle
f_{cry}	: Degree of crystallinity
x_{HM}	: Mole fraction of the hydrophobic monomer
ΔH_m	: Enthalpy changes during melting
ΔH^o_m	: Melting enthalpy of crystalline C18A units
W_g	: Gel fraction
$H_2O\%$	: Water content
E	: Young's modulus
W	: Toughness
G'	: Elastic modulus
G''	: Viscous modulus
ε	: Strain
$\dot{\varepsilon}$	: Strain rate
ε_m	: Maximum strain
ε_c	: Compressive strain
σ_{nom}	: Nominal stress
σ_f	: Fracture stress
σ_{true}	: True stress
γ_o	: Deformation amplitude
λ	: Deformation ratio
λ_o	: Prestretch ratio
λ_f	: Deformation ratio at break
$\lambda_{biax,max}$	: Maximum biaxial extension ratio
$I(q)$	: Scattering intensity
I_{max}	: Maximum intensity
q	: Scattering vector
U_{hys}	: Hysteresis energy
U_y	: Yield energy
L	: Thickness of lamellar clusters
V_a	: Activation volume
E_a	: Activation energy
ε_o	: Pre-exponential factor
k	: Boltzmann constant

LIST OF TABLES

LIST OF FIGURES

Page

SEMI-CRYSTALLINE HYDROGELS WITH SHAPE-MEMORY AND SELF-HEALING FUNCTIONS

SUMMARY

Semi-crystalline hydrogels are soft and functional materials having crystalline domains. Such domains in the hydrogels can be generated by incorporation of hydrophobic units with long alkyl side chains into hydrophilic polymer networks. Semi-crystalline hydrogels undergo reversible order-disorder (crystalline-amorphous) transitions in response to a temperature change leading to a dramatic change in their Young's moduli at a certain temperature. For instance, semi-crystalline hydrogels are soft and mechanically weak above the melting temperature T_m of their crystalline domains while they are hard and mechanically strong below the crystallization temperature T_{cry}. Osada et al. were the first to prepare such hydrogels by free radical copolymerization of stearyl acrylate (SA) and acrylic acid (AAc) in organic media in the presence of a chemical crosslinker. They showed that, at the high degree of crystallinity, the hydrogels exhibit shape-memory effect, which is known as the ability to return from a "temporary shape" to the "permanent shape" under the effect of a stimulus such as temperature. The crystalline domains in such hydrogels act as switching segments defining the temporary shape of the hydrogel, while the chemical crosslinks of the network determines the permenant shape. With the development of novel molecular design and synthetic technologies, second-generation semi-crystalline hydrogels also exhibit self-healing behavior in addition to the shape-memory effect. This was achieved by creating semi-crystalline hydrogels via non-covalent interactions instead of chemical crosslinks, providing them the self-healing ability, that is, the ability to repair themselves following a damage. This ability arises from the reversible association and disassociation of non-covalent interactions. In recent years, high-strength hydrogels with both shape memory and self-healing functions have attracted great interest due to their wide range of biotechnological applications. However, although semi-crystalline hydrogels with a high degree of crystallinity are mechanically strong, they are brittle and rupture during tensile deformations at less than 20% stretch ratio. Moreover, many biotechnological applications also require easy-processability for shape-memory and self-healing hydrogels using a simple synthetic route. The design of both shape-memory and self-healing hydrogels with an excellent mechanical performance such as a high toughness and stretchability, easy-processability and good biocompatibility is necessary for the fabrication of biodevices such as artificial organs, biosensors, actuators.

The aim of this thesis is to design and characterize high-strength semi-crystalline hydrogels with self-healing and shape memory functions. Within the framework of this thesis, hydrogels were prepared using a supramolecular approach by incorporating hydrophobic monomer units carrying long alkyl side chains within the hydrophilic polymer network. The crystalline domains and hydrophobic associations formed by alkyl side units in the swollen hydrophilic polymer chains created a physically cross-linked hydrogel with self-healing and shape-memory functions. In the study, acrylic acid, N,N-dimethylacrylamide, n-octadecyl acrylate and lauryl

methacrylate were used for the production of the biocompatible hydrogel networks. After the design of the hydrogels, their rheological, mechanical and thermomechanical properties were determined and their crystal structures were clarified by small and wide angle X-ray scattering technique. The effectiveness of shape-memory behavior of the hydrogels was determined by the bending test, and their strain recovery R_r and fixing rates R_f were calculated. The self-healing ability of the hydrogels was evaluated by manuel experiments as well as using uniaxial elongation and compression tests.

In the first part of the thesis study, a novel synthetic method for the preparation of melt-processable hydrogels with shape-memory and self-healing abilities was developed. The hydrogels consist of polyacrylic acid (PAAc) chains containing 20-50 mol% n-octadecyl acrylate segments together with surfactant micelles. The key of the supramolecular approach is the presence of an extractable surfactant as well as the absence of chemical crosslinks in the hydrogels. We found that, at temperatures above the melting point T_m of the crystalline domains, the hydrogel liquefies to form a semi-dilute polymer solution because of the presence of surfactant micelles that is effective in solving the hydrophobic associations. In this state, it can be poured into molds and easily processed in any desired manner. After cooling of the liquefied hydrogel from above to below T_m, and removal of the surfactant from the gel network, a hydrogel of any permanent shape with a high Young's modulus (26 MPa) and compressive strength (90 MPa) could be obtained. When the hydrogel is damaged, the remarkable original mechanical properties can fully be recovered via temperature-induced healing. The hydrogels also exhibit shape-memory effect with shape fixity and shape recovery ratios of 97 ± 2%. We propose that the crystalline domains in the hydrogels act as switching segments determining the temporary shape while the hydrophobic associations formed by melting of these domains act as physical netpoints.

In the second part of this thesis, we investigated the effect of incorporation of a weak hydrophobe into semicrystalline hydrogels on their mechanical properties. We found that the addition of a small amount of weak hydrophobe significantly increases the toughness and stretchability of semi-crystalline hydrogels without losing their high modulus and high strength. We designed a highly entangled physical network containing lamellar crystals formed by aligned side alkyl chains. The hydrogels consist of poly(N,N-dimethylacrylamide) (PDMA) chains containing n-octadecyl acrylate (C18A) and lauryl methacrylate (C12M) segments with side chain lengths of 18 and 12 carbons, respectively. We were able to produce more ordered and thinner lamellar crystals with a layered structure by including 0.1-0.4 mol % C12M into the polymer skeleton containing 70 mol % DMA and 30 mol % C18A segments. This ordering in the crystal structure of the hydrogels resulted in brittle-to-ductile transition due to the occurrence of necking behavior causing 10-fold increase of toughness. The significant increase in toughness due to the incorporation of C12M segments into the semicrystalline hydrogels could be explained with the appearance of active tie molecules interconnecting the lamellar clusters. The hydrogels also exhibit reversible tensile deformation induced by heating above the melting temperature of crystalline domains.

In the last part of this study, we report a simple one-step method of generating high-strength physical hydrogels exhibiting microstructural and mechanical anisotropy. As the precursor material, shape-memory semicrystalline hydrogels consisting of poly(N,N-dimethylacrylamide) chains interconnected by n-octadecyl acrylate (C18A) segments were used. To produce anisotropic microstructure and anisotropic mechanical properties, we imposed a prestretching process to the isotropic hydrogel specimens. In this process, the isotropic specimen was first heated above the melting temperature T_m of its crystalline domains and then prestretched to a predetermined prestretch ratio followed by cooling below T_m under strain to fix the elongated shape of the sample. An important microstructural and mechanical anisotropy were observed in the prestretched hydrogels, which could be adjusted by the magnitude of the prestretch ratio (λ_o). Directional brittle-to-ductile and ductile-to-brittle transitions could be triggered by tuning the prestretch ratio λ_o. Results of small- and wide-angle X-ray scattering measurements as well as mechanical tests show that the highest microstructural and mechanical anisotropy appear at a critical prestretch ratio due to the limited extensibility of the network chains. The hydrogel at λ_o=1.8 displays Young's moduli of 161 ± 14 and 76 ± 7 MPa, and toughness of 16 ± 1 and 1.3 ± 0.1 MJm^{-3} in the prestretching direction and perpendicularly to the prestretching direction, respectively.

ŞEKİL-HAFIZALI VE KENDİNİ ONARABİLEN YARI-KRİSTALİN HİDROJELLER

ÖZET

Yarı-kristalin hidrojeller, kristal yapılar oluşturan uzun yan zincirli hidrofobik segmentlerin suda şişen hidrofilik polimer zincirlere katılmasıyla elde edilen yumuşak fonksiyonel malzemelerdir. Hidrofilik polimer zincirleri arasında hidrofobik grupların varlığı, kristalin bölgelerin oluşumuna yol açmaktadır. Kristalin bölgelerin erime sıcaklığı (T_m) civarındaki küçük sıcaklık değişimlerinde ortaya çıkan tersinir düzenli-düzensiz (kristalin-amorf) geçişler, hidrojellerin Young modülünde keskin bir değişime neden olmaktadır. Bu hidrojeller, erime sıcaklığı üzerinde yumuşak ve mekanik olarak zayıf iken, kristalizasyon sıcaklığı üzerinde sert ve mekanik olarak güçlüdürler. Yarı-kristalin hidrojeller ilk olarak Osada ve ark. tarafından organik ortamda 18 karbonlu oktadesil akrilat (C18A) ve akrilik asidin (AAc) rastgele kopolimerizasyonu ile sentezlenmiştir. Yüksek miktarda kristalin bölgeler içeren hidrojeller, sıcaklık gibi uyarıcı bir etken altında geçici şeklinden kalıcı şekline dönme kabiliyeti olarak bilinen şekil hafıza etkisi sergilemektedir. Hidrojellerin çapraz bağlı ağyapısı kalıcı şekli belirlerken, kristalin bölgeler geçici şekli belirleyen anahtar segmentler olarak rol alır. Moleküler tasarım ve sentetik teknolojilerin gelişmesiyle birlikte ikinci nesil yarı-kristalin hidrojeller, şekil hafızası etkisinin yanısıra kendi-kendini onarabilme davranışı da göstermişlerdir. Kimyasal çapraz bağlar yerine kovalent olmayan etkileşimleri içeren yarı-kristalin hidrojeller, biyolojik dokularda görüldüğü gibi herhangi bir hasar sonrası kendi-kendini onarabilme becerisine sahiptirler. Bu yetenek, kovalent olmayan etkileşimlerin tersinir olarak ayrışıp tekrar birleşmesinden ileri gelir. Son zamanlarda, şekil-hafızalı, kendini onarabilen ve mekanik olarak dayanıklı hidrojeller, biyoteknolojik uygulama alanları tarafından büyük ilgi görmektedir. Yüksek kristaliniteye sahip yarı kristalin hidrojellerin mekanik olarak kuvvetli olup elastik modül ve çekme dayanımları sırasıyla 80−300 MPa ve 4-7 MPa'dır. Ancak, bu hidrojeller % 20'den daha düşük gerilme deformasyonunda kırılmakta ve kopmaktadırlar. Ayrıca, biyoteknolojik uygulamalarda basit bir sentetik yol kullanarak şekil-hafızalı ve kendini onaran hidrojellerin kolay işlenebilirliği talep edilmektedir. Mükemmel mekanik performans, yüksek tokluk, kolay işlenebilirlik ve biyouyumluluğa sahip şekil-hafızalı ve kendini onaran hidrojellerin tasarımı, yapay organlar, biyosensörler, aktüatörler gibi birçok biyo-cihazların üretimi için gereklidir.

Tezin amacı, şekil-hafıza ve kendini onarma fonksiyonlarına sahip yüksek mekanik dayanımlı yarı-kristalin hidrojelleri tasarlamak ve karakterize etmektir. Bu tez çalışması kapsamında hidrojeller, supramoleküler bir yaklaşımla, uzun alkil yan zincirleri taşıyan hidrofobik monomer ünitelerinin hidrofilik polimer ağı içine dahil edilmesi ile hazırlanmıştır. Suda şişmiş hidrofilik polimer ağyapısı içindeki hidrofobik birimler, kendi aralarında etkileşime girerek kristalin bölgeleri ve hidrofobik asosiyasyonları oluşturmuştur. Sırasıyla "anahtar segmentler" (switching segments) ve ağ noktası (net point) olarak rol oynayan kristalin bölgeler ve hidrofobik asosiyasyonlar, hidrojele şekil hafıza ve kendini onarabilme yeteneği kazandırmıştır. Biyouyumlu hidrojel üretimi için akrilik asit (AAc), N,N-

dimetilakrilamid (DMA), oktadesil akrilat (C18A) ve lauril metakrilat (C12M) gibi biyouyumlu monomerler kullanılmıştır. Hidrojel tasarımından sonra, hidrojellerin reolojik, mekanik ve termomekanik özellikleri incelenmiş ve dar (SAXS) ve geniş açılı X-ışını saçılımı (WAXS) teknikleri ile kristalin yapısı aydınlatılmıştır. Şekil-hafıza etkinliği, bükme testinin yanı sıra geri kazanma (R_r) ve sabitleme (R_f) oranlarının hesabı ile incelenmiştir. Kendini onarma kabiliyeti ise manuel denemelerle ve tek eksenli uzama ve basma testleri ile değerlendirilmiştir.

Tez çalışmasının ilk aşamasında, şekil-hafıza ve kendini onarma fonksiyonlarına sahip eriyik halinde işlenebilir yarı-kristalin hidrojellerin üretimi için sentetik bir yöntem sunulmuştur. Ağırlıkça % 60-80 su içeren bu hidrojeller, yüzey aktif maddenin oluşturduğu misellerle birlikte molce % 20-50 oktadesil akrilat segmentleri içeren poliakrilik asit (PAAc) zincirlerinden meydana gelirler. Tez çalışması kapsamında uygulanan supramoleküler yaklaşımın kilit noktası, hidrojel yapısında kimyasal çapraz bağların yokluğu ve surfaktan moleküllerinin varlığıdır. Hidrojellerin kristalin bölgelerinin erime sıcaklığı (T_m) üzerinde, surfaktan moleküllerinin varlığından dolayı hidrofobik assosiyasyonlar çözünerek hidrojel akıcı forma geçmiştir. Bu aşamada, kalıba akıtılarak jele istenilen şekli vermek çok kolaydır. T_m altına soğutulması ve jelin ağ yapısından surfaktanın moleküllerinin uzaklaştırılması sonucu 26 MPa Young modülü ve 90 MPa basma dayanımı değerlerine sahip hidrojelin kalıcı şekli ortaya çıkmıştır. Burada, güçlü hidrofobik asosiyasyonlar veya kristalin bölgeler, T_m altında ve üstünde sırasıyla hem fiziksel çapraz bağ noktaları hem de değiştirilebilir segmentler olarak rol almıştır. Bu sebeple hidrojel, %97 ± 2 değerinde şekil kurtarma ve sabitleme oranına sahip şekil hafıza etkisi göstermiştir. Ayrıca zarar gören hidrojelin sıcaklıkla indüklenerek kendini onarması sonunda mekanik özellikleri tamamen eski haline geri dönmüştür.

Çalışmanın ikinci aşamasında ise, az miktarda zayıf bir hidrofobun yarı kristalin hidrojellere dahil edilmesiyle yüksek modül ve mekanik dayanımını kaybetmeden hidrojelin tokluğunun ve gerilebilirliğinin önemli ölçüde arttığı saptanmıştır. Tok supramoleküler yarı kristalin hidrojeller, kütle polimerizasyonu tekniği kullanılarak, sırasıyla 18 ve 12 karbonlu yan zincir uzunluklarına sahip n-oktadesil akrilat (C18A) ile lauril metakrilat (C12M) segmentlerinin biyouyumlu bir polimer olan poli(N,N-dimetilakrilat) omurgasına eklenmesiyle sentezlenmiştir. Molce % 70 DMA ve % 30 C18A içeren polimer omurgasına molce % 0.1-0.4 C12M eklenerek daha düzenli ve daha ince tabakalı kristal yapılar üretilmiştir. Burada, C18A'ya ait uzun alkil yan zincirlerin oluşturduğu hekzagonal paketlenmeler alkil kristallerini meydana getirmişken, kısa yan zincirli C12M ve DMA'nın α-metil grupları hidrofobik etkileşimlere katkıda bulunmuştur. Ayrıca, tokluğun 10 misli artmasına neden olan boyun eğme davranışının ortaya çıkmasıyla kırılganlıktan sünekliğe geçiş gözlemlenmiştir. Az miktarda C12M'nin ilavesiyle yarı-kristalin hidrojellerin tokluğunu arttıran boyun verme davranışı, dış kuvvet altında tabakalı alkil kümeleri birbirine bağlayan aktif bağ moleküllerinin oluşumuyla açıklanabilmiştir. Hidrojeller ayrıca, kristalin bölgelerin erime sıcaklığı üzerinde (T_m) ısıtılarak indüklenen tersinir bir gerilme deformasyonu sergilemiştir.

Çalışmanın son aşamasında, mikroyapısal ve mekanik anizotropi sergileyen yüksek mekanik dayanımlı fiziksel çapraz bağlı yarı-kristalin hidrojellerin üretilmesi için tek adımlı basit bir yöntem sunulmuştur. Bu tip hidrojellerin hazırlanması için öncü materyal olarak, şekil-hafızalı, yarı-kristalli hidrojeller kullanılmıştır. Hidrojeller, kristalin bölgeler ve hidrofobik asosiyasyonlar oluşturan n-oktadesil akrilat (C18A) segmentleri ile birbirine bağlanan poli(N,N-dimetilakrilamid) zincirlerinden oluşmaktadır. Anizotropik mikroyapı oluşturmak için izotropik hidrojel üzerinde öngerilme (prestretching) işlemi uygulanmıştır. Öngerilme işleminde, suda şişmiş izotropik hidrojel numunesi, kristalin bölgelerinin erime sıcaklığının T_m üzerinde istenilen öngerilme oranında çekilerek deforme edilmiş, ardından T_m altında soğutularak deformasyon şekli gerilim kuvveti altında sabitlenmiştir. Böylece, öngerilme oranın (λ_o) değerine göre ayarlanabilen önemli bir mikroyapısal ve mekanik anizotropi elde edilmiştir. Sabitlenmiş deformasyon uzunluğun başlangıç uzunluğuna oranı olarak tanımlanan ön gerilme oranı λ_o 1,2 ile 8 aralığında değiştirilmiştir. Anizotropik mikroyapıya sahip hidrojellerde görülen kırılgan-sünek ve sünek-kırılgan geçişler, öngerilme oranının ayarlanmasıyla tetiklenebilmiştir. Hidrojellerin dar (SAXS) ve geniş açılı X-ışını saçılma (WAXS) ölçümleri ve mekanik testlerin sonuçlarına göre, en yüksek mikroyapısal ve mekanik anizotropi, polimer ağ zincirlerinin sınırlı ölçüde genişleyen bir konformasyona sahip olmasından dolayı kritik bir öngerilme oranında görülmüştür. Kritik ön gerilme oranı 1.8 olarak bulunmuştur. λ_o = 1.8'deki hidrojelin, öngerilme yönüne paralel ve dik yönde sırasıyla, Young' modülü 161 ± 14 ve 76 ± 7 MPa iken, tokluğu 16 ± 1 ve 1.3 ± 0.1 MJm^{-3}'dır.

1. INTRODUCTION

Hydrogels are water-swollen three-dimensional networks of physically or chemically cross-linked hydrophilic polymer chains. They have unique properties such as high water absorption capacities, drastic volume changes depending on the external stimuli, similarity to biological systems, and chemical reactions in the gel phase. Therefore, they are used as advanced technology material in many application areas such as contact lenses, dressings for wound healing, absorbents, cell encapsulation, scaffolds for tissue engineering, vehicles for controlled drug delivery systems, coatings for implantable devices, for cell culture, artificial muscles, sensor systems, and bioseparations, and actuators in soft machines [1-3]. According to the recent studies, hydrogels containing crystalline domains can be obtained by incorporating long hydrophobic side alkyl chains into a hydrophilic polymer network [4]. The presence of the hydrophobic groups among hydrophilic polymer chains leads to formation of crystalline structures. Moreover, such hydrogels exhibit relatively sharp physical or chemical changes in response to small temperature changes [5]. Osada et al. were the first to synthesize hydrogels with crystalline domains by copolymerization of acrylic acid with stearyl acrylate containing long alkyl side chains in the precence of a chemical crosslinker in organic media [6]. The hydrogels of Osada et al. exhibit a reversible order-disorder transition causing a dramatic change in their Young moduli at around the melting temperature T_m of crystalline domains. The order-disorder transition leading to the change in the mechanical properties is also responsible for the shape-memory effect, which is known as the ability to return original shape of a material from its temporary shape in the precence of external stimulus. The chemical crosslinks act as the netpoints to determine the permanent shape while the crystalline domains fix temporary shape of the hydrogels [7]. More recently, a novel way for the preparation of the chemically crosslinked semi-crystalline hydrogels with shape memory effect was reported. The hydrogels consisting of AAc and C18A monomer units together with a chemical cross-linker were synthesized in aquous solution containing sodium chloride (NaCl) and sodium dodecyl sulfate (SDS) by using micellar copolymerization technique [8]. Here, C18A dissolves in the micelles formed by the SDS molecules, while AAc dissolves in the water phase. To solubilize a large amount of C18A, the size of SDS micelles was increased by the addition of NaCl into aqueous semi-dilute SDS solutions [9-11]. Hence, hydrophobic units aligned in blocky incorporate into hydrophilic polymer chains. Due to the blocky structure of the network chains formed via micellar polymerization, the hydrogels exhibit a much larger extend of modulus change during the order-disorder transition and hence, a stronger shape-memory effect.

A further improvement in the field of semi-crystalline hydrogels was generating a high-strength shape memory hydrogels with self-healing ability by using non-covalent approach [12]. Here, the hydrogels consist of polyacrylic acid (PAAc) or poly(N,N-dimethylacrylamide) (PDMA) chains containing hydrophobic (meth)acrylate units with long alkyl side chains [12]. Such PDMA and PAAc hydrogels containing crystalline domains and hydrophobic associations have a high fracture energy of 20 ± 1 kJ m^{-2} and Young's modulus up to 308 ± 16 MPa. The mechanical properties of the hydrogels could be tuned by changing the degree of crystallinity. It was shown that the variation of the degree of crystallinity between 3 - 33% results in two orders of magnitude change in the modulus, toughness and elongation at break. The change of the temperature between below and above the melting temperature of the crystalline domains leads to 1000 fold change in their elastic moduli. They also show self-healing and shape memory behaviour induced by heating above T_m. The healed hydrogel maintains approximately 87% of the compressive stress of the virgin hydrogel samples.

As summarized above, a great improvement has been achieved in the past decade in the field of the semi-crystalline hydrogels. However, it is still necessary to add new properties to the semi-crystalline hydrogels like easy processability, high toughness, stretchability and anisotropic properties as well as effective shape-memory and self-healing functions to meet the needs of the developing technology. The easy processibility of the materials with high strength is a major demand of various applications including biomedical, packaging, sensors and actuators. Production of easy-processable semi-crystalline hydrogels with shape-memory effect is a crucial requirement for shape-memory applications. However, although the hydrogels developed so far are mechanically strong, they are brittle and break at a stretch of less than 20%. An essential challenge in the gel science is to design highly stretchable and tough semi-crystalline hydrogels with both shape-memory and self healing abilities. Another challenge to be addressed in the gel science is to produce high-strength hydrogels with anisotropic properties, as seen in many biological tissues such as muscle, skin, and articular cartilage having anisotropically oriented hierarchical structures [13].

1.1 Purpose Of The Thesis

The aim of the thesis is to design mechanically strong and tough semi-crystalline hydrogels with self-healing and shape memory properties. To achieve this aim, our strategy was to incorporate of hydrophobic monomer units carrying alkyl side chains into the hydrophilic polymer chains. Interactions between the hydrophobic monomer units in the aqueous medium create hydrophobic asociations and crystalline regions within the hydrogel and hence add water insolubility, self-healing and shape memory properties. The key point in the thesis study is the absence of chemical cross-links in the hydrogel network and the existence of physical cross-links formed by both hydrophobic asociations and the crystalline domains. Thus, the hydrogels exhibit self-healing behavior due to their supramolecular nature, that is, reversible dissociation and re-association of physical cross-links. In addition, the presence of both crystalline domains and hydrophobic associations acting as strong and weak physical cross-linkings, respectively lead to the appearance of shape-memory effect.
High-strength semi-crystalline hydrogels with self-healing and shape-memory functions were prepared via both micellar copolymerization and bulk photopolymerization techniques. Acrylic acid (AAc) and N, N-dimethylacrylamide (DMA) as the hydrophilic monomers, and n-octadecyl acrylate (C18A) and lauryl methacrylate (C12M) as hydrophobic ones were used to synthese the hydrogels. The rheological, mechanical and thermomechanical properties of the hydrogels were examined and their crystal structures were clarified using small (SAXS) and wide angle X-ray scattering (WAXS) techniques. The self-healing and shape-memory efficiencies of the hydrogels were determined by conducting self-healing and shape-memory tests with the hydrogel specimens.

The thesis comprises three major section and each of which has its own introduction, experimental, results and discussion, and conclusion.

In the first section, we present a supramolecular approach for the preparation of melt-processable mechanically strong semi-crystalline hydrogels with shape memory and self-healing abilities. The semi crystalline hydrogel with a water content of 60-70% comprises PAAc chains containing 20 to 50 mol% crystallizable n-octadecyl acrylate (C18A) segments together with surfactant micelles. The key of our approach is the absence of chemical cross-links and the presence of surfactant in the hydrogels. At temperatures above T_m of the crystalline domains, the hydrogel is in a liquid state because of the presence of surfactant micelles effective in solubilizing the hydrophobic associations. At this stage, the hydrogel can easily be shaped in any form by casting into molds. Cooling below T_m and removal of the surfactant from the hydrogel cause any permanent shape of hydrogel with a high elastic modulus (26 MPa) and mechanical strength (90 MPa). When the hydrogel is damaged, it can recover its original extraordinary mechanical properties via temperature-induced healing. The hydrogel also shows complete shape-recovery behavior because of the hydrophobic blocks in the gel network. We also show that the hydrophobic associations and crystalline domains in the hydrogels act as both physical netpoints determining the permanent shape and switching segments fixing the temporary shape above and below T_m, respectively.

In the second section, we report that the addition of a small amount of a weak hydrophobe into the semicrystalline hydrogels importantly increases their stretchability and toughness without reducing their high modulus and high strength. We designed the hydrogel consisting of highly entangled physical network with lamellar crystals formed by aligned side alkyl chains. The hydrogel network bases on poly (N,N-dimethylacrylamide) (PDMA) which is known as an useful hydrophilic biocompatible polymer. The layered hydrogel structure is formed by interconnected lamellar crystals created by incorporation of n-octadecyl acrylate (C18A) and lauryl methacrylate (C12M) segments with side chain lengths of 18 and 12 carbons, respectively, into the physcial network. Hexagonal packing of side alkyl chains of C18A units creates alkyl crystals in the hydrogels [4, 5, 8] while α-methyl groups and C12M units with shorter side alkyl chains contribute to the hydrophobic associations [11, 14, 15]. We were able to create thinner and more ordered lamellar crystals with a layered structure upon addition of 0.1-0.4 mol % C12M into the polymer backbone containing 70 mol % DMA and 30 mol % C18A segments.

Simultaneously, the hydrogel exhibits a brittle-to-ductile transition with the incorporation of C12M segments due to the occurence of necking behavior causing 10-fold increase of toughness. The significant toughness imrovement upon addition of C12M into the hydrogels could be clarified with the occurence of active tie molecules under external force interconnecting the lamellar clusters. The hydrogels also display reversible tensile deformation triggered by heating above T_m.

In the third section, we used semi-crystalline physical hydrogels with shape-memory function as the precursor materials for the production of anisotropic hydrogels. The precursor materials used are the same content as those reported in the previous sections. Above T_{m} of the crystalline domains, which is around 48 °C, the hydrogels have a relatively low and time-dependent moduli due to the limited lifetime of hydrophobic associations that hold the chains together. On the other hand, below T_{m}, about half of the associations convert to alkyl crystals thereby generating high-strength hydrogels with a high Young's modulus and tensile fracture stress [16-18]. In this section, we present a single step procedure to generate microstructural and mechanical anisotropy in semicrystalline hydrogels. We implement a prestretching on the water-swollen isotropic hydrogels above $T_{\mathrm{m},}$ and later we fix the elongated shape of the hydrogel by cooling below T_{m} under strain. The prestretch ratio λ_{o} described as the ratio of fixed elongated length to the initial length was varied between 1.2 and 8. As will be seen below, a significant mechanical and structural anisotropy in semi-crystalline hydrogels could be obtained by adjusting the prestretch ratio.

2. MELT-PROCESSABLE SHAPE-MEMORY HYDROGELS WITH SELF-HEALING ABILITY OF HIGH MECHANICAL STRENGTH[1]

Shape-memory polymers are materials having the capacity to remember one or more shapes under different conditions and therefore have attracted significant interest due to their great potential for applications in sensors, actuators, and implants for minimally invasive surgery [19-22]. Besides the bulk polymers, hydrogels capable of a shape-memory effect have drawn increasing attention in the biomedical field because of their softness, smartness, elasticity, similarity to biological tissues, and excellent permeability for transport of nutrient and metabolites [6-8,23-28]. Typically, shape-memory hydrogels have a hybrid network structure composed of chemical cross-links (netpoints) and crystalline or glassy, amorphous domains acting as physical cross-links (switching segments). While the netpoints determine the permanent shape of the hydrogel, the physical cross-links formed by solidification of the switching segments below the melting or glass transition temperatures fix the temporary shape gained by deformation of the gel sample at higher temperatures [22]. Shape memory hydrogels based on chemically cross-linked poly(acrylic acid) (PAAc) network chain segments containing hydrophobic domains have been prepared in organic media as well as in aqueous micellar solutions [6,8,29,30]. Upon swelling of the hydrogels in water, hydrophilic acrylic acid (AAc) segments provide flexibility to the network chain segments provide flexibility to the network chain segments so that hydrophobic units easily align to form crystalline domains with a melting temperature T_m between 30 and 50 $^{\circ}$C. The hydrogels exhibited 120- to 1000-fold increase in the modulus by decreasing the temperature from above T_m to a temperature from above T_m enabling a shape fixity ratio (R_f) as a measure of how good the deformed shape is maintained of > 99%.

---

[1] This chapter was published in "Bilici, Ç. and Okay, O. (2016). Melt-Processable Shape-Memory Hydrogels with Self-Healing Ability of High Mechanical Strength. *Macromolecules, 4*9, 7442-7449"

Although significant developments have been achieved in the field of shape-memory polymers and hydrogels, many applications demand on shape memory materials that can be melt-processed as a thermoplastic. Because polymers consisting of chemical and physical cross-links do not flow, the traditional thermoplastic processing methods such as injection molding cannot be used for the mass production of such materials. Hence, ease processability is an important topic for technological application of shape-memory polymers [20]. Moreover, a major challenge in the preparation of shape memory hydrogels is to combine melt-processability with a high mechanical strength and self-healing ability using a simple synthetic route.

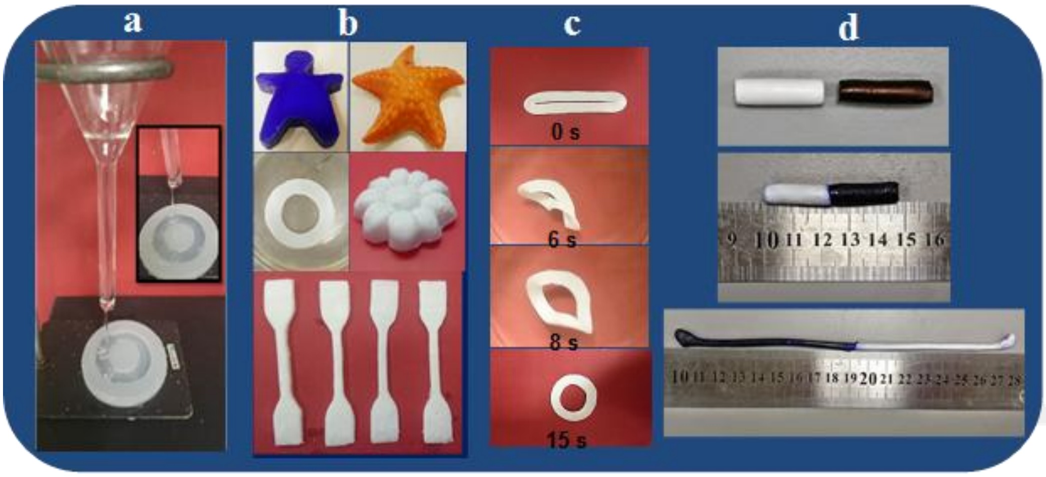

Figure 2.1 : (a) Images demonstrating the flow behavior of hydrogels containing surfactant. (b) Various permanent shapes after cooling and surfactant extraction, where two gel solutions were colored with dyes. (c) The shape recovery within 15 s from the temporary compressed ring to the permanent ring shape at 60 $^{\circ}$C. (d) Photographs of two virgin hydrogel samples after equilibrium swelling in water. One of the gel samples is colored for clarity. Gel samples were brought together in a closed container and fused together by heating to 80 $^{\circ}$C for one day. After stretching the combined gel samples at 56 $^{\circ}$C the healed gel sustains up to 1500% strain. All images are from hydrogel samples with 50 mol% C18A.

To address this problem, here we present a supramolecular approach for the preparation of melt-processable shape memory hydrogels with a good mechanical performance and self-healing ability. The supramolecular hydrogel with a water content of 60-80 wt % consists of PAAc chains containing 20 - 50 mol % crystallizable n-octadecyl acrylate (C18A) segments together with surfactant micelles. As compared to previous works, the key of our approach is the absence of chemical cross-links and the presence of an extractable surfactant in the hydrogels [6, 8, 29, 31, 32]. At temperatures above T_m of the crystalline domains, the hydrogel liquefies due to the presence of surfactant micelles effective for solubilizing the hydrophobic associations. At this stage, it can easily be processed in any desired form by pouring into molds, as shown in Figures 2.1a and b. Cooling below T_m and removing the surfactant result in a hydrogel of any permanent shape with a particularly high compressive strength of 90 MPa and a Young's modulus of 26 MPa. If damaged, the extraordinary mechanical properties can completely be recovered via temperature-induced healing (Figure 2.1d). The hydrogel also exhibits complete shape recovery due to the hydrophobic blocks of the polymer (Figure 2.1c). We have to mention that supramolecular shape memory polymers developed so far consisted of at least two segregated domains exhibiting different thermal transition temperatures [22]. One domain acted as the netpoints determining the permanent shape while the other acted as molecular switches fixing the temporary shape. In contrast, present hydrogels have only one hydrophobic domain forming strong associations or crystalline domains above or below T_m, respectively, and thus acting both as physical netpoints and switching segments.

2.1 Experimental Part

2.1.1 Materials

N-octadecyl acrylate (C18A, Sigma-Aldrich), sodium dodecylsulfate (SDS, Sigma-Aldrich), NaCl (Merck), ammonium persulfate (APS, Sigma-Aldrich), and sodium metabisulfite (SMS, Merck) were used as received. Acrylic acid (AAc, Merck) was freed from its inhibitor by passing through an inhibitor removal column (Sigma-Aldrich).

2.1.2 Hydrogel preparation

The supramolecular hydrogels were prepared by conducting the micellar copolymerization of AAc and C18A at 55 $^{\circ}$C in aqueous 1.5 M NaCl solutions containing 22 w/v % SDS. Because C18A is insoluble in SDS solutions, we added NaCl into the surfactant solution to induce the micellar growth and thus, to solubilize C18A in the grown SDS micelles [8]. C18A content in the comonomer feed was varied between 20 and 50 mol % C18A while the total monomer concentration was fixed at 1.0 M. The polymerization reaction was initiated using a redox initiator system consisting of 0.79 mM APS and 1 mM $Na_2S_2O_5$. The reactions were conducted for 24 h in plastic syringes of 4.8 mm internal diameter as well as between two glass plates (5x5 cm) separated by a 0.5 mm Teflon spacer.

2.1.3 Swelling and gel fraction measurements

Hydrogel samples were immersed first in ethanol for 3 days and then in a large excess of water at 24 $^{\circ}$C for 1 month by replacing water every day to extract any soluble species. SDS concentration in the external solutions (before refreshing) rapidly dropped below the detection limit of the methylene blue method (0.20 mgL^{-1}) after about 10 d indicating completeness of SDS extraction from gel samples [33]. Note that the pre-immersion of the gel samples in ethanol before contact with water is to prevent their initial swelling in water due to the presence of SDS, which otherwise resulted formation of cracks in the gel samples. The equilibrium swollen gel samples were taken out of water and dried at 55 $^{\circ}$C under vacuum to constant mass. The water content of the hydrogels was estimated as H_2O % = 1 – m_{dry}/m, where m and m_{dry} are the swollen and dry masses of the gel sample, respectively. The gel fraction W_g, i.e., the conversion of monomers to the water-insoluble polymer (mass of water-insoluble polymer / initial mass of the monomer) was calculated from the masses of dry, extracted polymer network and from the comonomer feed.

2.1.4 Rheological experiments

The gel samples in the form of sheets were subjected to rheological measurements between the parallel plates of the rheometer (Gemini 150 Rheometer system, Bohlin Instruments) equipped with a Peltier device for temperature control. The upper plate (diameter 40 mm) was set at a distance of 500 to 700 μm, depending on the swelling degree of the hydrogels. During all rheological measurements, a solvent trap was used to minimize evaporation. Further, the outside of the upper plate was covered with a thin layer of low-viscosity silicone oil to prevent evaporation of solvent. A frequency ω of 6.3 rad.s^{-1} and a deformation amplitude γ_o = 0.001 (0.1%) were selected to ensure that the oscillatory deformation is within the linear viscoelastic region. Thermal behavior of the gels was investigated by first keeping the samples at 65 $^{\circ}$C for complete melting and then, cooling down to 25 $^{\circ}$C, after keeping for 10 min at 25 $^{\circ}$C, heating back to 65 $^{\circ}$C. The cooling/heating steps were carried out at a fixed rate of 1 $^{\circ}$C/min. The changes in the dynamic moduli of gels were monitored during the course of the cycle as a function of temperature. The gel samples were also subjected to frequency-sweep tests at γ_o = 0.001 and at both 25 and 65 $^{\circ}$C over the frequency range 0.06 to 180 rad.s^{-1}.

2.1.5 Differential scanning calorimety (DSC) measurements

DSC measurements were conducted on a Perkin Elmer Diamond DSC under nitrogen atmosphere. The gel samples sealed in aluminum pans were scanned between 5 and 80 $^{\circ}$C with a heating and cooling rate of 5 $^{\circ}$C/min. From the DSC curves, enthalpy changes during melting, ΔH_m, were calculated from the peak areas. The degree of crystallinity f_{cry} was estimated by $f_{cry} = \Delta H_m / \Delta H_m^o$, where ΔH_m^o is the melting enthalpy of crystalline C18A units, which was taken as 71.2 kJ.mol^{-1} [31,32].

2.1.6 X-Ray diffraction (XRD) measurements

X-ray diffraction patterns of hydrogel samples were collected on a Rigaku SmartLab diffractometer using a Cu-Kα source (λ = 0.15418 nm) operating at 30 kV / 15 mA. The XRD patterns were collected in the 1-35^{o}, 2θ range with a scan rate of 1^{o}/min.

2.1.7 Mechanical and shape memory test

Uniaxial compression measurements were performed at 23 ± 2 $^{\circ}$C on a Zwick Roell test machine using a 500 N load cell. Before the test, an initial compressive contact to 0.01±0.002 N was applied to ensure a complete contact between the gel and the plates. Paraffin oil was used as lubricant to reduce friction and adhesion between the plates and the gel surface. The tests were conducted at a constant crosshead speed of 0.3 and 1 mm.min^{-1} below and above 15% compression, respectively. Load and displacement data were collected during the experiment. Compressive stres was presented by its nominal σ_{nom} and true values σ_{true}, which are the forces per cross-sectional area of the undeformed and deformed gel specimen, respectively. Assuming the gel volume remains constant during deformation, the true stress σ_{true} was calculated as $\sigma_{true} = \lambda\, \sigma_{nom}$ where λ is the deformation ratio (deformed length / original length). The compressive strain ε_c is defined as the change in the length relative to the initial length of the gel specimen, i.e., $\varepsilon_c = 1 - \lambda$. The strain is also given by the biaxial extension ratio λ_{biax} (=$\lambda^{-0.5}$) [34]. The Young's modulus E was calculated from the slope of stress-strain curves between 5 and 15% compressions.

Uniaxial elongation measurements were performed with a Zwick Z2.5 tensile test instrument equipped with a 20 N load cell on hydrogel samples immersed in a temperature controlled water tank, utilizing an Ecoline Star Edition RE306 (Lauda, Königshofen, Germany). The actual temperature of the samples was measured by a Voltcraft multi-thermometer DT-300 positioned near the sample. A preforce of 10 mN was applied before the start of the measurements. The gel samples were stretched at 56 °C and at a strain rate of 10 mm.min^{-1} up to 1500% strain ε $(= 1 - \lambda)$ due to the instrumental limitation. Stress-relaxation tests were carried out by stretching the gel samples at 56 °C and at a strain rate of 10 mm.min^{-1} up to a maximum strain ε_m of 100 and 200%, waiting at ε_m for 10 s, followed by retraction with a relaxation rate of 0.1 N.min^{-1} to zero relaxation force which was 20 mN. After waiting for 15 min at zero relaxation force, the test was repeated four times.

The shape memory behavior of the hydrogel with 50 mol % C18A was investigated using cyclic thermomechanical tests [35]. The gel sample was first stretched at 56 °C to ε_m of 100% at a strain rate of 10 mm.min^{-1}. After a waiting time of 5 min at ε_m to allow relaxation, the loaded sample was cooled to 35 °C while keeping the strain at ε_m. Finally, the sample was unloaded to zero relaxation force, 10 mN, and the strain ε_u (n) of the sample in the temporary shape was obtained. The recovery behavior was followed by reheating the sample up to 56 °C with a rate of 1 °C.min^{-1} and then keeping at this temperature. The total time at zero relaxation force was fixed at 50 min. After completion of the recovery process, the permanent elongation of the sample ε_p (n) was determined. The strain recovery rate R_r (n) and strain fixing rate R_f (n) of the nth cycle were calculated by

$$R_r(n) = \frac{\varepsilon_m - \varepsilon_p(n)}{\varepsilon_m - \varepsilon_p(n-1)} \tag{2.1}$$

$$R_f(n) = \frac{\varepsilon_u(n)}{\varepsilon_m} \tag{2.2}$$

The shape memory effect was also examined by a bending test as follows: The cylindrical hydrogel samples with a diameter of 4.8 mm and a length about 6 cm is folded at 60 °C and then cooled to 25 °C to keep the deformation. The deformed sample is then stepwise heated from 25 to 70 °C at 1-3 °C steps. The recovering of the permanent shape is recorded in terms of the deformation angle θ_d depending on temperature. The measurements of θ_d were conducted using an image analyzing system consisting of a microscope (XSZ single Zoom microscope), a CDD digital camera (TK 1381 EG) and a PC with the data analyzing system Image-Pro Plus. The recovered angle R_θ to the permanent one was calculated as $R_\theta = \theta_d / 180$.

2.1.8 Self healing tests

To quantify the healing efficiency, cylindrical gel samples of 5 mm diameter and 6 cm length were cut in the middle, and then the two halves were merged together within a plastic syringe (of the same diameter as the gel sample) at 80 °C by pressing the piston plunger for 24h. Thereafter, uniaxial compression and elongation tests were conducted as described above. The results were compared with those of the virgin gel samples.

2.2 Results and Discussion

Hydrogels were prepared by micellar copolymerization of AAc with 20-50 mol % hydrophobic monomer C18A at 55 °C and at a total monomer concentration of 1 M by free radical polymerization. The advantage of the micellar polymerization technique over the solution polymerization is the formation of copolymers in a blocky structure because of the local high concentration of hydrophobic monomer in the micelles [37], facilitating the formation of the aggregates [11,38,39]. An aqueous solution containing NaCl (1.5 M) and sodium dodecyl sulfate (SDS, 22 w/v%) was used as the micellar solution [8,10]. The addition of NaCl into the surfactant solution is to provide the growth of SDS micelles and hence to solubilize the hydrophobic monomer C18A in this micellar solution [8,36]. In order to obtain supramolecular PAAc hydrogels, there is no chemical cross-linker added during synthesis. The polymerization reaction was initiated using a redox initiator system consisting of ammonium persulfate (0.79 mM) and sodium metabisulfite (1 mM). After a reaction time of 24 h, the conversion of monomers to the water-insoluble polymer was found to be more than 90%. The micellar polymerization technique necessarily results in hydrogels containing SDS micelles while, after equilibrium swelling in water, all surfactant molecules could be removed from the gel network. In the following, as-prepared and water-swollen hydrogels will be denoted as those with and without SDS, respectively. Moreover, the hydrogels are coded as *x*% C18A in which *x* is the mole fraction of C18A in the feed. The supramolecular hydrogels with or without

SDS contain 64 to 88% water that increases with decreasing C18A content (Table 2.1).

Table 2.1 : Water contents, melting (T_m) and crystallization temperatures (T_{crys}) and the degree of crystallinity of the hydrogels. Standard deviations are in parenthesis while for the water contents, they are less than 10%.

C18A mol%	**Water%**		**T_m / °C**		**T_c / °C**		**Crystallinity%**	
	with SDS	without	with SDS	without	with SDS	without	with SDS	without
20	66	88	-	51 (0)	-	46 (0)	0	20 (1)
35	64	70	50 (1)	51 (0)	37 (1)	45 (1)	12 (2)	35 (3)
50	63	64	50 (0)	51(1)	38 (1)	44 (1)	17 (1)	56 (2)

[a]standard deviations in parentheses while for the water contents, they are less than 10%

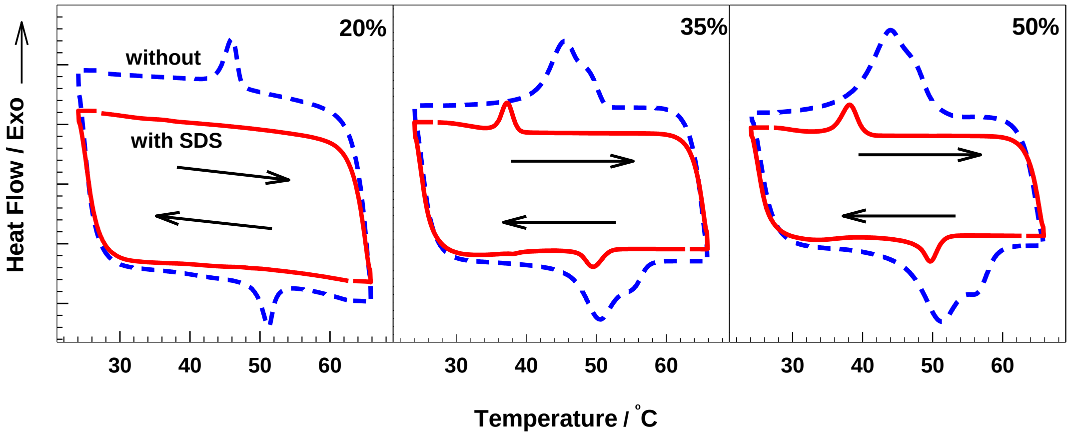

Figure 2.2 : DSC traces of the hydrogels with (solid curves) and without SDS (dashed curves). C18A content of the hydrogels is indicated.

DSC traces shown in Figure 2.2 reveal that, except 20% C18A hydrogel with SDS, they all exhibit melting and crystallization peaks. The melting (T_m) and crystallization temperatures (T_{crys}) of the physical gels are listed in Table 2.1 together with the degrees of crystallinity, estimated by assuming that the enthalpy change during melting of crystalline C18A units is 71.2 kJ/mol [31,32]. T_m of the hydrogels is at around 50 °C, regardless of the hydrophobe content or the presence of surfactant micelles, while re-crystallization of molten hydrophobic domains occurs at a lower temperature than melting. The degree of the crystallinity increases with increasing C18A content as well as after removal of SDS from the gel network. The latter is related with the formation of mixed micelles composed of SDS and C18A units of the polymer hindering the formation of crystalline domains [36]. Figure 2.3 shows the X-ray diffraction (XRD) patterns of the hydrogel sample containing 50 mol% C18A with and without SDS.

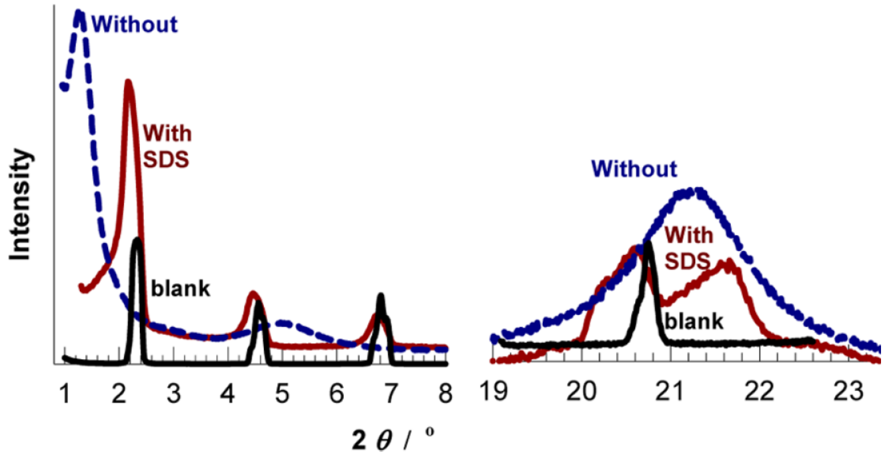

Figure 2.3 : XRD pattern of 50% C18A hydrogel without (blue, dashed curves) and with SDS (dark-red, solid curves) in 1-8° and 19-24° in 2θ ranges. Scan rate = 1°/min. The blank sample was prepared as the hydrogel sample but without C18A addition into the comonomer feed.

The pattern of the sample without SDS exhibits a sharp peak at 1.4^{o} and a broad, higher angle peak at 21.3^{o} corresponding to Bragg *d*-spacings of 6.3 and 0.42 nm, respectively. The *d*-spacing of 0.42 nm indicates packing of the side alkyl chains of C18A units in a paraffin-like hexagonal lattice, while the *d*-spacing of 6.3 nm reveals tail-to tail alignment of the side chains perpendicularly to the main chains [6,8, 24,41]. The hydrogel sample with SDS exhibit several peaks due to the presence of surfactant micelles. To eliminate the surfactant peaks, XRD measurements were also conducted using control samples obtained by micellar polymerization in the absence of the hydrophobe C18A. Thus, these samples correspond to a semi-dilute solution of PAAc and SDS micelles. XRD pattern of this sample denoted as blank is also shown in the figure. Comparison of the control with the gel sample containing SDS reveals that the gel exhibits a characteristic peak at 21.3^{o} (*d*-spacing 0.42 nm) as the swollen gel sample indicating hexagonal packing of the side alkyl chains in the presence of surfactant.

Figure 2.4 shows the frequency (ω) dependences of the elastic modulus G' (filled symbols) and viscous modulus G'' (open symbols) of the hydrogels at 25 and 65 $^{\circ}$C, i.e., at below and above T_m of crystalline domains. The data from hydrogels with (left panel) and without SDS (right panel) are shown.

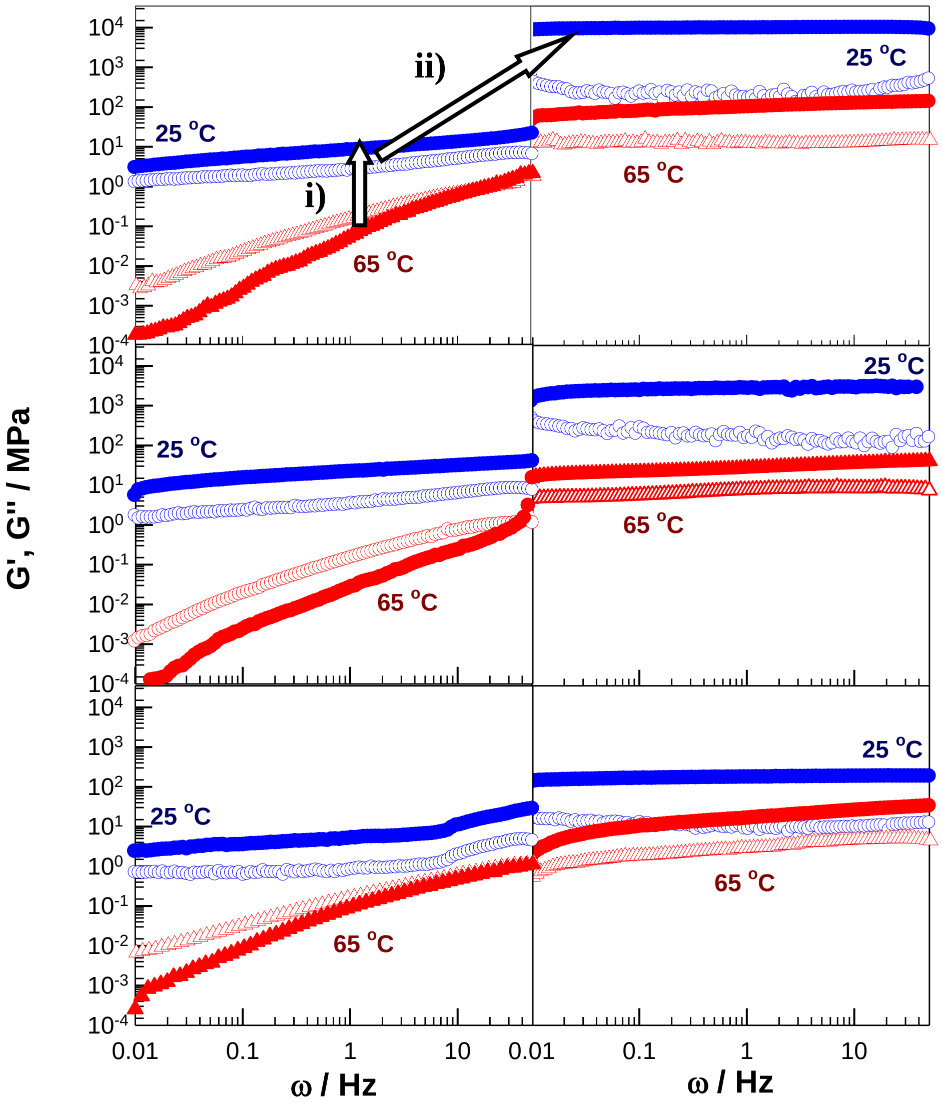

Figure 2.4 : *G'* (filled symbols) and *G''* (open symbols) of the hydrogels with (left panel) and without SDS (right panel) shown as a function of the frequency ω. γ_0 = 0.001. C18A = 50 (top), 35 (middle), and 20% (bottom). Temperature = 25 (circles) and 65 °C (triangles). The arrows indicate the changes in the moduli of 50% C18A hydrogel during two successive steps, namely, (i) cooling the gel containing SDS from 65 to 25 °C and (ii) extraction of SDS.

At 65 °C, the hydrogels with SDS exhibit a liquid-like response typical for a semi-dilute polymer solution, i.e., *G´´* exceeds *G´* over a wide range of frequencies while there is a crossover point between *G´* and *G´´* at a high frequency (≥ 160 rad.s^{-1}). Cooling the hydrogel containing SDS below T_{cry} leads to the formation of a weak gel while, after extraction of SDS, the gel exhibits frequency-independent elastic modulus of 0.2-8 MPa and a loss factor $\tan\delta$ (=*G''/G´*) close to 0.01, as typical for strong gels. Particularly remarkable is the drastic change in the viscoelastic properties of 50% C18A hydrogel during these successive steps, namely i) cooling the gel containing SDS from 65 to 25 $^{\circ}$C, and ii) extraction of SDS. These are illustrated in Figure 2.4 by the arrows. Starting from a viscoelastic liquid with *tan* δ = 3 at a frequency of 6.3 rad.s^{-1}, one may obtain a hydrogel with an elastic modulus of 8.4 MPa and *tan* δ = 0.02.

The variation of the temperature-dependent moduli of the hydrogels was investigated at a fixed frequency (6.3 rad.s^{-1}) during the cooling – heating cycles between 65 and 5 $^{\circ}$C. Figure 2.5 shows the dynamic moduli of the hydrogels with and without SDS during the cooling and heating scans. DSC traces of the gels with and without SDS are also shown in the figures by the solid and dashed curves, respectively. At around the transition temperatures, the dynamic moduli of the hydrogels change reversibly due to the formation and melting of the crystalline domains of the side chain alkyl crystals.

In Figure 2.6, G' and the loss factor *tan* δ of the hydrogels without and with SDS at below (25 $^{\circ}$C) and above (65 $^{\circ}$C) T_m are collected. The dashed horizontal lines denote *tan* δ values for sol-to-gel (=1) and weak-to-strong gel (=0.1) transitions. 50% C18A hydrogel without SDS undergoes a reversible 1100-fold change in G' (between 8.4 MPa and 7.5 kPa) between below and above T_m. Simultaneously, *tan* δ changes between below and above 0.1, demonstrating reversible weak-to-strong gel transition. Moreover, the hydrogels with SDS undergo reversible sol-gel transitions during thermal cycling, i.e., *tan* δ changes between below and above unity. Hydrogels become solutions at temperatures above 36, 46, and 49 $^{\circ}$C for 20, 35, and 50 mol% C18A samples, respectively. On cooling, they turn to their gel states at 34, 40, and 48 $^{\circ}$C, respectively. Thus, sol-to-gel and weak-to-strong gel transitions can be observed depending on the presence of the surfactant and on the temperature. The results also show easy transformation of a polymer solution into a strong hydrogel possessing around 8 MPa modulus.

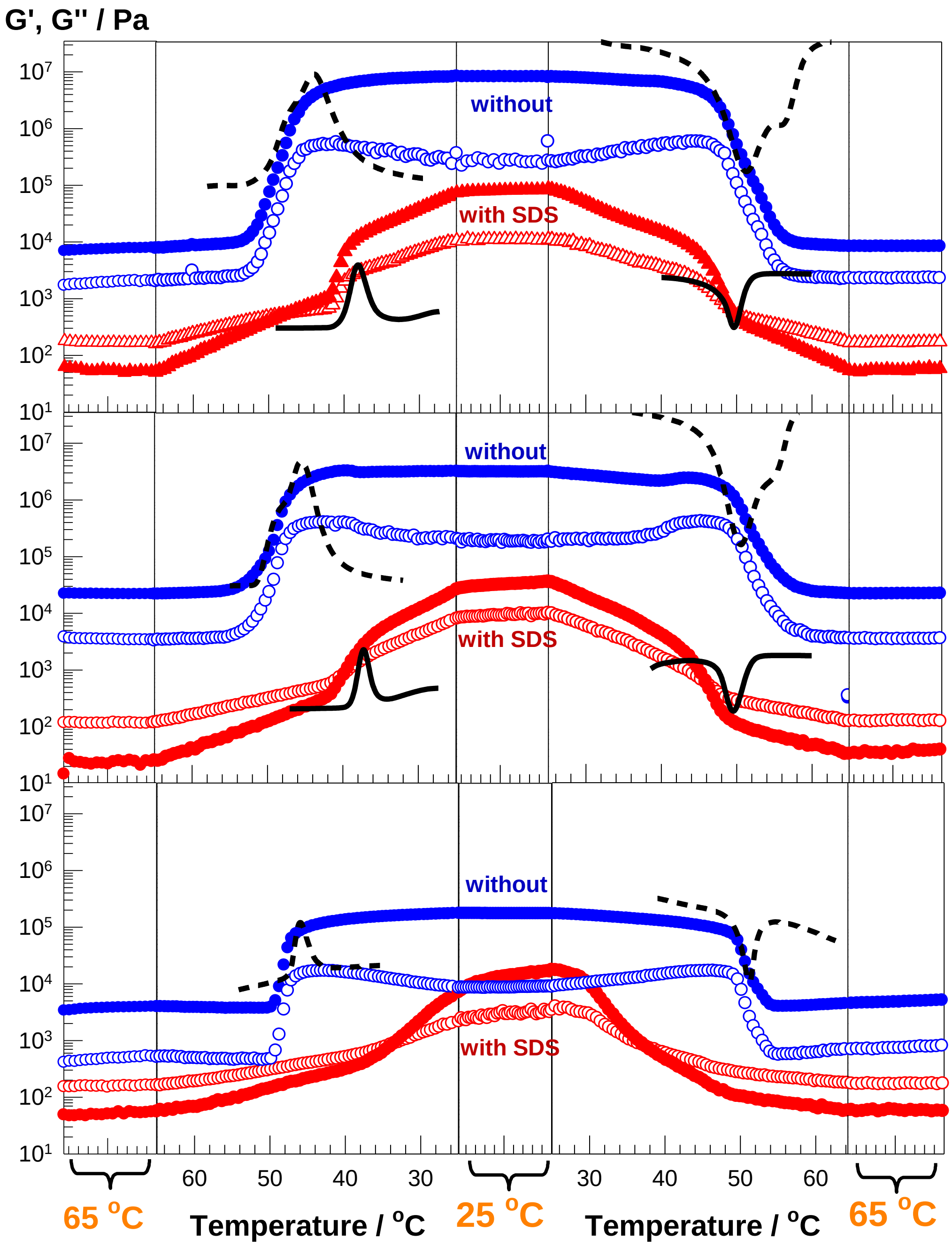

Figure 2.5 : *G'* (filled symbols) and *G''* (open symbols) of the hydrogels during the course of the cooling and heating periods. DSC traces of the hydrogels with and without SDS are also shown by the solid and dashed curves, respectively. *G'* and *G''* data of the gel samples with and without SDS are shown by triangles and circles, respectively. C18A = 50 (top), 35 (middle), and 20% (bottom panel). $\omega = 6.3$ rad.s^{-1}. $\gamma_0 = 0.001$.

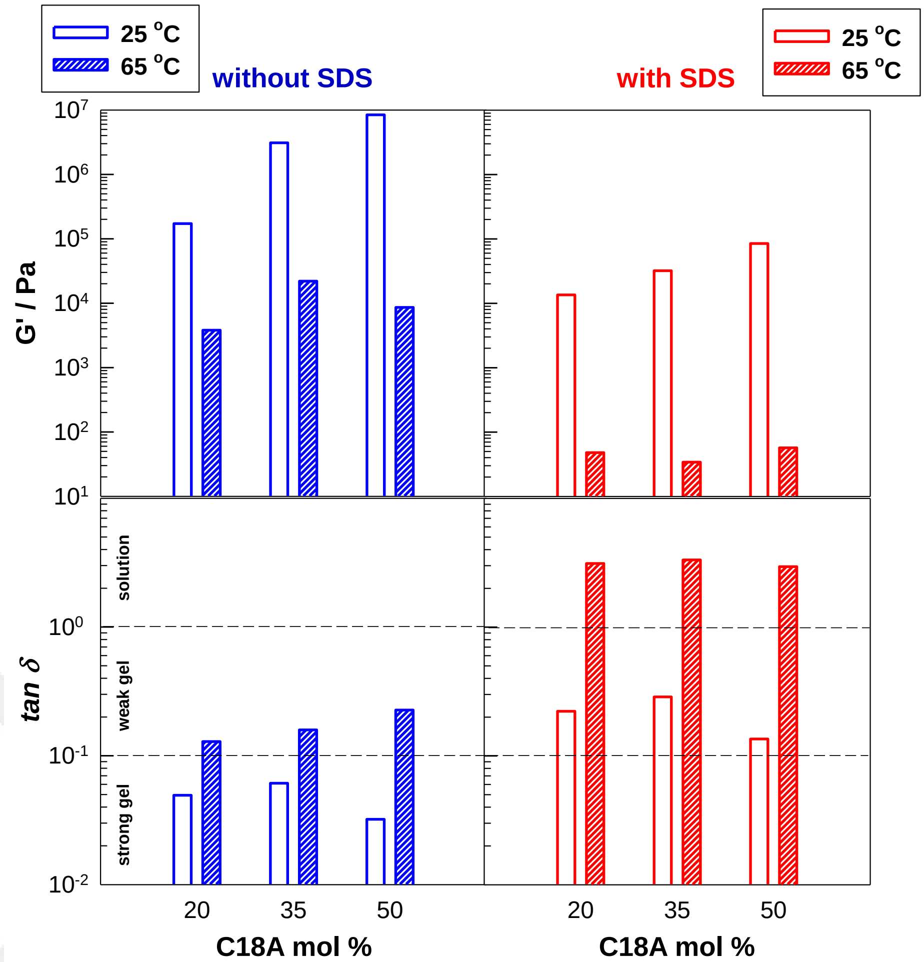

Figure 2.6 : *G′* and *tan* δ of the hydrogels without (left panel) and with SDS (right panel) at below and above the melting temperature. ω = 6.3 rad.s^{-1}. γ_o = 0.001.

Figure 2.1 demonstrates moldability and shape memory effect of 50% C18A hydrogels. After heating to 60 °C, the hydrogel with SDS is in a liquid state and could be shaped any desired shape by pouring into molds (Figure 2.1a,b). After cooling to 25 °C and extracting SDS from the gel, this permanent shape is fixed. By heating the gel sample above T_m, the gel becomes soft so that any temporary shape can be given which is then fixed by cooling it to 24 °C (Figure 2.1c). After heating again in a water bath at 60 °C, the gel sample returns to its permanent shape within 15 s (Figure 2.1c). The hydrophobic associations of C18A blocks of the hydrophilic polymer chains act as physical netpoints to determine the permanent shape while, above T_m, the same blocks forming side chain alkyl crystals act as molecular switches to fix the temporary shape of the hydrogel.

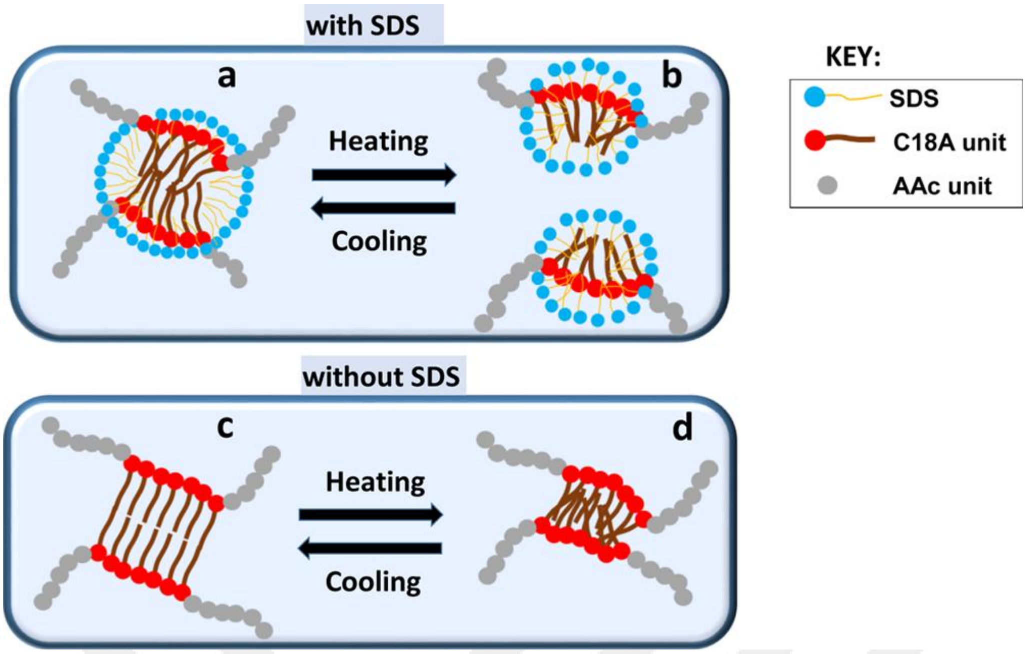

Figure 2.7 : Cartoon showing the physical cross-links of the hydrogels at various stages.

We propose that the moldability and the shape-memory capability of the hydrogels appear due to the temperature- and surfactant-induced changes in the properties of the physical cross-links, as depicted in Figure 2.7. For the hydrogel with SDS, mixed micelles consisting of C18A blocks of the polymer and SDS act as the physical cross-links (Figure 2.7a) [36]. Because of the weakening of hydrophobic interactions in the presence of a surfactant [10], the hydrogel is weak with an elastic modulus of 10^{-2}–10^{-1} MPa and a loss factor above 0.1 (Figure 2.4). Upon heating the hydrogel above T_m, the hydrophobic domains are solubilized by the SDS micelles to form a semidilute polymer solution (Figure 2.7b). Moreover, removing SDS from the hydrogel drastically changes the viscoelastic properties of the hydrogels due to the increasing extent of hydrophobic interactions (Figure 2.7c) Hydrophobic groups in the SDS-free hydrogel form stronger associations and larger number of crystalline domains to minimize their exposure to the gel phase; thereby the modulus increases to 10^{-1}–10^{1} MPa and the loss factor decreases below 0.1. Heating above T_m again destroys the crystalline domains while the associations formed act as the physical netpoints in the hydrogels (Figure 2.7c→d). Thus, the hydrophobic associations of C18A blocks of the hydrophilic polymer chains act as physical netpoints to determine the permanent shape while, below T_m, the same blocks forming side chain alkyl crystals act as molecular switches to fix the temporary shape gained by deformation of the hydrogel sample at a temperature above T_m.

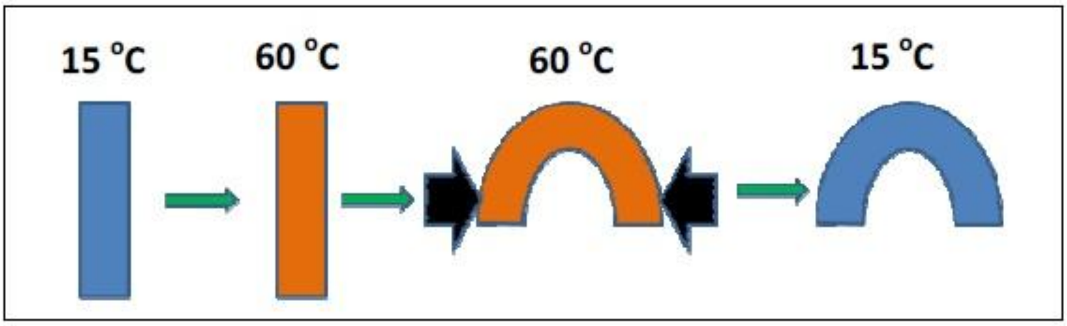

Figure 2.8 : Programming procedure for bending tests.

Shape memory properties of the hydrogels were determined by both bending experiments and uniaxial tensile tests conducted in aqueous environment. Bending test was carried out by first folding the cylindrical hydrogel sample at 60 °C to a deformation angle θ_d of 180° and then cooling to 15 °C to fix the deformation (Figure 2.8). The deformed sample was then stepwise heated from 15 to 70 °C in steps of 1−3 °C whereby the recovering of the permanent shape was recorded in terms of the deformation angle θ_d depending on temperature (see Figure 2.9).

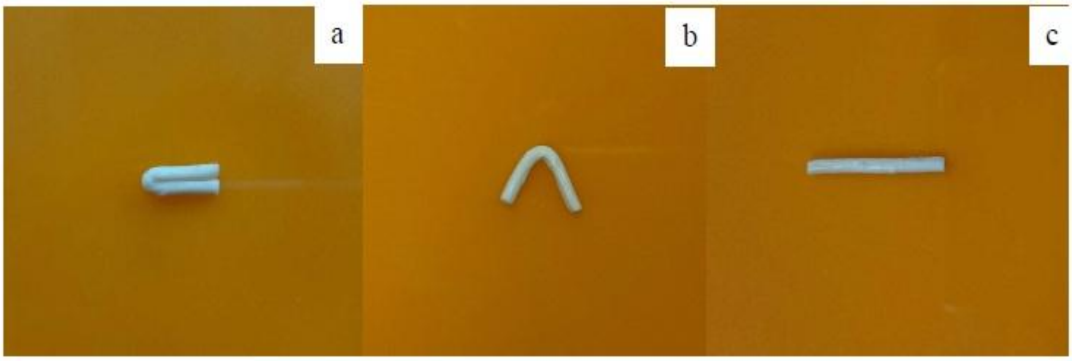

Figure 2.9 : Images of a hydrogel sample with 50 mol% C18A during the bending test. (a) After folding at 60 °C to a deformation angle of 180° and then cooling to 15 °C. (b, c): During heating from 15 °C to 70 °C. Temperature = 55 (b) and 65 °C (c).

Bending test results are shown in Figure 2.10 where the recovered permanent angle R_θ (= 1- θ_d / 180) of the folded hydrogels is shown as a function of the temperature. R_θ increases to 100% for the gels with 35 and 50 mol% C18A over a rather small temperature range, i.e., between 45-59 °C and 50-61 °C, respectively. Thus, the crystalline domains in these hydrogels are able to fix the temporary folded shape up to a temperature close to their melting temperature T_m (51 °C). In contrast, R_θ value of 20% C18A hydrogel steadily increases with temperature, which we attribute to the low crystallinity of this sample, i.e., its lower physical netpoint density (Table 2.1).

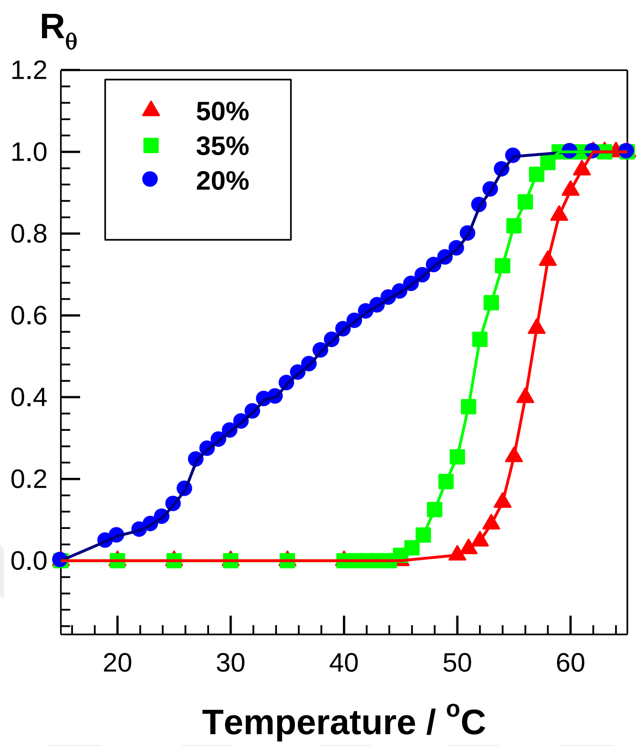

Figure 2.10 : The variation of the recoverability R_θ of the permanent angle of folded hydrogels with temperature. C18 mol% of the hydrogels is indicated.

The fixity of the permanent shape solely by hydrophobic associations was explored in stress relaxation experiments. The tests were conducted at 56 °C on hydrogel samples with 50 mol% C18A. At this temperature, no more crystalline domains exist and hence all C18A blocks in the hydrogel involve in hydrophobic associations or exist as non-associated free groups. Stress-relaxation tests were performed on a tensile tester Zwick Z2.5 with a tempered tank at 56 °C in order to determine the elastic recovery of the hydrogel samples at $T > T_m$. The specimens were stretched to a maximum strain ε_m of 100 and 200%, with a deformation rate of 10 mm.min^{-1} and then held shortly for a time period of 10s under constant strain. Afterward, the stress was released to a zero force of 10 mN at a rate of 0.1 N min^{-1} to enable the sample to recover from the imposed strain. When this zero force condition was maintained for 15 min, the elongation of the sample reached a plateau, and the recovered elongation became stable. This cycle was then repeated four times. The results of five successive stress-relaxation tests are shown in Figure 2.11 as the dependence of the nominal stress σ_{nom} on the strain ε., i.e., λ-1, where λ is the elongation ratio. The maximum strain ε_m is 100% (left) and 200% (right). In both cases, the first cycle shows the largest mechanical hysteresis and permanent deformation. We attribute this to decoupling of entanglement, disruption of weak associations, and reorientation of polymer chains. However, the following cycles are almost reversible with no additional permanent deformation. The average hysteresis energy U_{hys} for the 2nd to 5th cycles calculated from the area between the loading and unloading curves are 0.44 ± 0.05 and 0.8 ± 0.1 MJ.m^{-3} for ε_m = 100 and 200%, respectively. These are 2 orders of magnitude larger than U_{hys} of supramolecular hydrogels formed via hydrophobic associations [10,42] and reveal the existence of larger number of associations in the present hydrogels. Moreover, because U_{hys} is related to the extent of damage in the gel samples, i.e., to the number of bonds broken during the loading/unloading cycle [10,34], the reversibility of the successive cycles reveals that the damage done to the gel samples is recoverable in nature. Thus, the results indicate temperature-triggered healing ability of the hydrogels. The tests also confirm that the hydrophobic associations are very effective acting as netpoints determining the permanent shape of the hydrogels.

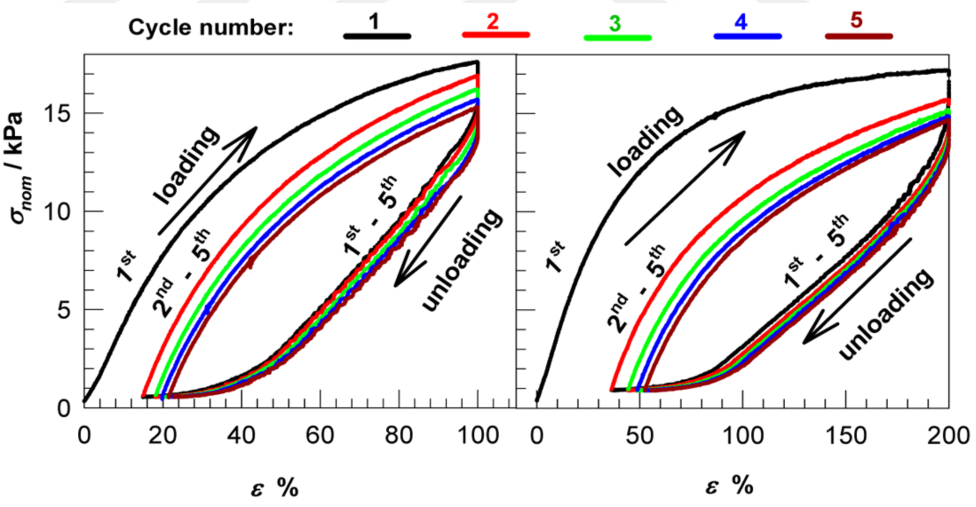

Figure 2.11 : Nominal stress σ_{nom} vs strain ε curves from stress relaxation tests conducted at 56 °C on hydrogel samples up to a maximum strain of 100 and 200%. Five successive loading / unloading cycles are shown. C18A = 50 mol%.

The hydrogel sample with 50 mol % C18A was also subjected to thermomechanical shape-memory cycles. The gel sample was first stretched at 57 °C to ε_m of 100% at a strain rate of 10 mm min^{-1}. After a waiting time period of 5 min at ε_m to allow relaxation, the loaded sample was cooled to 32 °C while keeping the strain at ε_m. Finally, the sample was unloaded to zero relaxation force, 10 mN, and the strain $\varepsilon_u(n)$

of the sample in the temporary shape was obtained. The recovery behavior was followed by reheating the sample up to 57 °C with a rate of 1 °C min^{-1} and then keeping at this temperature. The total time at zero relaxation force was fixed at 50 min. After completion of the recovery process, the permanent elongation of the sample $\varepsilon_p(n)$ was determined.

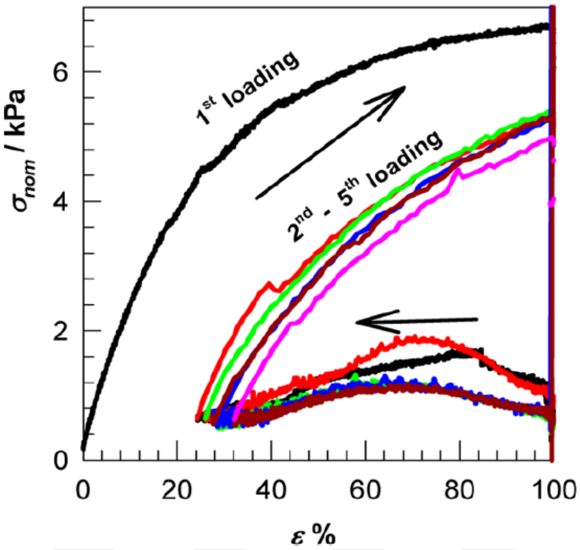

Figure 2.12 : Results of cyclic thermomechanical tests conducted on 50 mol% C18A hydrogel as the dependence of the nominal stress σ_{nom} on the strain ε. Five successive cycles are shown.

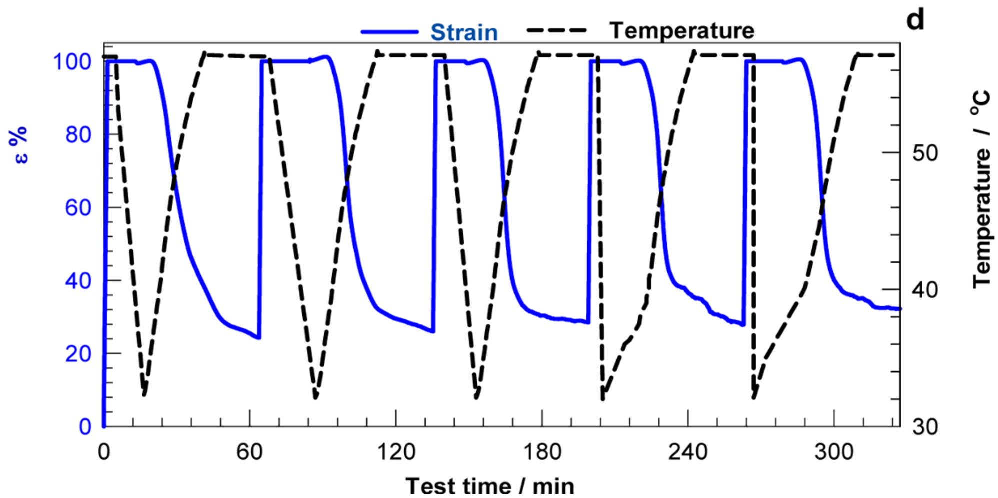

Figure 2.13 : Strain ε (solid curve) / temperature (dashed curve) vs time plots of five successive thermomechanical cycles.

The results of five cycles of the thermomechanical tests are shown in Figure 2.12 as stress σ_{nom} vs strain ε plots, while Figure 2.13 shows corresponding strain/temperature vs time plots. The hydrogel completely preserves its temporary shape after relaxation at 32 °C which is equivalent to a shape fixity ratio, R_f of >99%.

Moreover, similar to the results of stress-relaxation tests (Figure 2.11), the first thermomechanical cycle produces a permanent deformation in the hydrogel and the shape recovery ratio R_r (*1*) of this cycle is 76%. However, excellent reproducibility and reversibility of the shape changes were observed in the subsequent cycles (n = 2 - 5) with an average shape recovery ratio R_r (n) of 97± 2%. Considering the first cycle as the preconditioning cycle, the shape of the hydrogel is almost completely recovered by heating above T_m of crystalline domains.

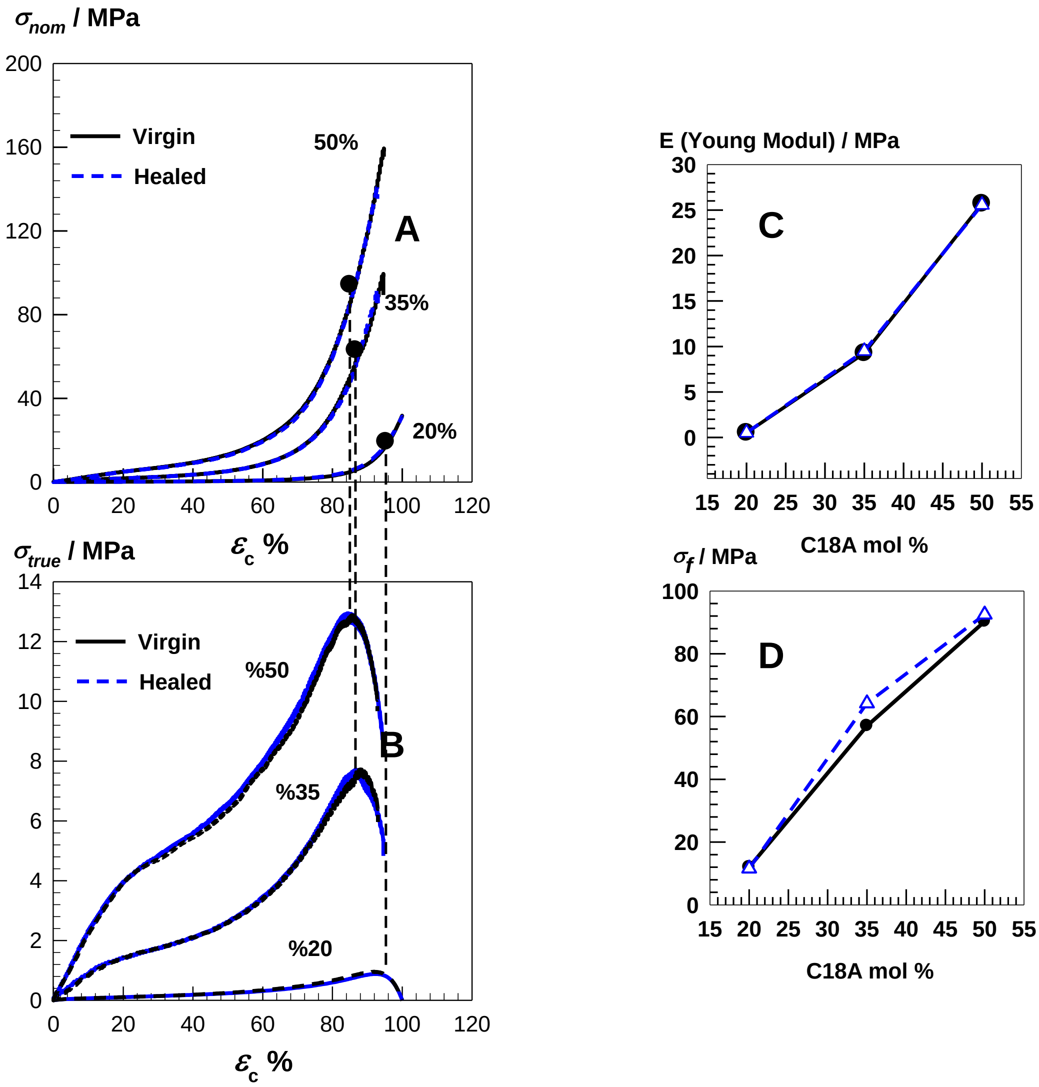

Figure 2.14 : (a, b) Typical stress-strain curves of the hydrogels under compression as the dependences of nominal σ_{nom} (a) and true stresses σ_{true} (b) on the compressive strain ε_c. Inset to b shows the σ_{true} vs λ_{biax} plots. Circles corresponding to the maxima in σ_{true} - λ (or, σ_{true} - λ_{biax}) plots are taken as the points of failure in the gel samples. C18A content of the hydrogels is indicated. Solid and dashed (blue) curves are results obtained from virgin and healed hydrogel samples, respectively. (c) Young's modulus E and (d) fracture stress σ_f of the virgin (filled symbols) and healed hydrogels (open symbols) plotted against their hydrophobe (C18A) content.

The mechanical properties of SDS-free hydrogels after cooling to $23 \pm 2\ ^{\circ}C$ was determined by uniaxial compression measurements. Solid curves in Figures 2.14a and 14b represent typical stress-strain curves of the hydrogels as the dependences of the nominal σ_{nom} (a) and true stresses σ_{true} (b) on the compressive strain ε_c (= l-λ), respectively. From σ_{nom} vs ε_c curves, it is seen that the hydrogels sustain up to about 94% compressions and they rupture under 30 - 160 MPa nominal stresses (Figure 2.14a). However, the corresponding σ_{true} vs ε_c plots pass through maxima below these strains (Figure 2.14b), indicating that the actual fracture points are below these stress values. This behavior is a result of the formation of microscopic cracks sustaining the stress under large strain [42,43]. Therefore, the fracture nominal stress σ_f and strain ε_f at failure were calculated from the maxima in σ_{true} - ε_c or σ_{true} - λ_{biax} plots, as indicated by the dashed vertical lines and circles in the figures. Filled circles in Figures 2.14c and 2.14d show Young's modulus E and fracture stress σ_f of the hydrogels plotted against the hydrophobe (C18A) content, respectively. All hydrogel samples sustain up to 85-92% compressive strain. They display particularly high mechanical strength (12 - 90 MPa) and Young's modulus (0.5 - 26 MPa), which increase with increasing hydrophobe content. All hydrogel samples were capable to sustain up to 85−92% compressive strain. They display particularly high compressive strength (12−90 MPa) and Young's modulus (0.5−26 MPa), which increase with increasing C18A content. Note that the measured Young's modulus is approximately 3 times the frequency independent elastic modulus of the hydrogels (0.2−8 MPa), consistent with an isotropic elastic material of Poisson's ratio close to 0.5.32 The hydrogels were also subjected to tensile testing experiments at 23 ± 2 °C. They exhibited a high Young's modulus (0.1−28 MPa) but a low stretchability (3−40% elongation) and low fracture stress (33−751 kPa) due to the high degree of crystallinity of the hydrogels (Table 2.2 and Figure 2.15).

Table 2.2 : Tensile properties of the hydrogels in equilibrium with water. Standard deviations are in parenthesis

C18A mol%	Elongation at break %	E / MPa	σ_f / kPa
20	40 (2)	0.14 (0.02)	33 (3)
35	28 (1)	2.6 (0.2)	367 (26)
50	2.7 (0.3)	28(2)	751 (69)

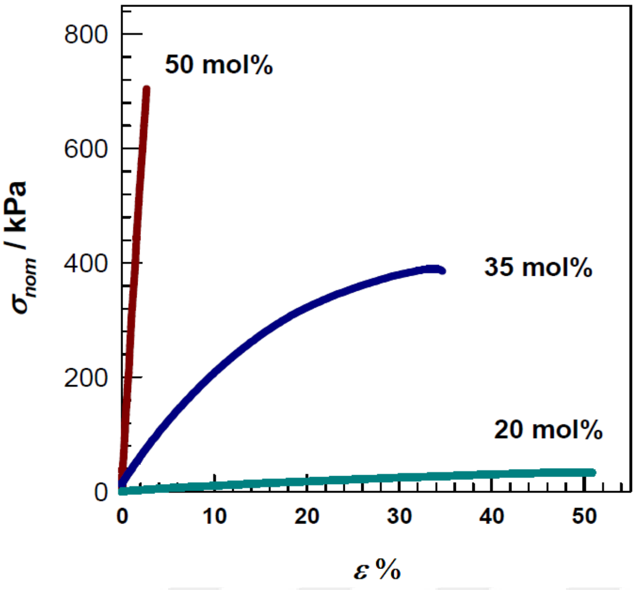

Figure 2.15 : Stress-strain curves of tensile tests conducted at 23 ± 2 °C. C18A content of the hydrogels is indicated.

Because of the supramolecular network structure of the present hydrogels, they exhibit self-healing ability when the damaged areas are heated above the melting temperature of the crystalline domains. The large mechanical hysteresis and the reversibility of the loading/unloading cycles shown in Figure 2.11 already demonstrate the self-healing ability of the hydrogels. This is also illustrated in Figure 2.1d where photographs of two virgin 50% C18A hydrogel samples after equilibrium swelling in water are shown. After pressing the gel surfaces together in a closed container at 80 °C for 24h, they merge into a single specimen. The dashed (blue) curves in Figures 2.14a and 2.14b show the stress-strain curves of the healed gel samples. A perfect superposition is observed between the stress-strain curves obtained from virgin (solid curves) and healed gel samples. The mechanical data of the healed hydrogels are represented by the open triangles in Figures 2.14c and 14b. The results reveal complete healing efficiency with respect to the compressive modulus, fracture stress and fracture strain after a healing time of 24h at 80 °C.

Healing tests were also conducted by uniaxial elongation tests at an elevated temperature. Figure 2.16 shows tensile test results of virgin and healed hydrogel samples at 56 °C.

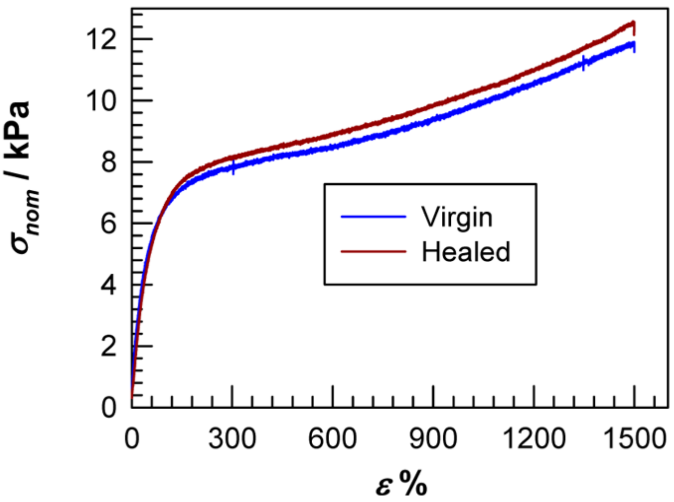

Figure 2.16 : Stress-strain curves of tensile tests conducted at 56 °C on virgin and healed hydrogel samples with 50 mol% C18A.

Note that because of the experimental limitation (dimensions of the water tank), the samples could only be elongated up to 1500%. A good superposition is observable in tensile stress-strain curves indicating a complete healing of the gel sample. Indeed, the Young's modulus *E* of both virgin and healed hydrogels is 12 kPa at 56 °C indicating complete recovery of the initial microstructure of the physical hydrogel.

The supramolecular approach described here can be extended to create a range of melt-processable hydrogels by varying the hydrophilic and hydrophobic monomers as well as hydrophobically modified polymer-surfactant systems. The key requirement is the presence of surfactant micelles in the physical gels effective for solubilizing the hydrophobic associations at a high temperature. Moreover, the surfactant should not form a complex with the polymer chains such as in oppositely charged surfactant-polymer systems, so that it could be removed from the physical network after determining the permanent shape of the hydrogel. A high mechanical strength and a complete shape memory effect require a hydrophobic monomer with a long alkyl side chain to form strong associations and crystalline domains acting as physical netpoints and molecular switches, respectively. We have to note that the elaborative surfactant removal step from the hydrogels, namely immersion in ethanol for 3 days and then in water for 1 month, is the limitation of the present approach for translation of thematerials into marked applications. Further work is in progress to develop an easy surfactant removal process from the hydrogels.

2.3 Conclusions

We present a supramolecular approach to the preparation of melt-processable shape memory hydrogels with self-healing ability. The hydrogels contain 60-80 wt% water and consist of PAAc chains containing 20 - 50 mol % C18A segments together with SDS micelles. The key of our approach is the absence of covalent cross-links and the presence of surfactant in the hydrogels. Above the melting temperature T_m of the crystalline domains, the hydrogel liquefies due to the presence of surfactant micelles effective for solubilizing the hydrophobic associations. At this stage, it can easily be processed in any desired shape by pouring into molds. Cooling below T_m and removing the surfactant results in a hydrogel of any permanent shape with a mechanical strength of 90 MPa and Young's modulus of 26 MPa. The hydrogel exhibited complete shape recovery due to the hydrophobic blocks of the polymer acting as physical netpoints and switching segments above and below T_m, respectively. If damaged, the extraordinary mechanical properties can completely be recovered via temperature-induced healing process. The synthetic strategy presented here offers the design of shape-memory hydrogels in various permanent shapes for the production of multifunctional smart hydrogel coatings, thin films, microspheres, tubings, rods, and wires to be used in various applications, including biomedical, packaging, sensors, and actuators.

3. YIELDING BEHAVIOR OF TOUGH SEMI-CRYSTALLINE HYDROGELS[2]

Hydrogels are unique soft materials with similarity to biological tissues and therefore attracted great interest for a wide range of application areas [44,45]. A significant achievement in the preparation of new generation hydrogels with extraordinary mechanical properties is the double-networking strategy developed by Gong and co-workers [46-48]. Double-network (DN) hydrogels consist of interpenetrated and interconnected polymer network components containing 60−90% water [46-50]. The highly crosslinked first-network consists of stretched network chains and therefore it is brittle in nature, while the loosely cross-linked second-network forming the major component of the DN exhibits viscoelastic and ductile behavior.

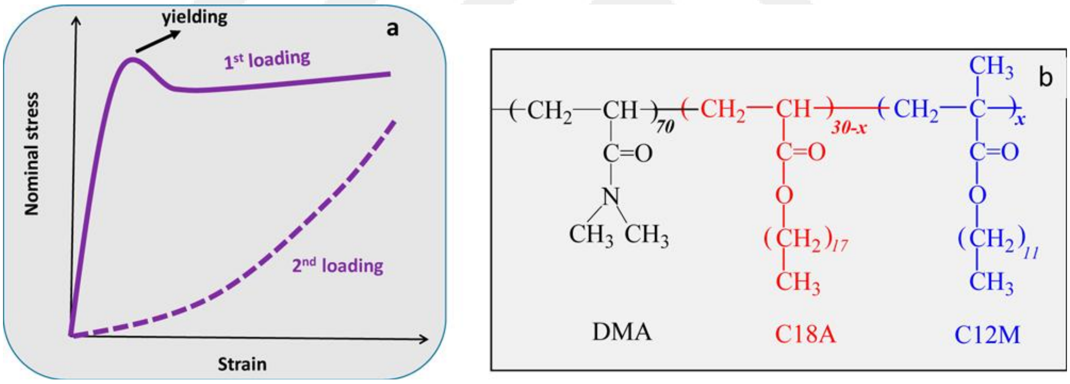

Figure 3.1 : (a) Scheme of stress−strain curves of a tough DN hydrogel in the first (solid curve) and second tensile loading before fracture (dashed curve). (b) Structure of the monomer units of the hydrogels.

The deformation of DNs possessing a high toughness usually proceeds via a yield phenomenon which is macroscopically evidenced by the appearance of necking [51-53]. Figure 3.1a schematically illustrates typical mechanical behavior of a DN hydrogel subjected to two successive tensile tests before fracture. The virgin DN

---

[2] This chapter was published in "Bilici C., Ide S., Okay O., (2017), Yielding behaviour of tough semicrystalline hydrogels, *Macromolecules*, 50, 9, 3647-3654".

shows a distinct yield point where the brittle first network starts to break up to form many cracks while the second ductile network keeps the macroscopic sample together, leading to excellent toughness [53]. However, breaking chemical bonds in the first network during the first loading results in an irreversible damage to the DN, as evidenced from the significant decrease of both the modulus and the toughness during the second loading (Figure 3.1a). This is the main disadvantage of DN hydrogels. To overcome this weakness, hybrid DNs have recently been synthesized consisting of physically and chemically cross-linked network components [54-56]. However, their fracture stresses are low as compared to the classical DNs due to the presence of noncovalent cross-links.

Because the DN synthesis is lengthy and complicated, a simple one-pot synthesis of such mechanically strong soft materials would be attractive for many applications. Moreover, in contrast to the irreversible deformation of the DNs, reversible tensile deformation at both prenecking and necking regimes is also required to create self-healing ability in such hydrogels. Recently, Gong et al. prepared polyampholyte single-network hydrogels of high toughness consisting of strong and weak physical bonds at high concentrations [57], while Hu et al. designed hybrid hydrogel systems formed via strong covalent bonds and clusters of hydrogel bonds [58]. Another group of high-strength single-network hydrogels is the semicrystalline hydrogels consisting of hydrophilic polymer chains interconnected by hydrophobic segments with long side alkyl chains such as n-alkyl(meth)acrylates forming lamellar crystals [6,23,30]. Osada was the first to prepare such hydrogels based on chemically cross-linked poly(acrylic acid) network chains containing hydrophobic domains [6]. Recently, supramolecular semicrystalline hydrogels with self-healing and shape memory functions have been prepared via micellar and bulk polymerization techniques [8,12,59]. It was shown that although the hydrogels with high crystallinity are mechanically strong, with elastic moduli and tensile strength of 80−300 MPa and 4−7 MPa, respectively, they are brittle and rupture at a stretch of less than 20% without yielding [12]. The challenge of producing stretchable and tough semicrystalline hydrogels of high mechanical strength is thus inherent.

Here, we report that the incorporation of a small amount of a weak hydrophobe into semicrystalline hydrogels significantly increases their toughness and stretchability without losing their high modulus and high strength. We design a highly entangled physical network formed via lamellar crystals consisting of aligned side alkyl chains.

The network bases on poly(N,Ndimethylacrylamide) (PDMA), which is a very useful hydrophilic biocompatible polymer with associative properties (Figure 3.1b) [60-62]. The interconnected lamellar crystals forming a layered hydrogel structure are created by incorporating noctadecyl acrylate (C18A) and lauryl methacrylate (C12M) segments with side chain lengths of 18 and 12 carbons, respectively, into the PDMA backbone (Figure 3.1b). As reported before, hexagonal packing of side alkyl chains of C18A segments create alkyl crystals in the hydrogels [6,8,23,30], while C12M segments with shorter side alkyl chains and α-methyl groups contribute to the hydrophobic associations [11,14,15]. As will be seen below, by including 0.1 - 0.4 mol % C12M into the polymer backbone consisting of 70 mol % DMA and 30 mol % C18A segments, we were able to generate more ordered and thinner lamellar crystals with a layered structure. Simultaneously, a brittle-to-ductile transition was observed due to the appearance of necking behavior leading to 10-fold increase of toughness. The significant toughness improvement upon incorporation of C12M into the semicrystalline hydrogels could be explained with the appearance of active tie molecules under external force interconnecting the lamellar clusters. The hydrogels also exhibit reversible tensile deformation induced by heating above the melting temperature of crystalline domains.

3.1 Experimental Part

3.1.1 Materials

The monomers N, N-dimethylacrylamide (DMA), n-octadecyl acrylate (C18A), lauryl methacrylate (C12M) and the initiator Irgacure 2959 were received from Aldrich and used without further purification.

3.1.2 Hydrogel preparation and gel fraction measurements

The hydrogels were prepared by bulk copolymerization of DMA with the hydrophobic monomers C18A and C12M in the presence of Irgacure 2959 as the photoinitiator at a concentration of 0.1 wt.% (with respect to the monomers). The hydrophobe content of the comonomer feed was fixed at 30 mol% while the amount of C12M was varied between 0 and 20 mol%. The monomers DMA, C18A, and C12M were first mixed and thoroughly stirred at 45 °C to obtain a homogeneous solution. After addition of the initiator Irgacure 2959 and bubbling nitrogen, the monomer mixtures containing the initiator were transferred into several pipettes of 7.5 mm in diameter as well as into rectangular plastic molds (200x13x0.5 mm). The polymerization was conducted at 23±2 °C for 1 day under UV lamp at a wavelength of 360 nm. After polymerization, the copolymer samples were immersed in a large amount of water for several days by replacing water every day to extract any soluble species. The water temperature was 70 °C and 23±2 °C for the first and following days, respectively. The initial high-temperature immersion period above the melting temperature of the crystalline domains of the hydrogels is to provide that the network chains assume their relaxed conformation. After equilibrium swelling in water at 23±2 °C, the gel samples were taken out of water and freeze-dried. The water content of the hydrogels was calculated as H_2O % = 10^2 $(1 - m_{dry}/m)$ where m and m_{dry} are the swollen and dried masses of the gel sample. The gel fraction W_g, that is, the conversion of monomers to the water-insoluble polymer was calculated from the masses of dry polymer network and from the comonomer feed.

3.1.3 Rheological experiments

Rheological measurements were performed on Gemini 150 Rheometer system, Bohlin Instruments, equipped with a Peltier device for temperature control. Hydrogel samples equilibrium swollen in water were subjected to dynamic experiments between the parallel plates of the rheometer. The upper plate (diameter 20 mm) was set at a distance of 500−1000 μm, depending on the swelling degree of the hydrogels. During all measurements, a solvent trap was used to minimize the evaporation. Viscoelastic behavior of the hydrogels depending on temperature was measured during heating-cooling cycles between 25 and 65 °C at a fixed rate of 1°C·min^{-1}. An angular frequency of ω = 6.28 rad·s^{-1} and a deformation amplitude γ_0 = 0.001 (0.1%) were selected to ensure that the oscillatory deformation is within the linear regime. The changes in the dynamic moduli of gels were monitored during the course of the cycle as a function of temperature. The samples were also subjected to frequency sweep tests at γ_0 = 0.001.

3.1.4 DSC measurements

DSC measurements were conducted on a Perkin Elmer Diamond DSC under a nitrogen atmosphere. The gel samples equilibrium swollen in water were cut into small specimens of about 10 mg weight and sealed in aluminum pans. Then, they were scanned between 25 and 65 °C with a heating and cooling rate of 5 °C·min^{-1}. From the DSC curves, enthalpy changes during melting, $\Delta H_{m,}$ were calculated from the peak areas. The degree of crystallinity, f_{cry}, that is, the fraction of C18A units in crystalline domains, was estimated by $f_{cry} = x_{HM}\, \Delta H_m / \Delta H°_m$, where x_{HM} is the mole fraction of the hydrophobic monomer in the comonomer feed and $\Delta H°_m$ is the melting enthalpy of crystalline C18A units. $\Delta H°_m$ was taken as 71.2 kJ.mol^{-1} from previous works on the melting behavior of long n-alkyl chains exhibiting a hexagonal crystal structure [31,32]

3.1.5 SAXS and WAXS measurements

SAXS (Small angle X-ray Scattering) and WAXS (Wide angle X-ray Scattering) data were collected at 23 °C with an exposure time of 900 s using HECUS-SWAXS system (Graz, Austria) [63-65]. Nickel filtered CuK_α radiation (λ= 0.154 nm) operating at 50 kV / 40 mA was used as X-ray source. Two linear position sensitive detectors (PSDs) were used for SAXS and WAXS data ranges.

3.1.6 Mechanical tests

Uniaxial elongation measurements were performed on swollen hydrogel samples at 23±2 °C on Zwick Roell test machine with 500 N load cell. All the tests were performed on rectangular hydrogel samples (1x5x20 mm) under following conditions: Strain rate = between 1.7x10^{-3} and 1.7x10^{-1} s^{-1}; sample length between jaws = 10 mm. Load and displacement data were collected during the experiments. The stress was presented by its nominal value σ_{nom}, which is the force per crosssectional area of the undeformed gel specimen, while the strain is given by λ, the deformation ratio (deformed length/initial length). The strain ε is also defined as the change in the length relative to the initial length of the gel specimen, i.e., $\varepsilon = \lambda - 1$. The Young's modulus E was calculated from the slope of stress–strain curves between 0.5-1.5% deformations. The yield energy U_y and the energy to break (toughness) W were calculated from the areas below the stress-strain curves up to the yield point and to the fracture point, respectively. The successive elongation tests were conducted at a constant strain rate of 8.3x10^{-2} s^{-1} to a maximum elongation ratio, followed by retraction to zero force and a waiting time of 5 min, until the next cycle of compression.

3.2 Results and Discussion

The hydrogels were prepared by bulk photopolymerization of DMA, C18A, and C12M in the presence of Irgacure 2959 as the photoinitiator at a concentration of 0.1 wt %. The monomers and the initiator were first mixed to obtain a homogeneous solution, and then the polymerization was conducted at 23 ± 2 °C for 1 day under UV lamp at a wavelength of 360 nm. The total amount of the hydrophobic monomers C18A and C12M in the comonomer feed was fixed at 30 mol % while the amount of C12M was varied between 0 and 20 mol %. In the following, the C12M content of the hydrogels is denoted by C12M %, which represents the mole percent of C12M in the comonomer feed. For instance, the hydrogel with 0.1% C12M was prepared from a comonomer feed consisting of 70 mol % DMA, 29.9 mol % C18A, and 0.1 mol % C12M. Preliminary experiments showed that a reaction time of 1 day was needed for the complete conversion of the monomers to the water-insoluble copolymer (Figure 3.2). After equilibrium swelling of the terpolymers in water, the water content of the hydrogels was between 26 and 37 wt % that increased with increasing C12M content (Figure 3.2). The increase in the water content is attributed to the decreasing crystallinity of the hydrogels upon increasing C12M %.

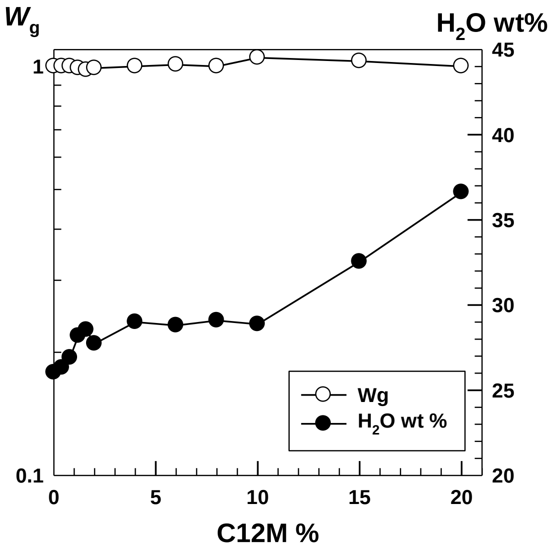

Figure 3.2 : Gel fraction W_g and the water content *H_2O wt%* of the hydrogels plotted against C12M %.

The hydrogels equilibrium swollen in water contained crystalline domains as evidenced by DSC, SAXS, WAXS, and rheological measurements. DSC scans of the hydrogels with ≤8% C12M showed melting and crystallization peaks while the peaks disappeared at higher C12M contents (Figure 3.3 and Figure 3.4a). Figure 3.4b shows the melting T_m and crystallization temperatures T_{cry} of the hydrogels plotted against their C12M contents. T_m and T_{cry} are between 40−48 and 34−40 °C, respectively, and they decrease upon increasing C12M %, indicating decreasing thermal stability of alkyl crystals in the hydrogels. This is expected as the added C12M segments do not contribute to the formation of alkyl crystals because of its short alkyl side chain [14,15].

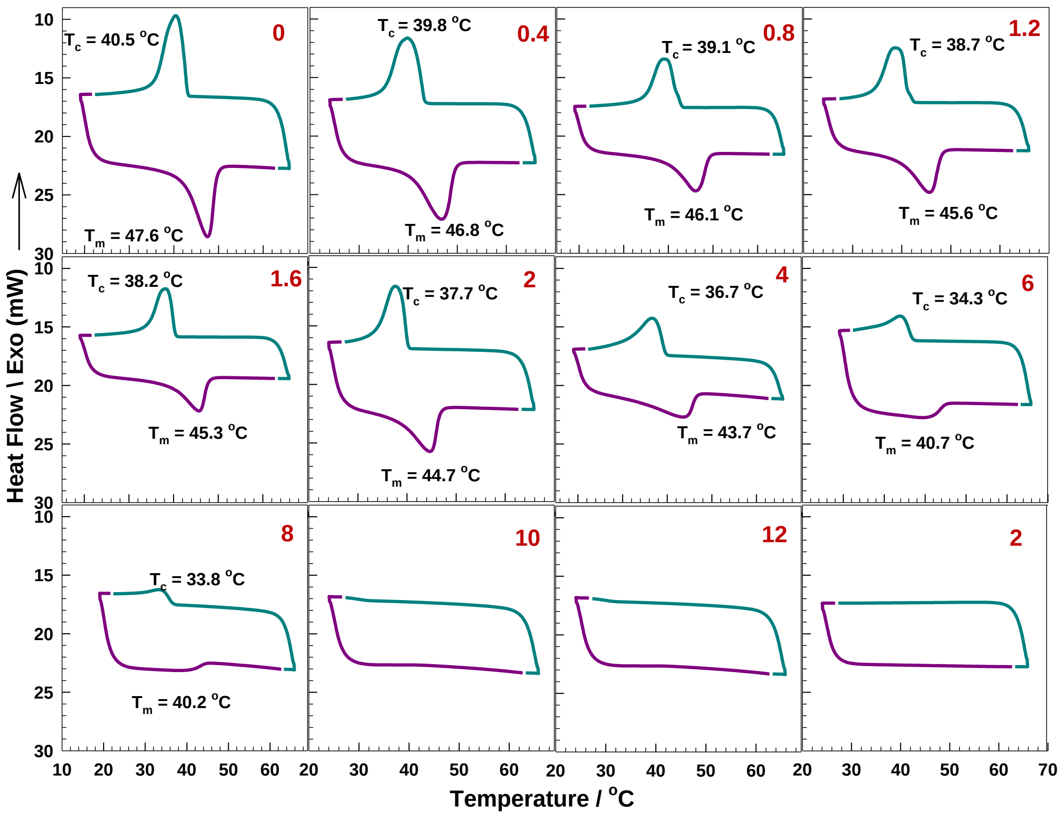

Figure 3.3 : DSC scans of the hydrogels containing various amounts of C12M as indicated. The melting (T_m) and crystallization temperatures (T_{cry}) of the hydrogels are also indicated.

In Figure 3.4c, the fraction f_{cry} of C18A segments in crystalline domains (moles of crystallized C18A/ mole of C18A) calculated from the area under the melting peaks are plotted against C12M %. The maximum degree of crystallinity observed in the absence of C12M is 38%, indicating that 38% of C18A segments form alkyl crystals while the remaining part contributes to the hydrophobic associations [10,11]. The crystallinity decreases with increasing C12M %, and no crystalline domains exist above 8% C12M. Thus, the relative content of the crystalline and noncrystalline domains can be adjusted by varying C12M content in the monomer feed.

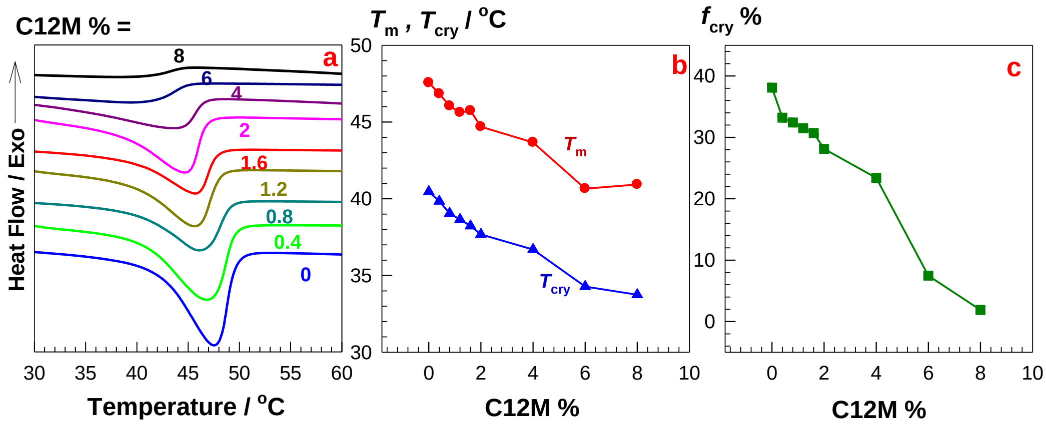

Figure 3.4 : (a) DSC traces of the hydrogels with various C12M contents. (b) Melting T_m and crystallization temperatures T_{cry} of the hydrogels plotted against C12M %. (c) The fraction f_{cry} of C18A segments in crystalline domains (moles of crystallized C18A/ mole of C18A) calculated from the area under the melting peaks against C12M %.

Figure 3.5a shows wide-angle X-ray scattering (WAXS) profiles of the hydrogels without and with 0.4 and 2% C12M where the scattering intensity $I(q)$ is plotted against the scattering vector q.

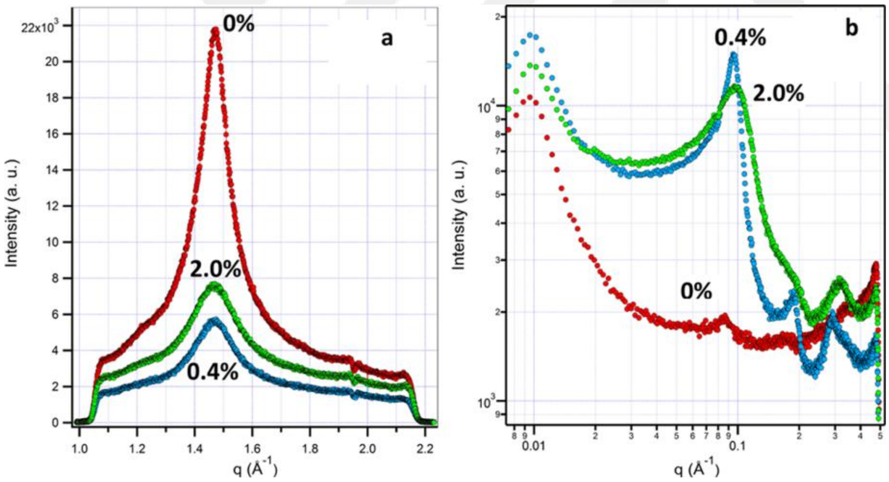

Figure 3.5 : WAXS (a) and SAXS (b) profiles of the hydrogel samples without and with 0.4 and 2 % C12M where the scattering intensity $I(q)$ is plotted against the scattering vector q. C12M contents are indicated.

Independent on the amount of C12M, WAXS data show a high intensity peak at q_{max} = 1.46 Å^{-1}, corresponding to a shortrange ordering with a constant lattice spacing d_1 of 0.43 nm. This spacing was reported before for the crystalline state of both dry and swollen n-alkyl(meth)acrylate (co)- polymers [6,8,16-18,23,24] and indicates side-by-side packing between the octadecyl (C18) side chains in the hydrogels, as illustrated in Figure 3.6. The constancy of d_1 spacing also indicate that side-by-side arrangement of alkyl chains is not affected by the incorporation of C12M segments into the polymer chains. Moreover, the peak intensity decreases and slightly broadens with the addition of C12M, which is consistent with slightly lower crystallinity of C12M-containing hydrogels (Figure 3.4c). This also reveals that the number of C18 chains per lamellar crystal decreases, i.e., a larger number but thinner lamellar crystals form with the incorporation of C12M segments.

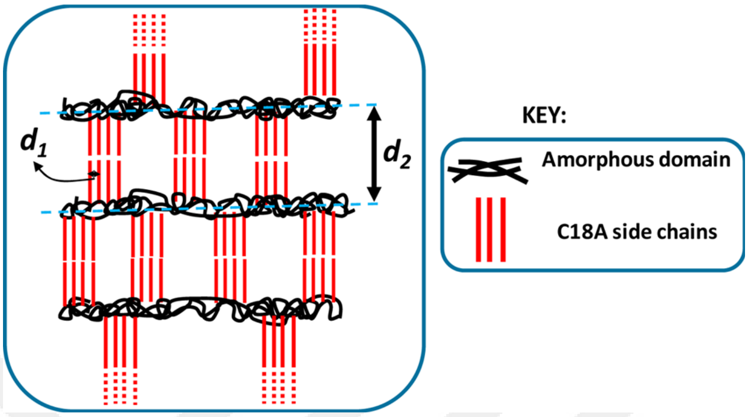

Figure 3.6 : Cartoon showing Crystalline and Amorphous Domains of the hydrogels.

Small-angle X-ray scattering (SAXS) profiles of the hydrogels in a semilogarithmic scale are shown in Figure 3.5b. The hydrogels containing C12M exhibit a high intensity peak at q_{max} = 0.094 and 0.096 Å^{-1}, indicating a long-range ordering with lattice spacings d_2 of 6.7 and 6.5 nm for 0.4 and 2% C12M, respectively. The hydrogel with 0.4% C12M exhibits the sharpest peak, while without C12M this peak is weak and broad at a q_{max} = 0.086 Å^{-1} (d_2 = 7.3 nm). Higher intensity and sharpening of the SAXS peak upon addition of C12M reveal formation of thinner lamellar crystals and increasing order in the hydrogels. The d_2 spacing also reveals tail-to-tail alignment of the side chains perpendicularly to the main chain, as reported before for semicrystalline hydrogels (Figure 3.6) [6-30]. Because the length l_{max} of the fully extended octadecyl (C18) chain is 2.43 nm [68] the d_2 spacing of the present hydrogels (6.5-7.3 nm) is larger than twice of the fully extended C18 chain length ($2l_{max}$ = 4.86 nm). The difference between d_2 and $2l_{max}$, which is between 1.6 and 2.4 nm for the present hydrogels, is attributed to the thickness of polymer backbone (amorphous domain) separating alkyl crystals (Figure 3.6) [6,23]. Thus, WAXS and SAXS data suggest side-by-side packing of alkyl chains in the hydrogels and formation of more ordered and thinner lamellar crystals with a layered structure after incorporation of C12M segments in the hydrogels. Moreover, the most significant change in the microstructure of the hydrogels appears upon addition of a small amount of C12M (0.4%). As will be seen in the next section, this is reflected in their mechanical properties.

Rheological measurements are another means of studying the transitions between crystalline and amorphous states depending on the temperature. Figure 3.7a shows temperature sweep results of the hydrogels without and with 0.4 and 2% C12M during heating from 25 to 65 °C at a heating rate of 1 °C min^{-1}. Here, the storage G′ (filled symbols) and loss modulus G″ (open symbols) of the hydrogels measured at an angular frequency ω of 6.3 rad s^{-1} are plotted against the temperature. The vertical lines in the figure represent the melting temperatures of the hydrogels, which are 48, 47, and 45 °C for 0, 0.4, and 2% C12M, respectively. At 25 °C, the hydrogels exhibit a storage modulus G′ of 7.6−8.3 MPa and a loss factor tan δ (= G″/G′) of 0.02−0.05, while upon heating above T_m, G′ decreases by more than 2 orders of magnitude and becomes 0.03−0.04 MPa at 25 °C. Simultaneously, tan δ increases to 0.3 as typical for weak gels.

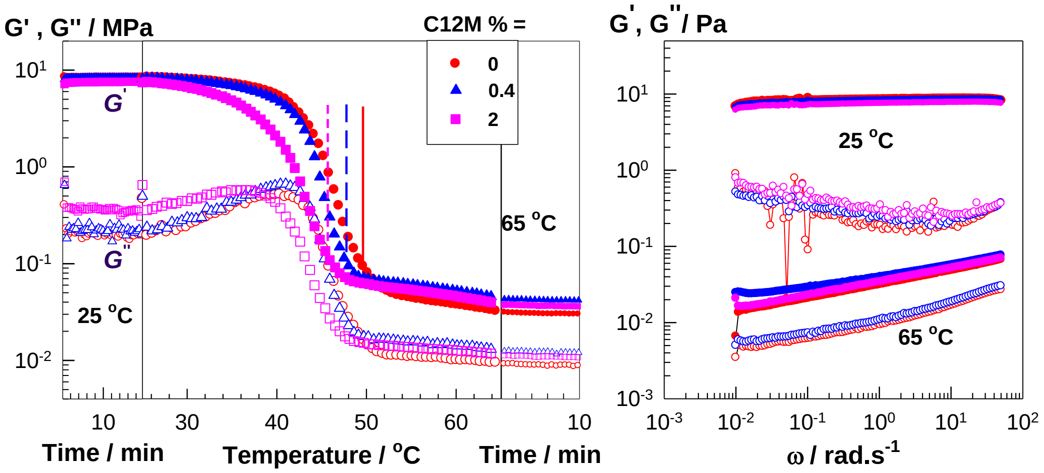

Figure 3.7 : (a) G′ (filled symbols) and G″ (open symbols) of the hydrogels during cooling and heating scans between 25 and 65 °C. The vertical lines represent the melting temperatures of the hydrogels without (solid line) and with 0.4 (long-dashed line) and 2% C12M (short-dashed line). ω = 6.3 rad s−1. γ_o = 0.001. (b) G′(filled symbols) and G″ (open symbols) of the hydrogels at below and above the melting temperature T_m plotted against the frequency ω. γ_o = 0.001. C12M contents of the hydrogels are indicated in (a).

The strong-to-weak gel transition observed during heating is completely reversible with a slight hysteresis (Figure 3.8), as typically observed in semicrystalline hydrogels [8,59]. As indicated by the arrow in Figure 3.7a, increasing C12M content, that is, decreasing T_m, of the hydrogels shifts the strong-to-weak gel transition to lower temperatures. The frequency sweep results of the hydrogels shown in Figure 3.9b reveal that below T_m G′ is independent of the frequency ω over the whole experimental window, while it is frequency dependent above T_m and proportional to $\omega^{-0.17\pm0.02}$ without any plateau in G′ vs ω curve.

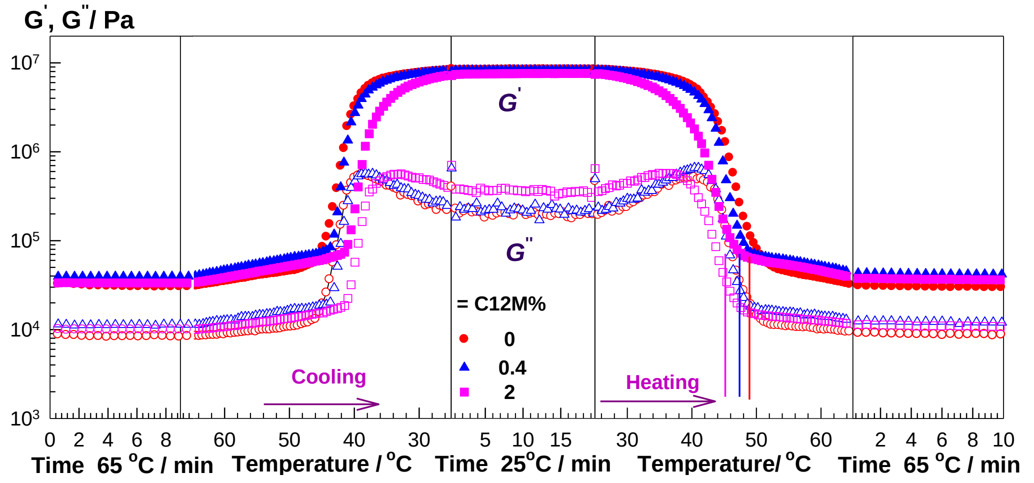

Figure 3.8 : G' (filled symbols) and G'' (open symbols) of the hydrogels without (triangles down) and with 0.4 (circles) and 2% C12M (triangles up) during cooling and heating scans. ω = 6.3 rad·s^{-1}. γ_o = 0.001.

Figure 3.9a compares stress−strain curves of the hydrogels prepared without (dashed curve) and with 0.2% C12M (solid curve).

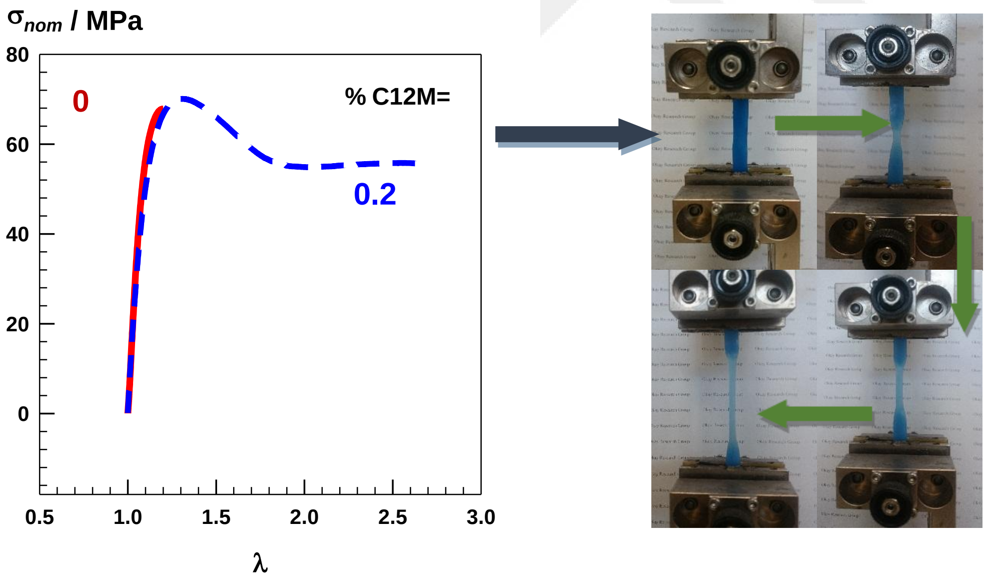

Figure 3.9 : (a) Typical tensile stress−strain curves of the hydrogels without (red dashed curve) and with 0.2% C12M (blue solid curve) as the dependence of nominal stress σnom on the elongation ratio λ. $\dot{\varepsilon} = 8.3 \times 10^{-2}$ s^{-1}. (b) Images demonstrating the necking behavior of the hydrogel with 0.2% C12M. The gel sample was colored for clarity.

The stress is presented by its nominal value σnom, which is the force per cross-sectional area of the undeformed gel specimen, while the strain is given by the deformation ratio λ (deformed length/initial length). The common feature of the two hydrogels is that the initial slope of the curves, i.e., the Young's modulus E, is almost the same, 71 ± 3 and 70 ± 5 MPa for 0 and 0.4% C12M, respectively. This reveals that inclusion of such a small amount of the weak hydrophobe C12M into the polymer backbone does not affect the cross-link density of the hydrogel. However, the gel sample prepared without C12M fails in a brittle fashion at a stretch (λ − l) of 20%, while the one with 0.2% C12M shows necking behavior, as seen in Figure 3.9b, leading to a 10-fold increase in toughness, calculated from the area below the stress−strain curve up to the fracture point, (from 1.0 ± 0.2 to 9.6 ± 0.3 MJ m^{-3}) and 8-fold increase in stretchability (from 20 to 167%). Thus, a brittle-to-ductile transition can be induced upon incorporation of a small amount of C12M into the polymer chains.

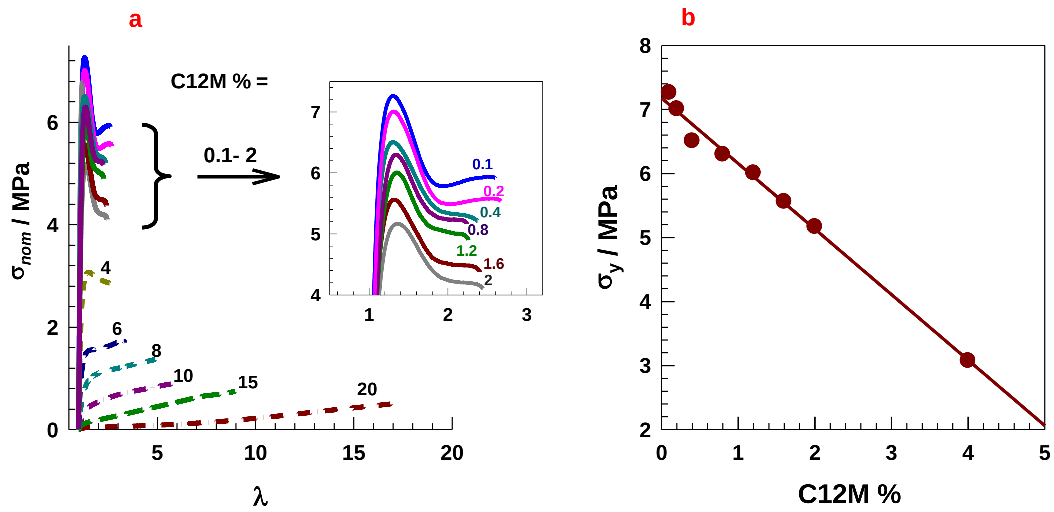

Figure 3.10 : Tensile stress−strain curves of the hydrogels with various C12M contents at $\dot{\varepsilon}$= 8.3 × 10^{-2} s^{-1} (a) and Yield stress σ_y plotted against C12M % (b). The solid lines are the best fits to the data.

Tensile tests were also conducted at different strain rates $\dot{\varepsilon}$ on hydrogel samples prepared at various C12M contents. Figure 3.10 shows stress-strain curves of the hydrogels at a fixed strain rate $\dot{\varepsilon}$ but at various levels of C12M, while in Figures 3.11a and 3.11b the curves were obtained by varying the strain rate $\dot{\varepsilon}$ at fixed levels of C12M. Both the amount of C12M and strain rate significantly affect the mechanical behavior of the hydrogels.

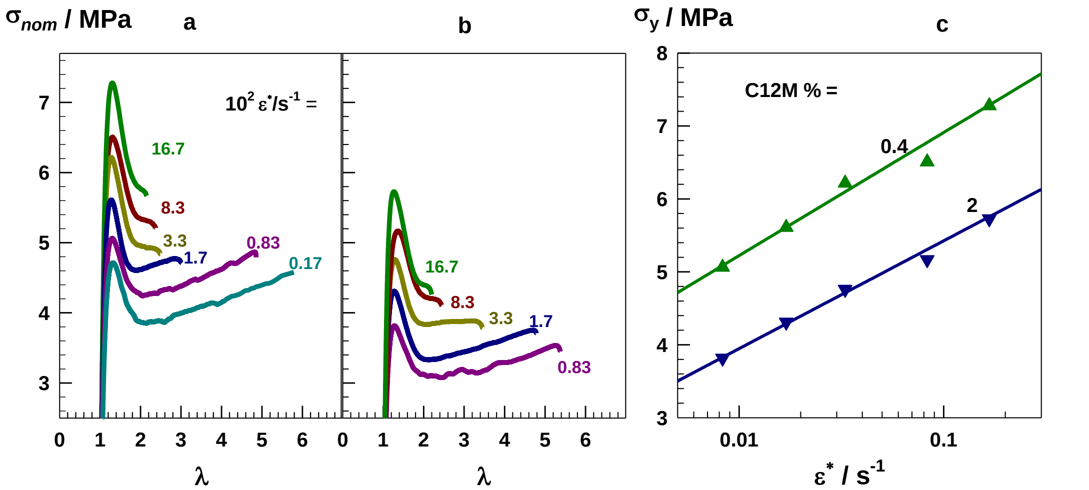

Figure 3.11 : (a,b) Tensile stress−strain curves of the hydrogels at various $\dot{\varepsilon}$ with 0.4 (a) and 2% C12M (b). Yield stress σ_y plotted against the logarithm of the strain rate $\dot{\varepsilon}$ (c). The solid lines are the best fits to the data.

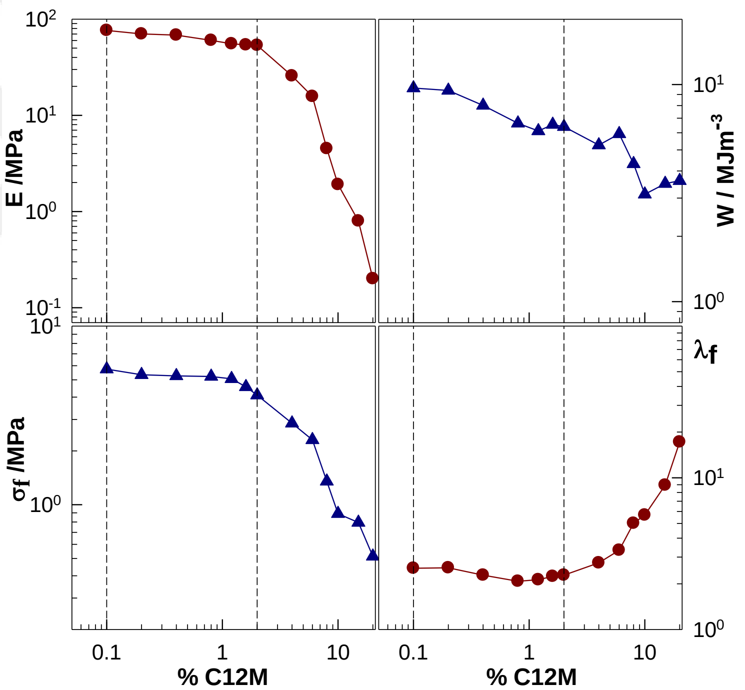

Figure 3.12 : Young's modulus E, fracture stress σ_f, toughness W, and elongation to break λ_f of the hydrogels plotted against C12M %. The dashed vertical lines represent the data obtained at 0.1 and 2% C12M. $\dot{\varepsilon} = 8.3\mathrm{x}10^{-2}$ s^{-1}.

Figure 3.12 shows Young's modulus E, fracture stress σ_f, toughness W, and elongation to break λ_f of the hydrogels plotted against C12M %. Between 0.1 and 2% C12M where a significant yielding appears (inset to Figure 3.9), the modulus, fracture stress, and toughness only slightly decrease with increasing C12M % while they rapidly decrease above 2% C12M. High stretchable hydrogels with a high elongation ratio at break (up to 1600%) could be produced at high C12M contents.

The variation of the yield stress σy with the C12M content and strain rate $\dot{\varepsilon}$ shows several interesting features. For instance, although the hydrogel without C12M is brittle, inclusion of 0.1% C12M; i.e., 1 C12M per 1000 segments into the polymer leads to the appearance of a significant necking and the highest yield stress σ_y of 7.3 MPa. Further addition of C12M linearly decreases the yield stress σ_y according to the relation σ_y = 7.1 ± 0.1 - C12M mol % (Figure 3.10b). The extrapolated value of σ_y to 0% C12M is thus 7.1 MPa, which is close to the fracture stress of the brittle hydrogel prepared without C12M (6.8 ± 0.3 MPa). Because no yielding appears at 0% C12M, this suggests that in the absence of C12M, the molecular mobility between crystalline domains is insufficient to produce yielding at the time scale of the mechanical tests ($\dot{\varepsilon}$ = 8.3 × 10^{-2} s^{-1}). At a fixed level of C12M (Figures 3.11a and 3.11b), the yield stress σy rises with the strain rate $\dot{\varepsilon}$, and this rise is linear when plotted against the logarithm of $\dot{\varepsilon}$ (Figure 3.11c), in accord with the Eyring model of mechanically induced dissociation of molecular bonds. [69-71].

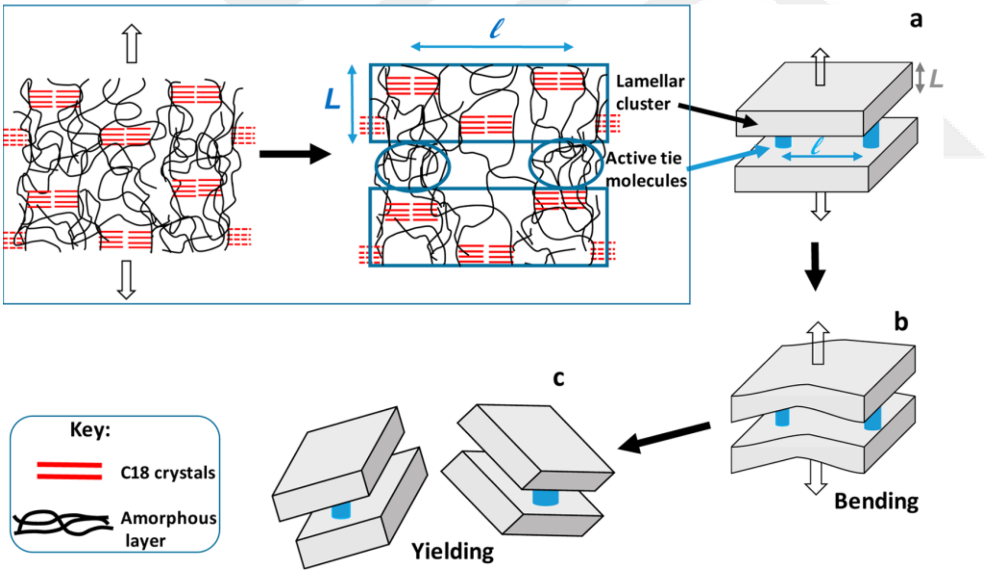

Figure 3.13 : Cartoon presenting two lamellar clusters interconnected by two active tie molecules (a) and deformation of lamellar clusters under force (b) and their destroying at the Yield Point (c). In part a, rectangles and circles indicate lamellar clusters and tie molecules, respectively.

$$\sigma_y = \frac{2kT}{V_a} \ln(\dot{\varepsilon}/\varepsilon_0) + \frac{2E_a}{V_a} \quad (3.1)$$

where V_a is the activation volume, E_a is the activation energy, ε_o is the pre-exponential factor, k is the Boltzmann constant, and T is the absolute temperature.

The slopes of the best-fit lines to the σ_y vs ln $\dot{\varepsilon}$ data give the activation volume V_a as 11.5 ± 0.4 and 13 ± 2 nm^3 for 0.4% and 2% C12M, respectively (Figure 3.11c). Because Va can be regarded as the size of the polymer segments in the hydrogels involved in the cooperative motion resulting in yielding, increasing V_a with rising C12M contentindicates increasing number of mobile segments, i.e., enhanced molecular mobility between crystalline domains. Moreover, the activation energy Ea is related to the height of energy barrier to overcome the mobile segments to move by the application of an external force. For the present hydrogels, this energy corresponds to the dissociation energy of hydrophobic associations, which is close to 0.98kT per methylene group of alkyl chains [72,73]. Because increasing C12M content decreases the average length of side alkyl chains, the magnitude of the energy barrier reduces so that the dissociation of physical crosslinks requires a lower mechanical stress. We have to note that even the brittle hydrogel formed in the absence of C12M exhibited yielding behavior at low strain rates $\dot{\varepsilon}$. For instance, a brittle-to-ductile transition in the hydrogels prepared without C12M can also be induced by reducing the strain rate from 8.3×10^{-2} to 4×10^{-3} s^{-1} although the corresponding yield stress was significantly lower than that of C12M-containing hydrogels [12]. We can explain the significant toughness improvement in semicrystalline hydrogels upon addition of C12M with the formation of layered lamellar crystals as revealed by SAXS measurements. Previous works conducted on semicrystalline polymers indicate that the existence of so-called active tie molecules interconnecting the lamellar clusters play a significant role in their mechanical strength and yielding behavior [74‒80]. For the present hydrogels, the applied external force during tensile testing results in the unfolding of the amorphous layers between lamellar crystals, leading to the appearance of lamellar clusters interconnected by tie molecules, as schematically illustrated in Figure 3.13a. Lamellar clusters consist of several lamellar crystals separated by amorphous domains, and tie molecules bridging them are part of the amorphous region but they are able to unfold under the external force. PDMA chains involved in hydrophobic associations through noncrystallized C18A and C12M segments can be considered as active tie molecules bridging the lamellar clusters. These molecules dissipate energy by transmitting the external load from one to the another lamellar cluster whereby the clusters are deformed, as illustrated in Figure 3.13b. As the hydrogel sample is stretched, the stress generated from the tie molecules may reach a critical value under which the lamellar clusters are broken and fragmented, leading to the yielding phenomenon (Figure 3.13c). In the absence of C12M, no yielding occursbecause the lamellar clusters do not form a layered structure and the deformation of the chains between the lamellae in the direction of elongation is too slow to pass over the potential energy barrier. Thus, there are no active tie molecules in the hydrogels without C12M. Addition of C12M segments induces self-assembly of lamellar clusters to form a layered structure. Simultaneously, the magnitude of the energy barrier decreases due to weakening of lamellar crystals, and the number of interlamellar active tie molecules increases so that yielding appears. Increasing activation volume Va with increasing C12M content also reveals the movement of larger domains during deformation of the hydrogels as the C12M content is increased. According to the lamellar cluster model of Nitta et al. [77−80], the bending force acting on the lamellar clusters through the tie molecules results in disintegration of the clusters into their fragments, and this occurs at the yield point. Assuming that the onset of disintegration of the lamellar cluster occurs when the elastic energy reaches a critical value U_y, the yield stress σ_y of semicrystalline polymers is given by [77−80].

$$\sigma_y = 2\sqrt{2EU_y}\,(L/l)^2 \tag{3.2}$$

where L is the thickness of lamellar clusters interconnected by tie molecules with a support span length l (l > L, Figure 3.13a). We estimated the yield energy U_y of the hydrogels from the area under the stress−strain curve up to the yield point. In Figure 3.14a, σ_y is plotted against $2EU_y$ for the hydrogels with various C12M contents (filled symbols) and at various strain rates (open symbols). It is seen that in accord with equation 3.2 all the data fall onto the same line with a slope 0.46 ± 0.01. The average l/L is 2.09 ± 0.03, indicating that the distance between adjacent active tie links is about twice the thickness of the lamellar clusters (Figure 3.14b). l/L ≈ 2 was also reported for semicrystalline polymers such as polyethylene and isotactic polypropylene [76,78,79] and reveals that the minimum size of fragmented clusters $L(l/2)^2$ is close to L^3. The thickness L of lamellar clusters was estimated as almost equal to the end-toend distance of unperturbed polymer chains in the melt [77]. This means that the minimum size L^3 of fragmented clusters corresponds to the spatial dimension of a single chain. Thus, the lamellar cluster model shown schematically in

Figure 3.13 well explains the yielding behavior of semicrystalline hydrogels, and the lamellar clusters are fragmented into polymer chains at the yield point.

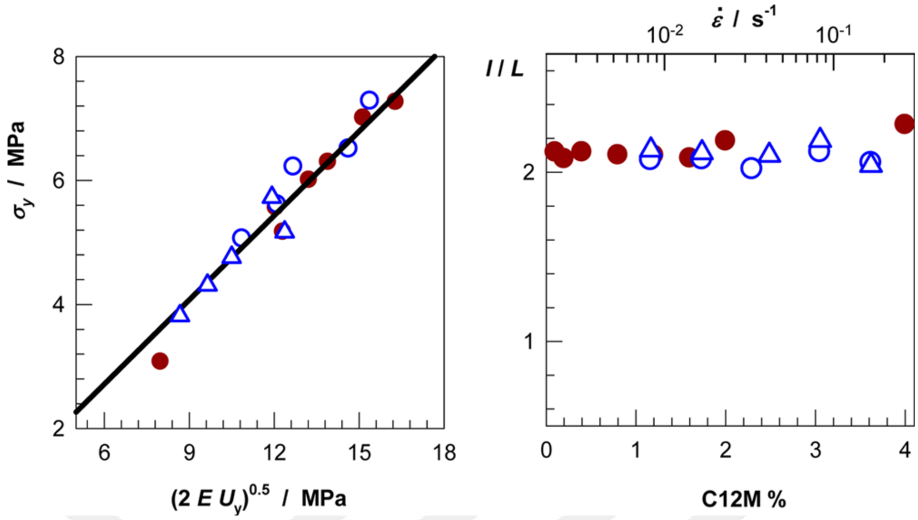

Figure 3.14 : (a) Yield stress σy plotted against $2EU_y$ for the hydrogels with various C12M contents at $\dot{\varepsilon}$= 8.3 × 10−2 s−1 (filled symbols) and at various strain rates $\dot{\varepsilon}$ with 0.4% (open circles) and 2% C12M (open triangles). (b) l/L data of all hydrogels shown as a function of C12M % (filled symbols) and $\dot{\varepsilon}$ (open symbols).

Because of the supramolecular nature of the present hydrogels, fragmented lamellar clusters could be repaired by melting the alkyl crystals above T_m and subsequent cooling to room temperature. The temperature-induced recovery of the crystal structure resulted in almost reversible stress−strain curves as illustrated in Figure 3.15a. The solid curve in the figüre presents the stress−strain curve of a virgin hydrogel sample with 0.4% C12M that is stretched to 100% elongation. The modulus E and the yield stress σf of the virgin hydrogel are 68 ± 2 and 6.5 ± 0.2 MPa, respectively (Figure 3.15b). The dotted curve in Figure 3.15a presents the stress−strain curve of the same hydrogel sample subjecting to a second tensile test up to 110% elongation. The modulus drastically decreases to 5.3 ± 0.1 MPa, and the yielding peak disappears, indicating the damage created in the lamellar clusters. This behavior is similar to that observed in DN hydrogels (Figure 3.1). Thus, the second loading curve has a much lower initial slope E due to the damage in the lamellar clusters and shows hardening at strain λ above 1.4 because gel deformation becomes homogeneous again. However, heating the damaged gel sample in a water bath at 70 °C to melt their crystalline domains and then cooling to 22 °C in water before the second tensile test results in the stress− strain curve shown in Figure 3.15a by the dashed curve. The gel recovers 93% of both the initial modulus (63 ± 5 MPa) and yield stress (6.0 ± 0.4), indicating that the hydrogels exhibit almost reversible tensile tests (Figure 3.15b).

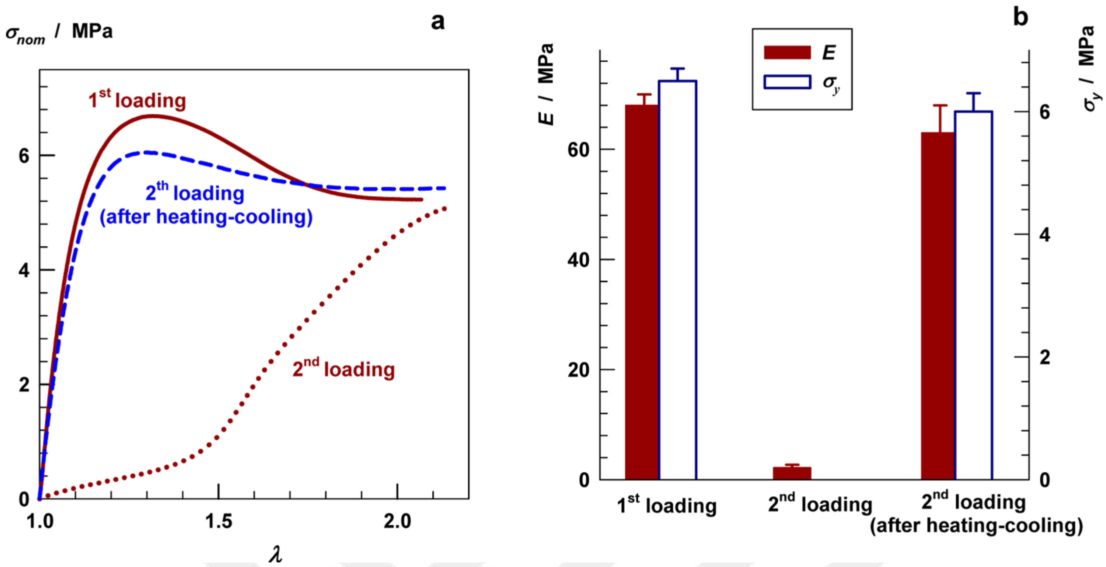

Figure 3.15 : (a) Two successive loading curves up about to 100% elongation for the hydrogel samples with 0.4% C12M. $\dot{\varepsilon}$= 8.3 × 10^{-2} s^{-1}. The second loading was conducted without (dotted curve) with heat treatment (dashed curve) of the hydrogel sample by first immersing it in a water bath at 70 °C and then cooling in water to 22 °C. (b) The Young's modulus E and yield stress σ_y of the hydrogel with 0.4% C12M during the first and second loading.

The synthetic strategy presented here, based on the use of weak and strong hydrophobes as the minor and major components of the hydrophobic part of the polymer, respectively, can be extended to a variety of hydrophobic and hydrophilic segments. In addition to bulk polymerization described here, solution and micellar polymerization techniques could also be used to prepare high-strength, tough, and stretchable semicrystalline hydrogels.

3.3 Conclusions

Supramolecular semicrystalline hydrogels with a high degree of crystallinity are mechanically strong soft materials exhibiting a Young's modulus of 80−300 MPa and tensile fracture stress of 4−7 MPa. However, they are brittle and rupture at a stretch of less than 20% without yielding. Here, we showed that the incorporation of a small amount of a weak hydrophobe into semicrystalline hydrogels significantly increases their toughness and stretchability without losing their high modulus and high strength. We design a highly entangled physical network based PDMA containing C18A and C12M segments with side chain lengths of 18 and 12 carbons, respectively. By including 0.1−0.4 mol % C12M into the polymer backbone consisting of 70% DMA and 30% C18A segments, we were able to generate more ordered and thinner lamellar crystals with a layered structure. Simultaneously, a brittle-to-ductile transition was observed due to the appearance of necking behavior leading to 10-fold increase of toughness while the modulus and tensile strength remain almost unchanged. The significant toughness improvement upon incorporation of C12M into the semicrystalline hydrogels could be explained with the appearance of active tie molecules interconnecting the lamellar clusters. The hydrogels also exhibit reversible tensile deformation induced by heating above the melting temperature of crystalline domains.

4. TOUGHNESS IMPROVEMENT AND ANISOTROPY IN SEMICRYSTALLINE PHYSICAL HYDROGELS[3]

Owing to their similarities to biological tissues, hydrogels as soft and smart materials have important functions in a variety of biological and biomedical applications [44]. Although hydrogels are traditionally brittle and exhibit a low modulus of elasticity in the range of kPa, significant progress has been achieved in the past 15 years in the design of mechanically strong and tough hydrogels [2]. Several techniques developed so far enable preparation of hydrogels with mechanical performances approaching to those of biological systems. Another challenge to be addressed in the gel science is to create mechanically strong hydrogels with anisotropic properties, as observed in many biological tissues such as skin, muscle, and articular cartilage possessing anisotropically oriented hierarchical structures [13]. To achieve this goal, nanofillers such as nanofibers [82,83], graphene oxide [84], nanosheets [85], nanotubes [86], or nanodisks [87,88] in a precursor dispersion were first oriented and then the oriented microstructure was fixed by gelation. Anisotropic hydrogels were also produced by directional freezing [89-91], or by orienting the network chains of isotropic hydrogels under an external force followed by fixing the anisotropic structure via in situ polymerization [92-96]. Kajiyama et al reported stress-induced orientation of lamellar crystals in covalently cross-linked semicrystalline hydrogels [97]. Although not reported, these hydrogels should exhibit anisotropic mechanical properties. Such hydrogels were also prepared via a two-step procedure consisting of prestretching the network chains of isotropic hydrogels to a certain strain and subsequent fixation of the stretched chain conformation by ionic cross-linking [93,94]. Another technique to create anisotropy in hydrogels is ion-diffusion-induced orientation and cross-linking of semi-rigid polyelectrolytes followed by double-networking with an amorphous

[3] This chapter was published in "Bilici C., Karaarslan D., Ide S., Okay O., (2018), Toughness improvement and anisotropy in semicrystalline physical hydrogels, *Polymer*, 151, 208-217".

second network [98-101]. Gong et al recently showed that prestretching of polyampholyte hydrogels accelerates the ion complexation dynamics and fixes the stretched chain conformation thereby producing mechanically anisotropic hydrogels [102]. Because the network chains of high-strength hydrogels are only slightly coiled, even at a modest strain their end-to-end distance approaches their contour length, which limits high prestretch ratios and hence the extent of anisotropic orientation. To overcome this hurdle, we report here a simple one-step method of producing high-strength anisotropic hydrogels. It occurred to us that shape-memory hydrogels would be a good candidate to generate anisotropic hydrogels in a single synthetic step. Such hydrogels generally contain two types of cross-links, namely chemical cross-links (netpoints) determining the permanent shape, and switching segments, e.g., glassy or crystalline domains fixing the temporary shape below their transition temperature T_{trans} [6-8,19,20,23,103,104]. Shape-memory hydrogels above T_{trans} exhibit a low modulus of elasticity so that they can be stretched to high elongations whereas upon cooling below T_{trans}, the stretched conformation of the network chains is fixed. This reveals that isotropic hydrogels with a very low stretchability can be made anisotropic providing that they have both netpoints and switching segments in their network structure. Previous work indeed shows appearance of mechanical anisotropy in a commercially available Verflex® thermoset shape-memory polymer induced by a large uniaxial strain [105].

Here, we use semicrystalline physical hydrogels with shape-memory function as the precursor material in generating anisotropic hydrogels. The precursor hydrogels consist of poly(N,N-dimethylacrylamide) (poly(DMA)) chains interconnected by n-octadecyl acrylate (C18A) segments forming crystalline domains and hydrophobic associations acting as switching segments and netpoints, respectively (Figure 4.1) [59,106,107]. Above the melting temperature T_{m} of C18 crystals which is around 48 °C, the hydrogels exhibit a relatively low and time-dependent modulus due to the finite lifetime of hydrophobic associations holding the chains together, whereas below T_{m}, about half of the associations turns into alkyl crystals thereby producing mechanically strong hydrogels with a high Young's modulus (up to 160 MPa) and tensile fracture stress (up to 6.7 MPa) [8,59,106]. Microstructural and mechanical anisotropy in semicrystalline hydrogels was generated via a single-step procedure as shown in Figure 4.2a. We impose a prestretching on the water-swollen isotropic hydrogel samples above T_{m} of their crystalline domains followed by cooling below

T_m under strain to fix the elongated shape of the gel samples. The prestretch ratio λ_o defined as the ratio of fixed elongated length to the initial length was varied between 1.2 and 8.

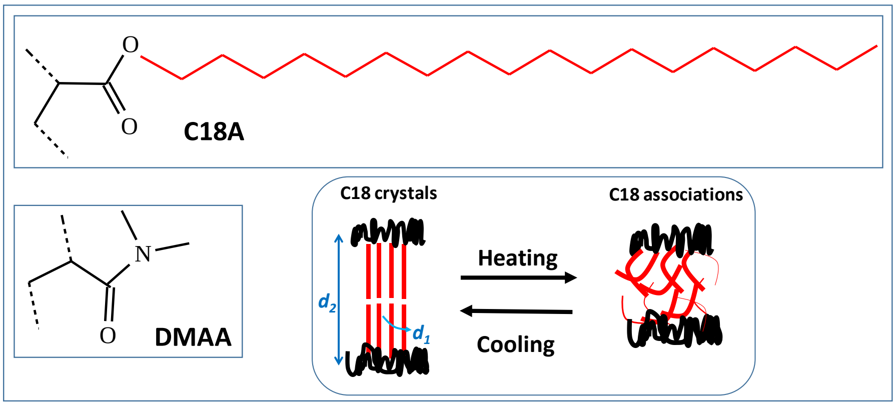

Figure 4.1 : Structure of DMA and C18A segments of the hydrogels and a cartoon showing alkyl crystals and hydrophobic associations. [a] Red lines and curves in the bottom panel represent side alkyl chains of C18A segments in crystals and hydrophobic associations, respectively, while black curves represent the amorphous domains.

As will be seen below, a significant microstructural and mechanical anisotropy was achieved in high strength physical hydrogels, that could be tuned by the magnitude of the prestretch ratio λ_o. For instance, the dashed red curve in Figure 4.2b presents typical nominal stress (σ_{nom}) – elongation ratio (λ) curve of an isotropic poly(DMAA-co-C18A) hydrogel specimen consisting of 70 mol % N,N-dimethylacrylamide (DMA) and 30 mol % C18A segments. The hydrogel is brittle and ruptures at a stretch of 20%. The blue solid curves in the figure are stress-strain curves of the same hydrogel at λ_o = 1.8, measured in directions parallel (ǁ) and perpendicular (⊥) to the prestretching direction. The prestretch ratio of 1.8 creates significant anisotropy as well as brittle-to-ductile transition along the prestretching direction. In the following, we discuss the relation between the microstructure and mechanical properties of poly(DMAA-co-C18A) hydrogels containing 30 mol % C18A together with and without 0.1 mol % non-crystallizable hydrophobic monomer lauryl methacrylate (C12M). Small- and wide-angle X-ray scattering measurements and mechanical tests, conducted parallel and perpendicular to the prestretching direction, reveal a critical prestretch ratio λ_o at which the hydrogel exhibits the highest microstructural and mechanical anisotropy due to the finite extensibility of the network chains.

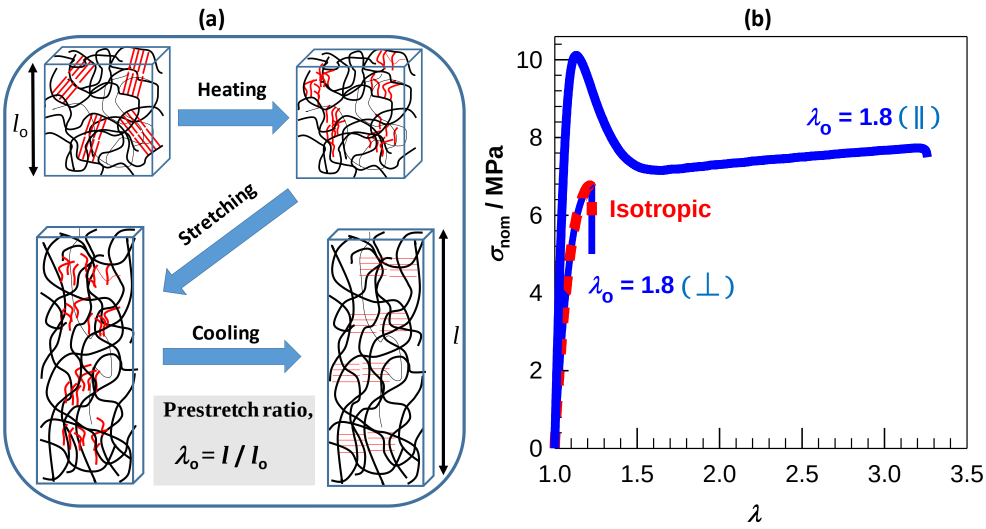

Figure 4.2 : Cartoon presenting prestretching technique to generate anisotropic hydrogels. Red straight lines and curves are C18 alkyl chains in crystals and associations, respectively. (b): Stress-strain curves of isotropic (red dashed curve) and anisotropic 0C12M hydrogels at a prestretch ratio λ_o = 1.8 (blue curves) obtained parallel (∥) and perpendicular to the prestretching direction (⊥).

4.1 Experimental Part

4.1.1 Materials

The monomers N, N-dimethylacrylamide (DMA), n-octadecyl acrylate (C18A), lauryl methacrylate (C12M) and the initiator Irgacure 2959 were received from Aldrich and used without further purification.

4.1.2 Preparation of isotropic hydrogels

The hydrogels were prepared by bulk copolymerization of DMA with the hydrophobic monomers C18A and C12M in the presence of Irgacure 2959 as the photoinitiator at a concentration of 0.1 wt.% (with respect to the monomers). The hydrophobe content of the comonomer feed was fixed at 30 mol% while the amount of C12M was 0 and 0.1 mol% for the hydrogels denoted as 0 C12M and 0.1 C12M, respectively. The monomers DMAA, C18A, and C12M were first mixed and thoroughly stirred at 45 °C to obtain a homogeneous solution. After addition of the initiator Irgacure 2959 and bubbling nitrogen, the monomer mixtures containing the initiator were transferred into several pipettes of 7.5 mm in diameter as well as into rectangular plastic molds (1x5x20 mm). The polymerization was conducted at 23±2 °C for 24 h under UV lamp at a wavelength of 360 nm. After polymerization, the copolymer samples were immersed in a large amount of water for several days by replacing water every day to extract any soluble species. The water temperature was 70 °C and 24±1 °C for the first 3 days and following days, respectively. The initial high-temperature immersion period above the melting temperature of the crystalline domains of the hydrogels is to provide that the network chains assume their relaxed conformation. The gel fraction and the water content of the hydrogels were determined as described before [12,106]. Two hydrogel samples at DMA/C18A/C12M molar ratios of 70/30/0 and 70/29.9/0.1 were prepared which are denoted as 0 C12M and 0.1 C12M, respectively (Table 4.1).

4.1.3 Preparation of prestretched hydrogels and their characterization

Water-swollen isotropic hydrogel specimens in the form of thin films of about 1x5x20 mm in dimensions were used for the preparation of anisotropic hydrogels. Two metal clamps were first placed on both sides of the gel specimen separated by a distance l_0 in wet condition, as shown in Figure 4.3a. The clamps together with the gel specimen were immersed in a water bath at 80 °C for 5 min during which the modulus significantly reduced and the strong gel became a weak gel with a loss factor above 0.1. This is illustrated in Figure 4.3b where the storage G' and loss moduli G'' of a 0 C12M hydrogel specimen at 25 and 80 °C are shown as a function of frequency ω. Upon heating from 25 to 80 °C, G' decreases about 3-orders of magnitude and becomes frequency dependent indicating strong-to-weak gel transition. The specimen was then stretched in water at 80 °C to a clamp-to-clamp distance l_1 and then immersed in a water bath at 20 °C by fixing the strain. After removing strain, clamp-to-clamp distance l_1 remained unchanged indicating complete shape-fixing efficiency. The prestretch ratio λ_o calculated as $\lambda_o = l_1 / l_0$ was varied between 1.2 and 8. Prestretched hydrogels equilibrium swollen in water were subjected to swelling, rheological, differential scanning calorimetry (DSC), small (SAXS) and wide angle X-ray scattering (WAXS) measurements, and uniaxial tensile tests as described before [12,106], and detailed in Supporting Information section. SAXS and WAXS measurements as well as uniaxial tensile tests were carried out in directions parallel and perpendicular to the prestretching direction.

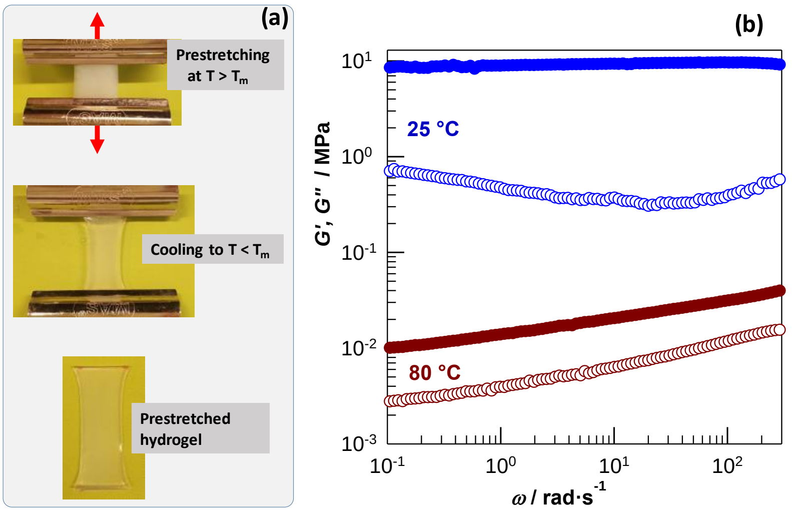

Figure 4.3 : (a): Images showing prestretching of a 0 C12M hydrogel specimen at 80 °C and then cooling below T_m to obtain a prestretched gel at $\lambda_o = 2$. (b): Storage modulus *G'* (filled symbols) and loss modulus *G''* (open symbols) of 0 C12M hydrogel at 25 and 80 °C. Strain amplitude = 0.1%.

4.1.4 Swelling tests and gel fractions of isotropic and anisotropic hydrogels

After equilibrium swelling of the hydrogels in water at 23±2 °C, the gel samples were taken out of water and freeze-dried. The weight swelling ratio was calculated as $q_w = m/m_{dry}$, where m and m_{dry} are the swollen and dried masses of the gel sample. The gel fraction W_g, that is, the conversion of monomers to the water-insoluble polymer was calculated from the masses of dry polymer network and from the comonomer feed. The gel fraction W_g of the hydrogels reported here were unity indicating complete conversion of the monomers into the polymer.

4.1.5 Rheological experiments

Rheological measurements were performed on Gemini 150 Rheometer system, Bohlin Instruments, equipped with a Peltier device for temperature control. Hydrogel samples equilibrium swollen in water were subjected to dynamic experiments between the parallel plates of the rheometer. The upper plate (diameter 20 mm) was set at a distance of 900−1100 µm, depending on the swelling degree of the hydrogels. During all measurements, a solvent trap was used to minimize the evaporation. The hydrogel samples were subjected to frequency sweep tests at a strain amplitude γ_o = 0.001.

4.1.6 DSC measurements

DSC measurements were conducted on a Perkin Elmer Diamond DSC under a nitrogen atmosphere. The gel samples equilibrium swollen in water were cut into small specimens of about 10 mg weight and sealed in aluminum pans. Then, they were scanned between 25 and 65 °C with a heating and cooling rate of 5 °C·min^{-1}. From the DSC curves, enthalpy changes during melting, ΔH_m, were calculated from the peak areas. The degree of crystallinity, x_c, that is, the fraction of C18A units in crystalline domains, was estimated by $x_c = x_{HM}\, \Delta H_m / \Delta H_m^o$, where x_{HM} is the mole fraction of the hydrophobic monomer in the comonomer feed and ΔH_m^o is the melting enthalpy of crystalline C18A units. ΔH_m^o was taken as 71.2 kJ.mol^{-1} from previous works on the melting behavior of long n-alkyl chains exhibiting a hexagonal crystal structure [31,32].

4.1.7 SAXS and WAXS measurements

SAXS (Small angle X-ray Scattering) and WAXS (Wide angle X-ray Scattering) data were collected at 23 °C with an exposure time of 900 s using HECUS-SWAXS system (Graz, Austria) [63-65]. Nickel filtered CuK_α radiation (λ= 0.154 nm) operating at 50 kV / 40 mA was used as X-ray source. Two linear position sensitive detectors (PSDs) were used for SAXS and WAXS data ranges.

4.1.8 Mechanical tests

Uniaxial elongation measurements were performed on swollen hydrogel samples at 23±2 ^{o}C on Zwick Roell test machine with 500 N load cell. All the tests were performed on rectangular hydrogel samples (1x5x20 mm) under following conditions: Strain rate = 5 min^{-1}; sample length between jaws = 10 mm. Load and displacement data were collected during the experiments. The stress was presented by its nominal value σ_{nom}, which is the force per cross-sectional area of the undeformed gel specimen, while the strain is given by λ, the deformation ratio (deformed length/initial length). The strain ε is also defined as the change in the length relative to the initial length of the gel specimen, i.e., $\varepsilon = \lambda - 1$. The Young's modulus E was calculated from the slope of stress–strain curves between 0.5-1.5% deformations. The successive elongation tests were conducted at a constant strain rate of 5min^{-1} to a maximum elongation ratio, followed by retraction to zero force and a waiting time of 5 min, until the next cycle of elongation.

4.2 Results and Discussion

Semicrystalline hydrogels with an isotropic microstructure were prepared by bulk copolymerization of DMAA with the hydrophobic monomers C18A and C12M, followed by swelling of the resulting copolymers in water. The hydrogel denoted by 0 C12M was prepared at a DMA/C18A molar ratio of 70/30 without addition of C12M, whereas the hydrogel denoted by 0.1 C12M was prepared in the presence of 0.1 mol % C12M, i.e., at a DMA/C18A/C12M molar ratio of 70/29.9/0.1. The characteristics of isotropic 0 C12M and 0.1 C12M hydrogels are collected in Table 4.1. 0 C12M is a brittle hydrogel and ruptures at a stretch of 20 %, whereas 0.1 C12M is a tough hydrogel sustaining up to 160 % stretches. As reported before [106], the toughness improvement upon incorporation of 0.1 mol % C12M into the backbone of 0 C12M hydrogel is due to the formation of more ordered lamellar clusters interconnected by active tie molecules creating an effective energy dissipation mechanism. In the following we discuss the changes in the microstructure and mechanical properties of 0 C12M and 0.1 C12M hydrogels depending on the prestretch ratio λ_o which was varied between 1.2 and 8.

Table 4.1 : Characteristics of isotropic 0 C12M and 0.1 C12M hydrogels prior to prestretching.[a]

Code	DMA mol%	C18A mol%	C12M mol%	q_w	T_m °C	x_c %	E MPa	σ_f /MPa	λ_f	W MJm^{-3}
0C12M	70	30.0	0	1.35	48	38	71(4)	6.7(0.1)	1.2(0.1)	1.1(0.1)
0.1C12M	70	29.9	0.1	1.36	47	37	74(7)	5.4(0.2)	2.6(0.2)	9.6(0.4)

[a] q_w = Equilibrium weight swelling ratio in water at 23±2 °C. T_m = Melting temperature. x_c = Degree of crystallinity. E = Young's modulus. σ_f = Fracture stress, λ_f = Fracture strain. W = Energy to break (toughness). Standard deviations are in parentheses while for the q_w 's, they are less than 10%.

4.2.1 Microstructure of the hydrogels

Figure 4.4a shows the equilibrium weight swelling ratio q_w (swollen gel mass / dry mass) of 0C12M and 0.1C12M hydrogels in water at 23±2 °C plotted against the prestretch ratio λ_o. Prestretching first decreases q_w for both hydrogels up to λ_o =

2.0±0.1, as indicated by the dashed vertical line, but then it again increases with a further increase of λ_o. Because the swelling degree of the hydrogels is determined by their cross-link density, the results reveal that prestretching at λ_o below and above 2.0±0.1 has opposite effects on the number of crystals acting as effective cross-links, that is, the crystallinity first increases but then decreases with increasing λ_o. Figures 4.4b,c show DSC scans of 0 C12M and 0.1 C12M hydrogels, respectively, at various prestretch ratios λ_o. The melting temperature T_m does not change with λ_o and remains at 48.3±0.5 and 47.4±0.5 °C for 0 C12M and 0.1 C12M, respectively. However, the degree of crystallinity x_c calculated from the area under the melting peak depends on the prestretch ratio, as seen in Figure 4.4d.

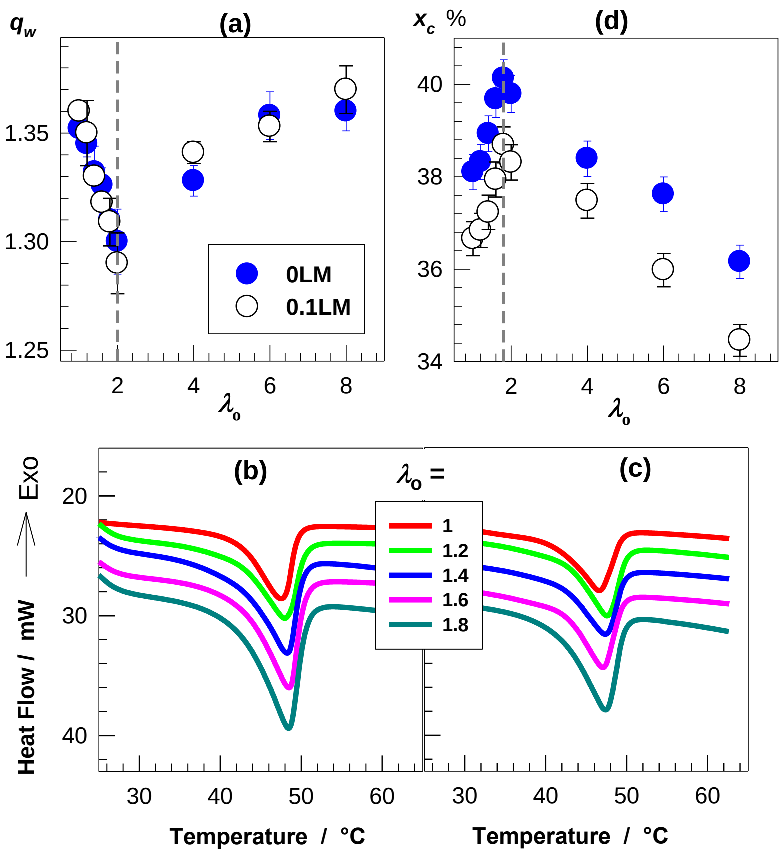

Figure 4.4 : (a, d): The weight swelling ratio q_w at 23±2 °C (a) and the degree of crystallinity x_c (d) of 0 C12M (filled circles) and 0.1 C12M hydrogels (open circles) both plotted against the prestretch ratio λ_o. (b, c): DSC scans of 0 C12M (b) and 0.1 C12M hydrogels (c) at various prestretch ratios λ_o.

In accord with the swelling results, the crystallinity x_c increases with increasing λ_o for λ_o < 1.8±0.2 whereas for λ_o > 1.8±0.2, it again decreases. Thus, prestretching of the hydrogels in the melt state first facilitates the alignment of alkyl side chains and increases the number of crystalline domains acting as physical cross-links. However, above the threshold value of λ_o = 1.8±0.2, the crystallinity again decreases while swelling ratio increases continuously suggesting disruption of crystalline domains and hence decreasing the cross-link density of the hydrogels.

For a deeper understanding of the microstructure of the hydrogels, WAXS and SAXS measurements were conducted in directions both parallel and perpendicular to the prestretching direction. Figures 4.5a,b show WAXS patterns of 0 C12M hydrogels at various λ_o from directions parallel (∥) and perpendicular (⊥) to the prestretching direction, respectively. The data for $\lambda_o \leq 1.4$ and $\lambda_o \geq 1.4$ are shown in the upper and bottom panel, respectively. In both directions, the high intensity peak appears at a scattering vector q_{max} = 1.52±0.01 Å^{-1} corresponding to a lattice spacing d_1 of 4.13±0.02 Å, which is typical for side-by-side packed alkyl chains (Figure 4.1) [6,8,23,24,67,108]. Thus, the peak position and hence the dimension of the unit cell do not change depending on the prestretch ratio or, on the direction of the measurements.

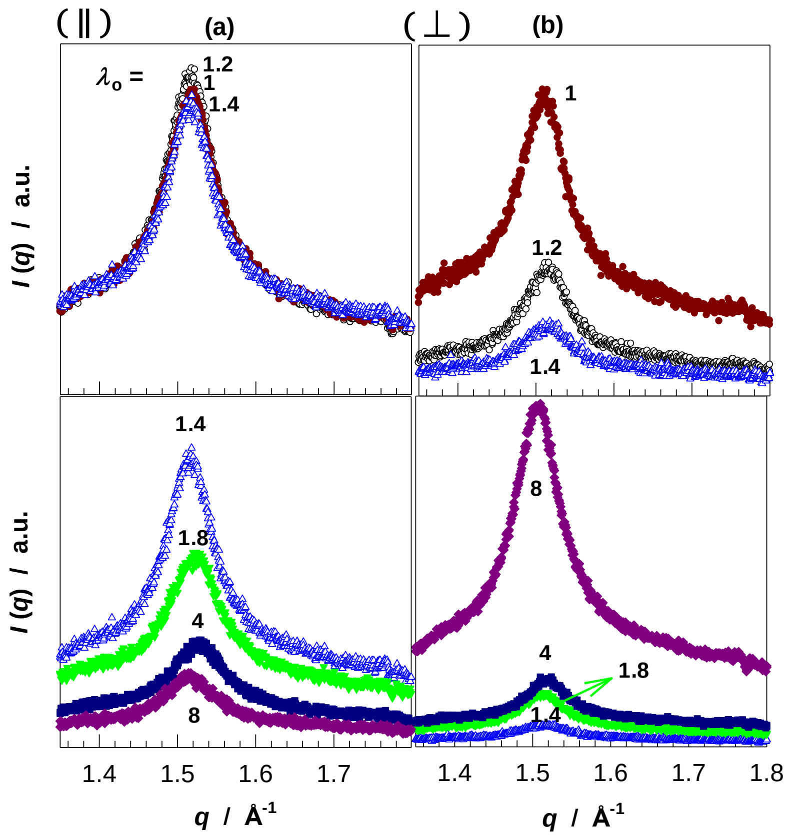

Figure 4.5 : WAXS profiles of 0 C12M hydrogels at various prestretch ratios λ_o indicated. The data were recorded in directions parallel (left panel, a) and perpendicular (right panel, b) to the prestretching direction.

However, the peak intensity shows a strong prestretch ratio and directional dependencies. Along the prestretching direction (Figure 4.5a), the high intensity peak is sharp and the maximum intensity I_{max} is almost constant between λ_o = 1 and 1.4, but then it decreases and the peak broadens at high λ_o's, as expected due to the decreasing crystallinity at $\lambda_o > 2$ (Figure 4.4d). In contrast, I_{max} in perpendicular direction first decreases with λ_o up to λ_o = 1.4 and then it again increases with increasing λ_o and a sharp high intensity peak appears at the highest prestretch ratio of 8. The constancy of d_1 spacing at 4.13±0.02 Å and opposite variations of the peak intensities with λ_o in parallel and perpendicular directions were also observed in 0.1 C12M hydrogels prepared with 0.1 mol % C12M (Figure 4.6). The results reveal higher number density of lamellar crystals perpendicularly to the prestretching direction at large prestretch ratios.

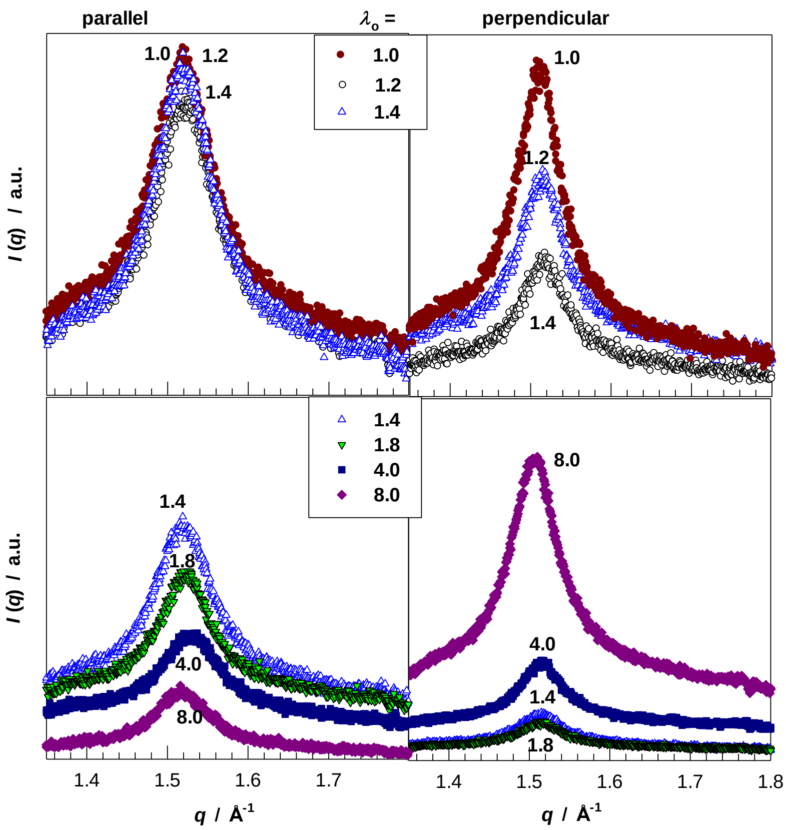

Figure 4.6 : WAXS profiles of 0.1 C12M hydrogels at various prestretch ratios λ_o indicated. The data were recorded in directions parallel (left panel) and perpendicular to the prestretching direction (right panel).

SAXS profiles of 0 C12M hydrogels between λ_o = 1.2 and 8 are shown in Figures 4.7a, b in directions parallel and perpendicular to the prestretching direction, respectively. All hydrogels with and without C12M exhibit a high intensity peak at

q_{max} = ~0.095 Å^{-1} corresponding to a lattice spacing d_2 of 6.6±0.1 nm (Figures 4.7 and 4.8).

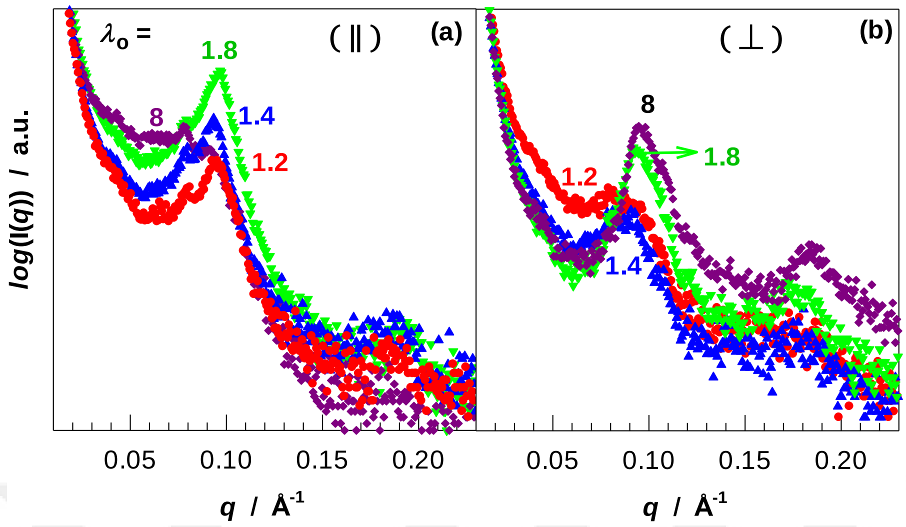

Figure 4.7 : SAXS profiles of 0 C12M hydrogels at various prestretch ratios λ_o indicated. The data were recorded in directions parallel (a) and perpendicular (b) to the prestretching direction.

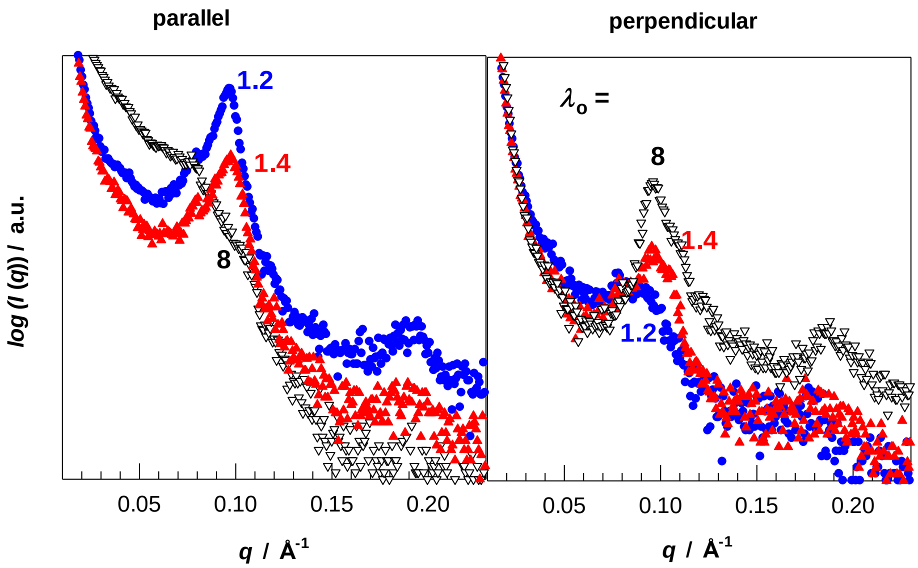

Figure 4.8 : SAXS profiles of 0.1 C12M hydrogels at various prestretch ratios λ_o indicated. The data were recorded in directions parallel (left) and perpendicular (right) to the prestretching direction.

This reveals tail-to-tail alignment of octadecyl (C18) side chains perpendicularly to the main chain [6,7,23], as illustrated in Scheme 1. Because the fully extended C18 chain length is 2.43 nm [106], this also reveals that the thickness of amorphous poly(DMAA) domains between alkyl crystals is around 1.7 nm. The peak intensity in parallel direction increases with prestretch ratio up to 1.8 while in perpendicular direction, broad peaks with lower intensities were recorded. The result thus reveals that the lamellar crystals align along the prestretching direction while those in perpendicular direction become more disordered. Moreover, remarkable is the almost structureless SAXS pattern at $\lambda_o = 8$ in parallel direction while the appearance of the highest intensity peak in perpendicular direction which we attribute formation of ordered crystallites vertical to the prestretching direction. Thus we may conclude that randomly oriented lamellar stacks in the hydrogels align along the stretching direction at $\lambda_o \leq 1.8$ while a change in the alignment from parallel to perpendicular stretching direction appears at high stretch ratios.

4.2.2 Correlation between mechanical properties and microstructure of the hydrogels

Figure 4.9a shows uniaxial tensile stress-strain curves of 0 C12M hydrogels at various prestretch ratios λ_o between 1.2 and 8. The curves for the reference hydrogel without prestretching ($\lambda_o = 1$) are also shown by the dashed curves. The tests were carried out parallel (∥, left panel) and perpendicular to the prestretching direction (⊥, right panel). Except the reference non-prestretched hydrogel, all hydrogels exhibit anisotropic mechanical properties. Moreover, in accord with the microstructural changes in the hydrogels, their mechanical performance shows different prestretch ratio dependences at below and above 1.8. For the sake of clarity, the data for $\lambda_o \leq 1.8$ and $\lambda_o \geq 1.8$ are shown in the upper and bottom panels of Figure 4.9a, respectively. Two distinct regimes can be seen from the plots:

(i) $\lambda_o \leq 1.8$: The brittle reference hydrogel becomes tough along the prestretching direction while it remains brittle in perpendicular direction. The brittle-to-ductile transition could be induced even at the lowest prestretch ratio λ_o of 1.2; both the yield stress and the fracture strain increase continuously with λ_o.

(ii) $\lambda_o \geq 1.8$: The yield stress and fracture strain start to decrease with increasing λ_o along the prestretching direction and at the highest prestretch ratio of 8, the hydrogel fractures without yielding. Simultaneously, strain hardening behavior appears and the stress continuously increases up to the fracture point. In perpendicular direction, hydrogel starts to toughen with increasing λ_o with the appearance of yielding behavior at $\lambda_o = 4$, above which both the yield stress and fracture strain continuously increase with λ_o up to 8.

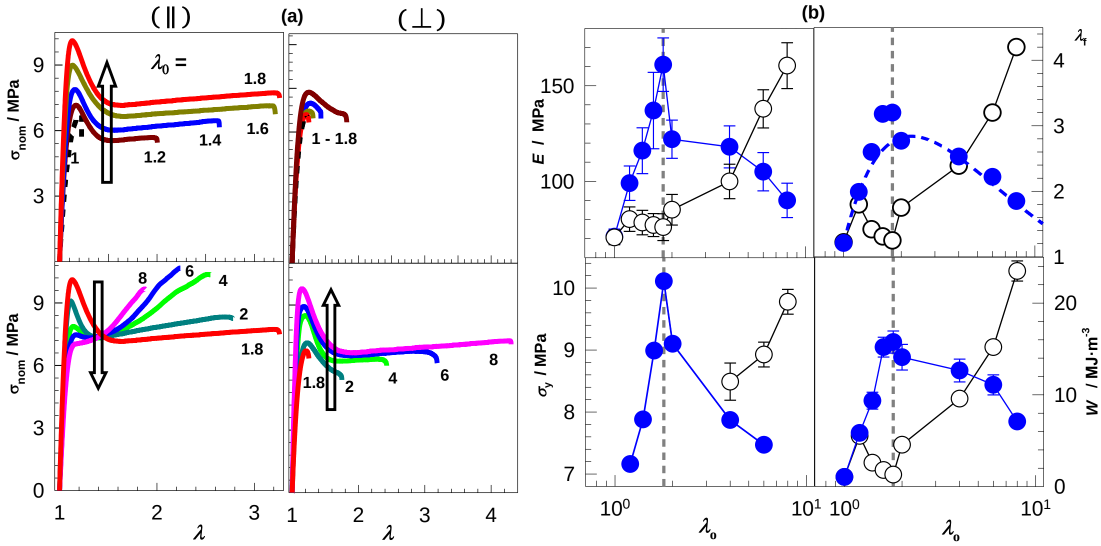

Figure 4.9 : (a): Stress-strain curves of 0 C12M hydrogels at various stretch ratios λ_o indicated. The measurements were conducted in directions parallel (∥) and perpendicular (⊥) to the prestretching. Strain rate: 5 min^{-1}. (b): Prestretch ratio dependences of Young's modulus E, yield stress σ_y, fracture strain λ_f, and energy to break (toughness) W of the hydrogels measured along parallel (filled symbols) and perpendicular to the prestretching direction (open symbols). The vertical dashed line represents the data at λ_o = 1.8. The dashed curve was calculated using eq 3 for $\lambda_{f,n}$ = 1.2±0.1.

The opposite effect of λ_o at below and above 1.8 on the mechanical properties is also illustrated in Figure 4.9b where the Young's modulus E, yield stress σ_y, fracture strain λ_f, and the energy to break W (toughness) of the hydrogels measured at parallel (filled symbols) and perpendicular directions (open symbols) are plotted against λ_o. General trend at below and above λ_o = 1.8 is the increase of the modulus, toughness, yield stress, and fracture strain with increasing λ_o in parallel and perpendicular directions, respectively. The maximum degree of mechanical anisotropy in the hydrogels appears at the prestretch ratio of 1.8, as indicated by vertical gray lines in the figures. For instance, the hydrogel at this prestretch ratio sustains 220 and 25% elongations and exhibits Young's moduli of 161±14 and 76±7 MPa, toughness of 16±1 and 1.3±0.1 MJ·m^{-3} along and vertical to the prestretching direction, respectively. The extent of mechanical anisotropy is generally given by the ratio of a mechanical property such as the modulus measured in directions parallel to perpendicular to the orientation of the material [13]. At λ_o = 1.8, the anisotropy with respect to the modulus and toughness attains a maximum value of 2.1±0.2 and 12±1, respectively. Interestingly, the modulus anisotropy at λ_o = 8 is 0.56, i.e., 1/1.8, indicating the existence of the same extent of modulus anisotropy in favor of perpendicular direction.

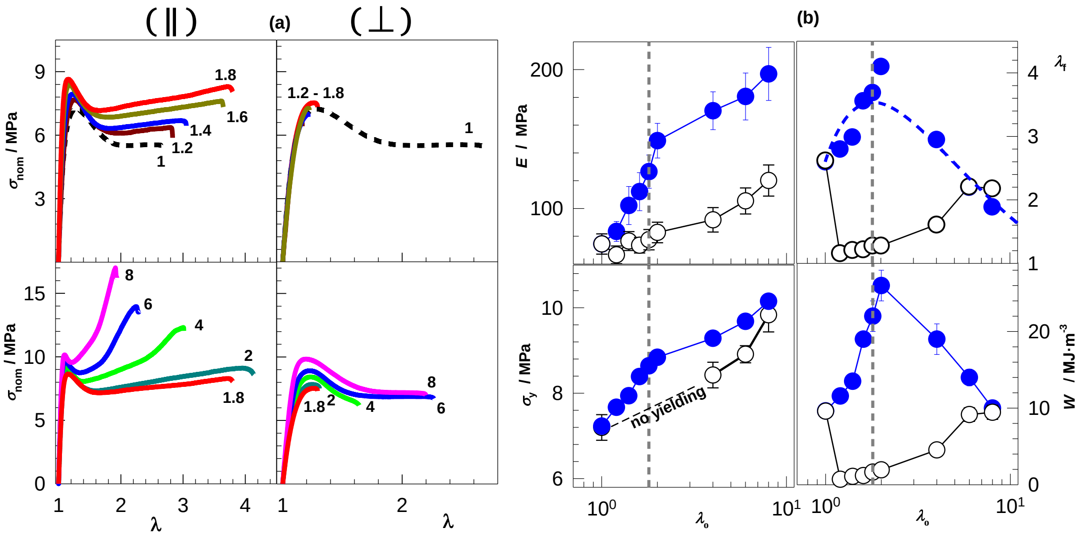

Figure 4.10 : (a): Stress-strain curves of 0.1 C12M hydrogels at various stretch ratios λ_o measured in parallel (ǁ) and perpendicular to the prestretching directions (⊥). Strain rate: 5 min^{-1}. (b): E, σ_y, λ_f, and W of the hydrogels along parallel (filled symbols) and perpendicular directions (open symbols) plotted against λ_o. The dashed curve was calculated using eq 3 for $\lambda_{f,n}$ = 2.6±0.2.

Similar results were also observed for 0.1 C12M hydrogels prepared with 0.1 mol% C12M. Figures 4.10a, b show stress-strain curves and mechanical parameters of 0.1 C12M hydrogels at various prestretch ratios. The non-prestretched 0.1 C12M hydrogel is already tough and exhibits isotropic mechanical properties. Its stretchability and toughness further increase along the prestretching direction while it becomes brittle in perpendicular direction. Interesting is the appearance of tough-to-brittle transition in vertical direction by imposing the lowest prestretch ratio of 1.2. Thus, brittle-to-ductile and ductile-to-brittle transitions in 0 C12M and 0.1 C12M hydrogels could be induced in parallel or perpendicular directions, respectively, at low prestretch ratios. The results thus reveal that the orientation of the alkyl crystals in a given direction leads to directional toughness improvement in semicrystalline hydrogels. This finding is in accord with our previous report showing that incorporation of 0.1-0.4 mol % C12M segments into the backbone of semicrystalline hydrogels generate more ordered lamellar clusters with a layered structure, which was accompanied by a brittle-to-ductile transition [106]. In the present work, ordered lamellar clusters were generated by prestretching of the network chains instead of

C12M addition so that a directional improvement in the mechanical performance of the hydrogels was observed.

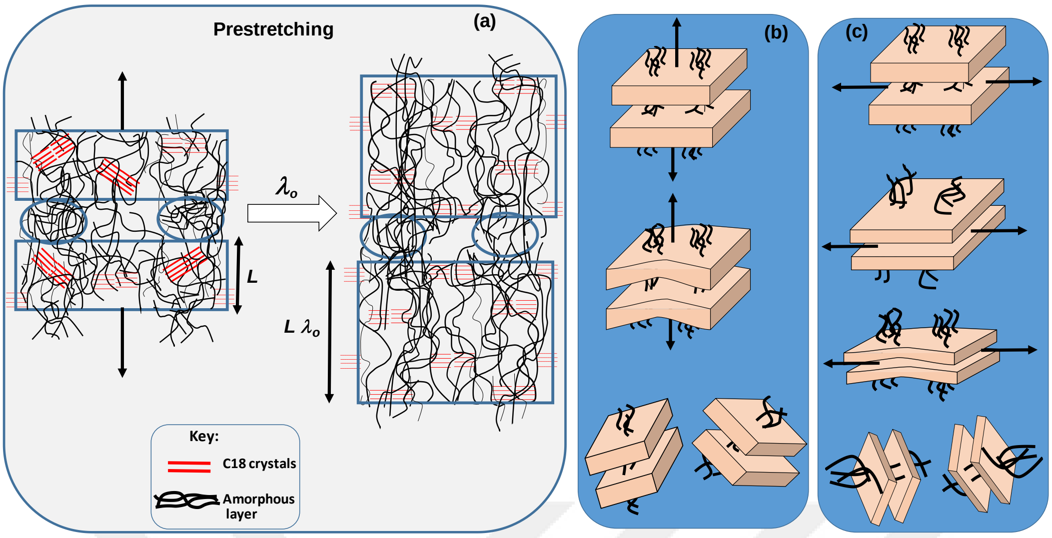

Figure 4.11 : (a): Cartoon showing lamellar clusters interconnected by active tie molecules before and after prestretching. Lamellar clusters and tie molecules are enclosed in rectangles and circles, respectively. (b, c): Stretching lamellar clusters parallel (b) and perpendicular to the prestretching direction.

As schematically illustrated in Fig. 4.11a, lamellar clusters (enclosed in rectangles) are composed of several lamellar crystals separated by amorphous domains. The tie molecules bridging the clusters have an important role in the mechanical properties of semicrystalline polymers [74-80]. Prestretching the hydrogel above T_m followed by cooling below T_m creates aligned lamellar crystals to the prestretching direction (Figure 4.11a). Moreover, because the thickness L of the lamellar clusters is in the range of the end-to-end distance of the polymer chains in unperturbed state [78,79], this thickness will increase to $\lambda_o L$ in prestretched hydrogels producing thicker lamellar clusters. Stretching the hydrogel parallel to the prestretching direction produces a stress on the lamellar clusters through the tie molecules leading to their bending and finally fragmentation at the yield point (Figure 4.11b). Because of the increased thickness of lamellar cluster with increasing prestretch ratio λ_o, a higher stress and a lower deflection will be required for fragmentation of thicker lamellar clusters. Indeed, as shown in Figures 4.10b and 11b, the yield stress σ_y increases whereas the yield strain λ_y decreases with increasing λ_o up to 1.8 for both 0 C12M and 0.1 C12M hydrogels. On the other hand, stretching the hydrogel perpendicular to the prestretching direction does not produce a significant stress on the lamellar clusters, as illustrated in Figure 4.11c. Tie molecules and amorphous domains of the clusters are pulled away from the clusters leading to the formation of thinner and closer clusters. Thus, the hydrogels exhibit a low modulus and toughness when measured perpendicular to the prestretching direction. Fragmentation of the thin clusters and appearance of yield point thus require high prestretch ratios at which the tie molecules are highly stretched.

Fragmentation of lamellar clusters results in dissipation of energy while being stretched so that resistance to crack propagation is observed. Because the clusters are irreversibly broken at the yield point, this suggests that the yielding behavior will disappear if a hydrogel specimen is subjected to second stretching. This was indeed observed. Figure 4.9a shows nominal stress σ_{nom} vs strain ε (= λ - l) plots from five successive tensile cycles conducted parallel to the prestretching direction on 0 C12M hydrogel at λ_o = 1.8. The tests were carried out up to a maximum strain of 110% where up and down arrows in the figure indicate loading and unloading steps, respectively.

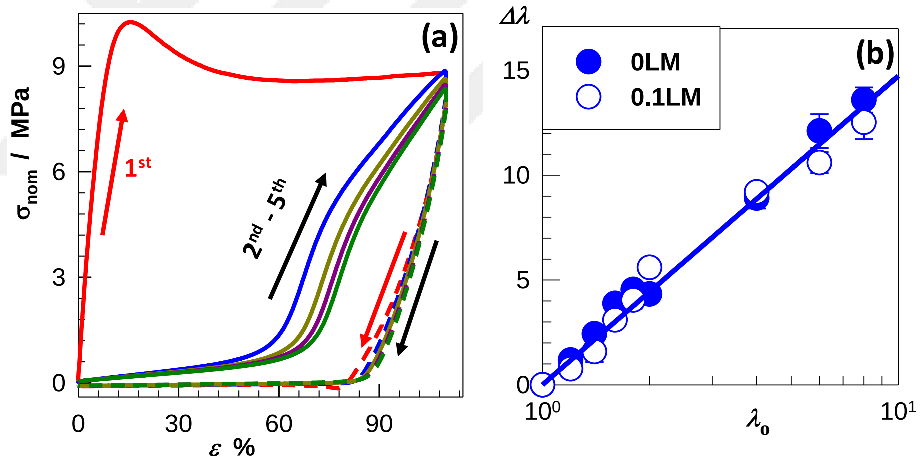

Figure 4.12 : (a). σ_{nom} vs strain ε (= λ - l) plots from five successive tensile cycles up to a maximum strain of 110% conducted parallel to the prestretching direction on 0 C12M hydrogel at λ_o = 1.8. Up and down arrows indicate loading and unloading steps, respectively. Strain rate: 5 min^{-1}. (b): Excess chain extension at break $\Delta\lambda$ of 0 C12M and 0.1 C12M hydrogels plotted against logarithm of the prestretch ratio λ_o. The line is the best-fitting curve to the experimental data with a slope 6.4±01.

It is seen that the first loading significantly deviates from the following loadings and produces 4- to 5-fold larger hysteresis energy as compared to the following cycles (Figure 4.13). The modulus of the first loading curve is around 100-fold larger as compared to that of the following loadings revealing the occurrence of an irreversible damage in the hydrogel due to the broken lamellar clusters at the yield point. Similar results were also obtained at larger prestretch ratios λ_o when the tests are conducted perpendicular to the prestretching direction (Fiure 4.13).

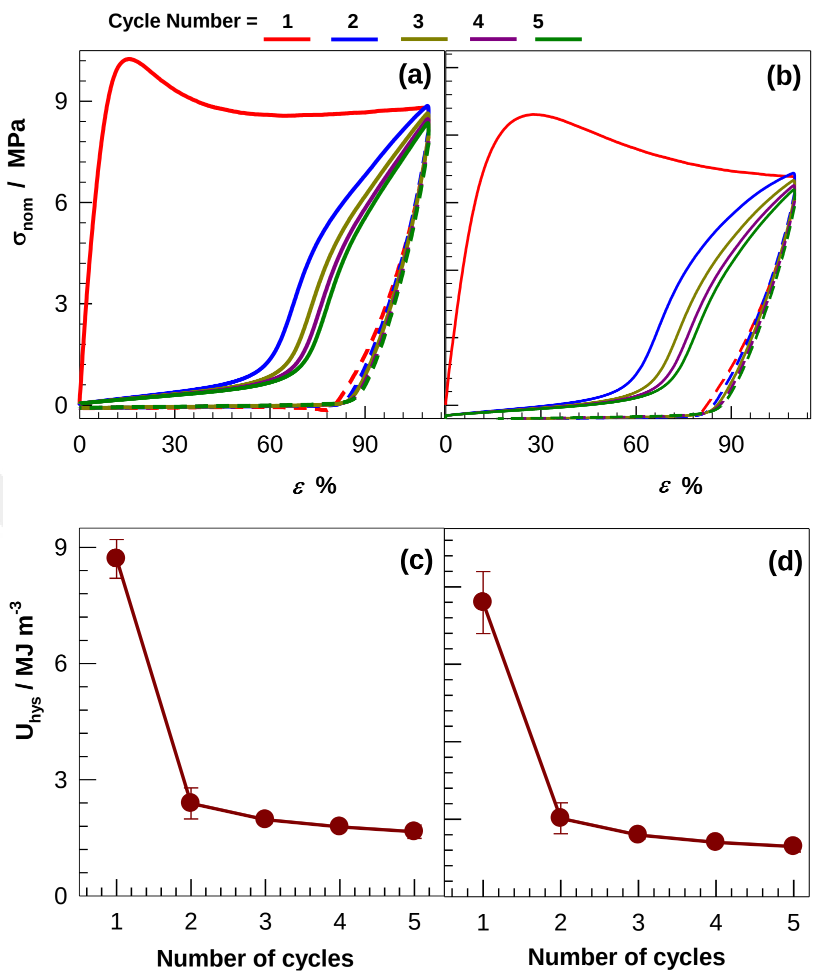

Figure 4.13 : (a, b): Nominal stress σ_{nom} vs strain ε (= λ - l) plots of 0 C12M hydrogel specimens from five successive tensile cycles up to a maximum strain of 110%. The tests were conducted parallel (a) and perpendicular to the prestretching direction (b). λ_o = 1.8 (a) and 4 (b). (c, d): Hysteresis energies U_{hys} calculated from the area between the loading and unloading curves of the mechanical cycles in Figures a and b, respectively, plotted against the cycle number.

After the yield point, that is, after fragmentation of lamellar clusters, tie molecules are stretched out from the fragmented clusters until they can be pulled out no further without rupture. As seen in Figures 4.9b and 10b, the stretch at rupture of tie molecules, that is the fracture strain λ_f of both hydrogels along the prestretching direction exhibits a maximum at around λ_o = 1.8. We have to mention that because tensile tests on the hydrogels start from the value $\lambda = \lambda_o$ instead of λ = 1, the true fracture strain $\lambda_{f,true}$ with respect to the as-prepared state is the product λ_f and λ_o, which is larger than the nominal value λ_f. Let $\lambda_{f,n}$ be the fracture strain of non-prestretched hydrogel, the excess chain extension at break $\Delta\lambda$ of prestretched hydrogels over $\lambda_{f,n}$ can thus be given by:

$$\Delta\lambda = \lambda_{f,true} - \lambda_{f,n} = \lambda_f \lambda_o - \lambda_{f,n} \tag{4.1}$$

In Figure 4.12b, the excess chain extension $\Delta\lambda$ for 0 C12M and 0.1 C12M hydrogels along the prestretching direction is plotted in a semi-logarithmic scale against the prestretch ratio λ_o. The best fitting curve to the data shown in the figure indicates that the excess chain extension at break is linear in $ln(\lambda_o)$, given by the equation,

$$\Delta\lambda = n \ln(\lambda_o) \tag{4.2}$$

where n is a constant and equal to 6.4±0.1. By substituting of eq 4.1 into eq 4.2, we obtain:

$$\lambda_f = (\lambda_o)^{-1} \left[\lambda_{f,n} + n \ln(\lambda_o)\right] \tag{4.3}$$

presenting the prestretch ratio dependence of the fracture strain of the hydrogels (dashed curves in Figs. 4.9b, 10b). Taking derivative of λ_f with respect to λ_o and equating to zero, one may calculate λ_f and λ_o at the maximum point in λ_f vs λ_o curves as:

$$\lambda_{f,\max} = \frac{n}{\lambda_o} \quad or \quad \lambda_{f,true,\max} = n \tag{4.3a}$$

$$\lambda_{o,\max} = \exp\left(1 - \frac{\lambda_{f,n}}{n}\right) \tag{4.3b}$$

Eq 4.3a reveals that the constant n = 6.4±0.1 is the maximum extension ratio ($\lambda_{f,true,max}$) of tie molecules with respect to the as-prepared state, above which they rupture. Because $\lambda_{f,n}$ = 1.2±0.1 and 2.6±0.2 for 0 C12M and 0.1 C12M hydrogels, respectively, eq 4.3b reveals that the maximum extension ratio n of tie molecules is reached at $\lambda_{o,max}$ = 2.0±0.2 for the present hydrogels, which is close to the critical prestretch ratio of around 1.8. Thus, the period λ_o < 1.8 corresponds to the flexible regime where the tie molecules between fragmented clusters are coiled so that λ_f increases with increasing λ_o. However, at larger values of λ_o, the maximum extension n of tie molecules is reached earlier, that is, at a lower strain as λ_o is increased. The results also reveal that the limited extensibility of tie molecules above $\lambda_o = 4$ is responsible for the appearance of strain hardening behavior in hydrogels (Figures 4.9 and 4.10).

4.3 Conclusions

An ongoing challenge in the gel science is to create mechanically strong hydrogels with anisotropic properties, as observed in many biological tissues possessing anisotropically oriented hierarchical structures. We present a simple one-step physical method for production of high-strength physical hydrogels with anisotropic properties. As the precursor material, we use semicrystalline hydrogels consisting of poly(N,N-dimethylacrylamide) chains interconnected by n-octadecyl acrylate (C18A) segments forming crystalline domains and hydrophobic associations. To generate anisotropic microstructure, we impose a prestretching on the isotropic hydrogel sample above the melting temperature T_m of its crystalline domains followed by cooling below T_m under strain to fix the elongated shape of the gel sample. A significant microstructural anisotropy and directional improvement in the modulus, stretchability and toughness were achieved, that could be tuned by the magnitude of the prestretch ratio λ_o. Directional brittle-to-ductile and ductile-to-brittle transitions could also be induced by adjusting the prestretch ratio λ_o. Small- and wide-angle X-ray scattering measurements and mechanical tests highlight a critical prestretch ratio λ_o at which the hydrogel exhibits the highest microstructural and mechanical anisotropy due to the finite extensibility of the network chains. At $\lambda_o = 1.8$, the hydrogel exhibits Young's moduli of 161±14 and 76±7 MPa, and toughness of 16±1 and 1.3±0.1 MJ m^{-3} along and perpendicular to the prestretching directions, respectively.

5. CONCLUSION

Within the framework of this thesis, we focused on the design of mechanically strong semi-crystalline hydrogels with shape-memory and self-healing functions. The hydrogels were generated by incorporation of hydrophobic units containing long alkyl side chains into hydrophilic polymer backbone. To prepare the hydrogels, we used both micellar copolymerization and bulk photopolymerization techniques. In the first part of the thesis, the hydrogels were synthesized via micellar copolymerization of acrylic acid (AAc) and n-octadecyl acrylate (C18A) in aqueous sodium chloride (NaCl) solutions containing sodium dodecyl sulfate (SDS) at 55 $^{\circ}$C. No chemical cross-linker was included in the monomer feed to produce a physical network. In the second and third part of the thesis, the hydogels were synthesized by bulk photopolymerization of N,N dimethylacrylamide (DMA), C18A and lauryl methacrylate (C12M) monomers in the presence of ırgacure 2959 as an initiator. The key point in our studies is to use a supramolecular approach, that is, the absence of chemical cross-links in the hydrogel network and the existence of physical cross-links formed by both hydrophobic asociations and the crystalline domains. In aquous medium, interactions between hydrophobic units formed by long alkyl side chains result in the formation of both hydrophobic associations and crystalline domains providing water insolubility, good mechanical performance, shape memory and self-healing abilities for the hydrogel.

In the first section, we prepared melt-procesable, self-healable, shape-memory hydrogels in aqueous solutions of surfactant micelles and in the absence of a chemical cross-linker. The hydrogels with water content of 60-80% consist of PAAc chains containing 20−50 mol % C18A segments together with SDS micelles. Above the melting temperature of the crystalline domains (T_m), the hydrogel was in liquid state due to the solubilizing effect of surfactant micelles to the hydrophobic associations. At this stage, the hydrogel could be shaped by pouring into a desired mould. By cooling below T_m and removing the surfactant, a hydrogel of any permanent shape with a compressive strength of 90 MPa and a Young's modulus of

26 MPa was obtained. However, the hydrogels thus obtained were brittle and they rupture at a stretch of less than 20% without yielding. In the second section of the thesis, we intended to improve both the toughness and stretchability of the supramolecular semi-crystalline hydrogels. We realized that the incorporation of a small amount of a weak hydrophobic monomer into the semi-crystalline hydrogels leads to a significant increase in toughness and stretchability without losing their high mechanical performance. The hydrogels have entangled physical network of poly (DMA) chains containing C18A and lauryl methacrylate (C12M) segments with side chain lengths of 18 and 12 carbons, respectively. By incorporation of 0.1 to 0.4 mol % C12M segments into polymer containing 30% C18A and 70% DMA, we were able to produce thinner and more ordered lamellar crystals with a layered structure. C12M-modified hydrogels exhibited necking behaviour causing 10-fold increase of toughness without changing of the modulus and tensile strength due to the brittle-to-ductile transition. The significant toughness enhancement resulting from incorporation of C12M into the semi-crystalline hydrogels could be explaned with the formation of active tie molecules interconnecting the lamellar clusters. In the last section of this study, research was conducted to create microstructural and mechanical anizotropy in the semi-crystalline hydrogels. We presented a simple one-step way for the generation of high-strength physical hydrogels with anisotropic properties. The composition of the hydrogel network was the same as in the previous sections of this study. A prestretching process was imposed on the isotropic hydrogel samples to produce anisotropic microstructures. In this prestretching process, the gel sample was first prestretched above T_m of its crystalline domains followed by cooling below T_m under strain to fix its elongated shape. The degree of anisotropy with respect to the microstructure and mechancial properties such as the modulus, stretchability and toughness could be adjusted by the magnitude of the prestretch ratio λ_o, which was defined as the ratio of fixed elongated length to the initial length. Small- and wide-angle X-ray scattering measurements as well as mechanical tests reveal a critical prestretch ratio λ_o at which the hydrogel exhibits the highest mechanical and microstructural anisotropy. At $\lambda_o = 1.8$, the hydrogel exhibits Young’s moduli of 161±14 and 76±7 MPa, and toughness of 16±1 and 1.3±0.1 MJ m^{-3} along and perpendicular to the prestretching directions, respectively.

All of the hydrogels reported here exhibited complete shape-recovery because of their hydrophobic segments acting as physical netpoints and switching segments above and below T_m, respectively. When they were damaged, their excellent original mechanical properties could fully be recovered by a temperature-induced healing process. The hydrogels also exhibit reversible tensile deformation induced by heating above T_m. In concluding, we developed during this thesis studies new synthetic strategies for the production of multi-functional semi crystalline hydrogels with extraordinary mechanical properties together with shape-memory and self-healing functions. The presented hydrogels as multi-functional smart materials can be used in various applications including biomedical, packaging, sensors, and actuators. They all are promising intelligent materials for tissue engineering, artifical organs and soft bio-device.

REFERENCES

[1] **Chaterji, S., Kwon, K., Park, K.** (2007). Smart polymeric gels: Redefining the limits of biomedical devices, *Prog. Polym. Sci.*,32, 1083-1122.

[2] **Fratzl, P.** (2007). Biomimetic materials research: what can we really learn from nature's structural materials? *J. R. Soc. Interface*, 4, 637-642.

[3] **Slaughter, B. V., Khurshid S. S.** et al. (2009). Hydrogels in Regenerative Medicine, *Adv. Mater.,21*, 3307-3329.

[4] **Matsuda, T., Kagami, Y. and Osada, Y**. (1995). Synthesis and Dynamic Properties of Hydrogel with Order-Disorder Transition, *Polymer Preprints, Jpn.,* 469.

[5] **Lee, J.W., Park, J.K., Lee, K.H.** (2000). Thermosensitive Permeation from Side-Chain Crystalline Ionomers, *Journal of Polymer Science, 38*, 823-830.

[6] **Matsuda, A., Sato, J., Yasunaga, H., Osada, Y**. (1994). Order-disorder transition of a hydrogel containing an n-alkyl acrylate, *Macromolecules*, 27, 7695-7698.

[7] **Osada, Y., Matsuda, A.** (1995). Shape Memory in Hydrogels, *Nature, 376*, 219.

[8] **Bilici, C., Okay O.,** (2013). Shape Memory Hydrogels via Micellar Copolymerization of Acrylic Acid and n-Octadecyl Acrylate in Aqueous Media, *Macromolecules*, 46, 3125-3131.

[9] **Tuncaboylu, D. C., Sari, M., Oppermann, W. and Okay, O. (**2011). Tough and Self-Healing Hydrogels Formed via Hydrophobic Interactions, *Macromolecules, 44*, 4997-5005.

[10] **Tuncaboylu, D. C., Sahin, M., Argun, A., Oppermann, W. and Okay, O. (**2012). Dynamics and Large Strain Behavior of Self-Healing Hydrogels with and without Surfactants, *Macromolecules*, *45*, 1991-2000.

[11] **Tuncaboylu, D. C., Argun, A., Sahin, M., Sari, M., Okay, O**. (2012). Structure Optimization of Self-Healing Hydrogels Formed via Hydrophobic Interactions, *Polymer*, *53*, 5513-5522.

[12] **Kurt, B., Gulyuz, U., Demir, D.D. and Okay, O**. (2016). A simple non-covalent approach to generate high-strength self-healing hydrogels with shape memory effect, *European Polmer Journal*, 81, 12-23.

[13] **Sano, K., Ishida, Y., Aida, T.** (2018) Synthesis of anisotropic hydrogels and their applications. *Angew. Chem. Int. Ed*., 57, 2-14.

[14] **Hempel, E., Budde, H., Höring, S., Beiner, M.** (2006). On the crystallization behavior of frustrated alkyl groups in poly(n-octadecyl methacrylate). *J. Non-Cryst. Solids,* 352, 5013−5020.

[15] **Hiller, S., Pascui, O., Budde, H., Kabisch, O., Reichert, D., Beiner, M. (**2004). Nanophase separation in side chain polymers: new evidence from structure and dynamics. *New J. Phys*. 6, 10.

[16] **Floudas, G., Stepánek, P.** (1998). Structure and dynamics of poly(ndecyl methacrylate) below and above the glass transition. *Macromolecules,* 31, 6951−6957.

[17] **Miller, R. L., Boyer, R. F., Heijboer, J**. (1984). X-ray scattering from amorphous acrylate and methacrylate polymers: Evidence of local order. *J. Polym. Sci., Polym. Phys. Ed.,* 22, 2021−2041.

[18] **Shang, S., Huang, S. J., Weiss, R. A.** (2009). Synthesis and characterization of itaconic anhydride and stearyl methacrylate copolymers. *Polymer,* 50, 3119−3127.

[19] **Lendlein, A., Kelch, S.** (2002). Shape-memory polymers. *Angew. Chem-Int. Ed.* 41, 2034-2057.

[20] **Liu, C., Quin, H., Mather, P. T.** (2007). Review of progress in shape-memory polymers. *J. Mater. Chem.* 17, 1543-1558.

[21] **Behl, M.; Lendlein, A.** (2007). Actively moving polymers. *Soft Matter,* 3, 58-67.

[22] **Behl, M., Razzaq, M. Y., Lendlein, A.** (2010). Multifunctional shape-memory polymers, *Adv. Mater.*, 22, 3388-3410.

[23] **Tanaka, Y., Kagami, Y., Matsuda, A., Osada, Y.** (1995). Thermoreversible transition of the tensile modulus of a hydrogel with ordered aggregates. *Macromolecules,* 28, 2574-2576.

[24] **Uchida, M., Kurosawa, M., Osada, Y.** (1995). Swelling process and order-disorder transition of hydrogel containing hydrophobic ionizable groups. *Macromolecules,* 28, 4583-4586.

[25] **Nöchel, U., Reddy, C. S., Uttamchand, N. K., Kratz, K., Behl, M., Lendlein, A.** (2013). Shape-memory properties of hydrogels having a poly(ε-caprolactone) crosslinker and switching segment in an aqueous environment. *Eur. Polym. J.*, 49, 2457-2466.

[26] **Balk, M., Behl, M., Nöchel, U., Lendlein, A.** (2012). Shape-memory hydrogels with switching segments based on oligo(ω-pentadecalactone). *Macromol. Mater. Eng.*, 297, 1184-1192.

[27] **Hao, J., Weiss, R. A.** (2013). Mechanically tough, thermally activated shape memory hydrogels. *ACS Macro Lett.*, 2, 86-89.

[28] **Han, Y.; Bai, T.; Liu, Y.; Zhai, X.; Liu, W.** (2012). Zinc ion uniquely induced triple shape memory effect of dipole–dipole reinforced ultra-high strength hydrogels. *Macromol. Rapid. Commun*., 33, 225-231.

[29] **Lin, X. K., Chen, L., Zhao, Y. P., Dong, Z. Z.** (2010). Synthesis and characterization of thermoresponsive shape-memory poly(stearyl acrylate-co-acrylamide) hydrogels, *J. Mater. Sci.*, 45, 2703-2707.

[30] **Zhang, H., Han, D., Yan, Q., Fortin, D., Xia, H., Zhao, Y.** (2014). Light-healable hard hydrogels through photothermally induced melting–crystallization phase transition, *J. Mater. Chem. A.*, 2, 13373-13379.

[31] **Mogri, Z., Paul, D. R.** (2001). Gas sorption and transport in side-chain crystalline and molten poly(octadecyl acrylate). *Polymer*, 42, 2531-2542.

[32] **Bisht, H. S., Pande, P. P., Chatterjee, A. K.** (2002). Docosyl acrylate modified polyacrylic acid: synthesis and crystallinity. *Eur. Polym. J.* 38, 2355-2358.

[33] **ISO 7875-1,** (1996). Water quality. Determination of surfactants. Part 1: Determination of anionic surfactants by measurement of the methylene blue index (MBAS). *USO/TC*, 147.

[34] **Webber, R. E., Creton, C., Brown, H. R., Gong, J. P**. (2007). Large strain hysteresis and Mullins effect of tough double-network hydrogels. *Macromolecules*, 40, 2919-2927.

[35] **Sauter, T., Heuchel, M., Kratz, K., Lendlein, A.** (2013). Quantifying the shape-memory effect of polymers by cyclic thermomechanical tests, *Polym. Rev.*, 53, 6-40.

[36] **Can,V., Kochovski, Z., Reiter, V., Severin, N., Siebenbürger, M., Kent, B. ….. Okay, O.** (2016). Nanostructural evolution and self-healing mechanism of micellar hydrogels. *Macromolecules*, 49, 2281-2287.

[37] **Peer, W. J.** (1989). Polymerization of hydrophobically modified polyacrylamide: Effects of surfactants and comonomers. In Polymers in Aqueous Media - Performance Through Association, *Advances in Chemistry; American Chemical Society*, 223, 381−397.

[38] **Hill, A.; Candau, F.; Selb, J.** (1993). Properties of hydrophobically associating polyacrylamides: influence of the method of synthesis. *Macromolecules*, 26, 4521−4532.

[39] **Candau, F.; Selb, J.** (1999). Hydrophobically modified polyacrylamides prepared by micellar polymerization, *Adv. Colloid Interface Sci*. 79, 149−172.

[40] **Miyazaki, T., Kaneko, T., Gong, J. P., Osada, Y.** (2001). Effects of carboxyls attached at alkyl side chain ends on the lamellar structure of hydrogels. *Macromolecules*, 34, 6024-6028.

[41] **Livshin, S., Silverstein, M. S.** (2008). Crystallinity and cross-linking in porous polymers synthesized from long side chain monomers through emulsion templating, *Macromolecules*, 41, 3930-3838.

[42] **Algi, M. P., Okay, O.** (2014). Highly stretchable self-healing poly(N,N-dimethylacrylamide) hydrogels, *Eur. Polym. J.*, 59, 113-121.

[43] **Argun, A., Can, V., Altun, U., Okay, O.** (2014). Non-ionic double and triple network hydrogels of high mechanical strength. *Macromolecules*, 47, 6430-6440.

[44] **Calvert, P.** (2009). Hydrogels for soft machines. *Adv. Mater.*, 21, 743-756.

[45] **Tanaka, Y., Gong, J. P., Osada, Y**. (2005). Novel hydrogels with excellent mechanical performance. *Prog. Polym. Sci.*, 30, 1-9.

[46] **Gong, J. P., Katsuyama, Y., Kurokawa, T., Osada, Y**. (2003). Double network hydrogels with extremely high mechanical strength. *Adv. Mater.*, 15, 1155-1158.

[47] **Tanaka, Y., Kuwabara, R., Na, Y.-H., Kurokawa, T., Gong, J. P., Osada, Y.** (2005). Determination of fracture energy of high strength double network hydrogels. *J. Phys. Chem. B,* 109, 11559-11562.

[48] **Gong, J. P.** Why are double network hydrogels so tough? (2010). *Soft Matter,* 6, 2583-2590.

[49] **Nakajima, T., Furukawa, H., Tanaka, Y., Kurokawa, T., Osada, Y., Gong, J. P.** (2009). True chemical structure of double network hydrogels. *Macromolecules*, 42, 2184-2189.

[50] **Es-haghi, S. S., Leonov, A. I., Weiss, R. A.** (2014). Deconstructing the double-network hydrogels: The importance of grafted chains for achieving toughness. *Macromolecules,* 47, 4769-4777.

[51] **Ahmed, S., Nakajima, T., Kurokawa, T., Haque, Md.A., Gong, J. P.** (2014). Brittle−ductile transition of double network hydrogels: Mechanical balance of two networks as the key factor. *Polymer*, 55, 914-923.

[52] **Matsuda, T., Nakajima, T., Fukuda, Y., Hong, W., Sakai, T., Kurokawa, T., Chung, U., Gong, J. P.** (2016). Yielding criteria of double network hydrogels. *Macromolecules,* 49, 1865-1872.

[53] **Es-haghi, S. S., Leonov, A. I., Weiss, R. A**. (2013). On the necking phenomenon in pseudo-semi-interpenetrating double-network hydrogels. *Macromolecules*, 46, 6203-6208.

[54] **Sun, J.-Y., Zhao, X., Illeperuma, W. R. K., Chaudhuri, O., Oh, K. H., Mooney, D. J., Vlassak, J. J., Suo, Z.** (2012). Highly stretchable and tough hydrogels. *Nature*, 489, 133-136.

[55] **Li, J., Suo, Z., Vlassak, J. J. Stiff**, (2014). Stiff, strong, and tough hydrogels with good chemical stability. *J. Mater. Chem. B,* 2, 6708-6713.

[56] **Chen, Q., Wei, D., Chen, H., Zhu, L., Jiao, C., Liu, G., Huang, L., ... Zheng, J.** (2015). Simultaneous enhancement of stiffness and toughness in hybrid double network hydrogels via the first, physically linked network. *Macromolecules*, 48, 8003-8010.

[57] **Sun, T. L., Kurokawa, T., Kuroda, S., Ihsan, A. B., Akasaki, T., Sato, K., ... Gong, J. P.** (2013). Physical hydrogels composed of polyampholytes demonstrate high toughness and viscoelasticity. *Nat. Mater*., 12, 932-937.

[58] **Hu, X., Vatankhah-Varnoosfaderani, M., Zhou, J., Li, Q., Sheiko, S. S.** (2015). Weak hydrogen bonding enables hard, strong, tough, and elastic hydrogels. *Adv. Mater.,* 27, 6899-6905.

[59] **Bilici, C., Can, V., Nöchel, U., Behl, M., Lendlein, A., Okay, O.** (2016). Melt-processable shape-memory hydrogels with self-healing ability of high mechanical strength. *Macromolecules*, 49, 7442-7449.

[60] **Uemura, Y., McNulty, J., Macdonald, P. M.** (1995). Associative behavior and diffusion coefficients of hydrophobically modified poly(N,Ndimethylacrylamides). *Macromolecules*, 28, 4150-4158.

[61] **Peppas, N. A.** (1987). Hydrogels in Medicine and Pharmacy. Wiley: New York.

[62] **Relogio, P., Martinho, J. M. G., Farinha, J. P. S**. (2005). Effect of surfactant on the intra- and intermolecular association of hydrophobically modified poly(N,N-dimethylacrylamide). *Macromolecules*, 38, 10799-10811.

[63] **Masalci, O., Kazanci, N., Orujalipoor, I., Ide, S.** (2015). Nano-structural analysis of a lyotropic liquid crystal (TTAB + water + decanol ternary) system by salt (NH4Br) addition. *Mol. Cryst. Liq. Cryst. Sci. Technol.*, 609, 70-79.

[64] **Ozcan, Y., Ide, S., Butun, V., Jeng, U-S., Lai, Y-H., Su, C-H.** (2013). Micellization behavior of tertiary-amine-methacrylate-based block copolymers characterized by small-angle X-ray scattering and dynamic light scattering. *Mater. Chem. Phys.*, 138, 559-564.

[65] **Goktas, M., Cinar, G., Orujalipoor, I., Ide, S., Tekinay, A.B., Guler, O.** (2015). Self-assembled peptide amphiphile nanofibers and PEG composite hydrogels as tunable ECM mimetic microenvironment. *Biomacromolecules*, 16, 1247-1258.

[66] **Alig, I., Jarek, M., Hellmann, G. P.** (1998). Restricted segmental mobility in side-chain crystalline comblike polymers studied by dielectric relaxation measurements. *Macromolecules*, 31, 2245−2251.

[67] **Plate, N. A., Shibaev, V. P.** (1974). Comb-like polymers. Structure and properties. *Macromol. Rev.*, 8, 117-253.

[68] **Stokes, R. J., Evans, D. F.** (1997). *Fundamentals of Interfacial Engineering,* Wiley-VCH, p 215.

[69] **Kauzmann, W., Eyring, H.** (1940). The viscous flow of large molecules. *J. Am. Chem. Soc.*, 62, 3113-3125.

[70] **Ward, I. M., Hadley, D. N.** (2000). *Mechanical Properties of Solid Polymers,* Wiley: Chichester, UK.

[71] **McCrum, N. G., Buckley, C. P., Bucknall, C. B**. (1997). *Principles of Polymer Engineering*, Oxford University Press: New York.

[72] **Annable, T., Buscall, R., Ettelaie, R., Whittlestone, D**. (1993). The rheology of solutions of associating polymers: Comparison of experimental behavior with transient network theory. *J. Rheol.*, 37, 695-726.

[73] **Tripathi, A., Tam, K. C., McKinley, G. H.** (2006). Rheology and dynamics of associative polymers in shear and extension: Theory and experiments. *Macromolecules,* 39, 1981-1999.

[74] **Guo, H., Zhang, Y., Xue, F., Cai, Z., Shang, Y., Li, J., ... Jiang, S.** (2013). In-situ synchrotron SAXS and WAXS investigations on deformation and α−β transformation of uniaxial stretched poly(vinylidene fluoride). *Cryst. Eng. Comm*, 15, 1597-1606.

[75] **Spitalsky, Z., Bleha, T., Cifra, P.** (2002). Energy elasticity of tie molecules in semicrystalline polymers. *Macromol. Theory Simul*., 11, 513-524.

[76] **Humbert, S., Lame, O., Chenal, J.-M., Rochas, C., Vigier, G.** (2010). Small strain behavior of polyethylene: In situ SAXS measurements. *J. Polym. Sci., Part B: Polym. Phys.*, 48, 1535-1542.

[77] **Nitta, K.-H., Takayanagi, M.** (2003). Novel proposal of lamellar clustering process for elucidation of tensile yield behavior of linear polyethylenes. *J. Macromol. Sci., Part B: Phys.*, 42, 107-126.

[78] **Nitta, K.-H., Takayanagi, M.** (1999). Role of tie molecules in the yielding deformation of isotactic polypropylene. *J. Polym. Sci., Part B: Polym. Phys.*, 37, 357-368.

[79] **Nitta, K.-H., Takayanagi, M.** (2000). Tensile yield of isotactic polypropylene in terms of a lamellar-cluster model. *J. Polym. Sci., Part B: Polym. Phys.*, 38, 103-1044.

[80] **Gao, R., Kuriyagawa, M., Nitta, K.-H., He, X., Liu, B.** (2015). Structural interpretation of Eyring activation parameters for tensile yielding behavior of isotactic polypropylene solids. *J. Macromol. Sci., Part B: Phys.*, 54, 1196-1210.

[81] **Creton, C.** (2017). 50th Anniversary perspective: Networks and gels: Soft but dynamic and tough. *Macromolecules* ,50, 8297-8316.

[82] **Lu, Q., Bai, S., Ding, Z., Guo, H., Shao, Z., Zhu, H., Kaplan, D.L.** (2016). Hydrogel assembly with hierarchical alignment by balancing electrostatic forces. *Adv. Mater. Interfaces*, 3, 1500687.

[83] **Lin, X.Y., Wang, Z.J., Pan, P., Wu, Z.L., Zhenga, Q.** (2016). Monodomain hydrogels prepared by shear-induced orientation and subsequent gelation. *RSC Adv*. 6, 95239-95245.

[84] **Zhu, Z., Li, Y., Xu, H., Peng, X., Chen, Y-N., Shang, C., Wang, H.** (2016). Tough and thermosensitive poly(N-isopropylacrylamide)/graphene oxide hydrogels with macroscopically oriented liquid crystalline structures. *ACS Appl. Mater. Interfaces*, 8, 15637-15644.

[85] **Liu, M., Ishida, Y., Ebina, Y., Sasaki, T., Hikima, T., Takata, M., Aida, T.** (2015). An anisotropic hydrogel with electrostatic repulsion between cofacially aligned nanosheets. *Nature*, 517, 68-72.

[86] **Kaneda, K., Uematsu, K., Masunaga, H., Tominaga, Y., Shigehara, K., Shikinaka, K.** (2014). Flow-orientation of internal structure and anisotropic properties on hydrogels consisted of imogolite hollow nanofibers. *Sen'i Gakkaishi*, 70,137-144.

[87] **Paineau, E., Dozov, I., Bihannic, I., Baravian, C., M Krapf, M-E., Philippe, A-M., ... Davidson, P**. (2012). Tailoring highly oriented and micropatterned clay/polymer nanocomposites by applying an a.c. electric field. *ACS Appl. Mater. Interfaces*, 4, 4296-4301.

[88] **Isabettini, S., Stucki, S., Massabni, S., Baumgartner, M.E., Reckey, P.Q., Kohlbrecher, J., ... Kuster, S.** (2018). Development of smart optical gels with highly magnetically responsive bicelles. *ACS Appl. Mater. Interfaces*, 10, 8926-8936.

[89] **Yetiskin, B., Okay, O.** (2017). High-strength silk fibroin scaffolds with anisotropic mechanical properties. *Polymer*, 112, 61-70.

[90] **Millon, L.E., Mohammadi, H., Wan, W.K.** (2006). Anisotropic polyvinyl alcohol hydrogel for cardiovascular applications. *J. Biomed. Mater. Res. B Appl. Biomater*. 79, 305-311.

[91] **Wan, W., Bannerman, A.D., Yang, L., Mak, H.** (2014). Poly(vinyl alcohol) cryogels for biomedical applications. *Adv. Polym. Sci.*, 263, 283-321.

[92] **Kaneko, T., Ogomi, D., Mitsugi, R., Serizawa, T., Akashi, M.** (2004). Mechanically drawn hydrogels uniaxially orient hydroxyapatite crystals and cell extension. *Chem. Mater.* 16, 5596-5601.

[93] **Choi, S., Kim, J.** (2015). Designed fabrication of super-stiff, anisotropic hybrid hydrogels via linear remodeling of polymer networks and subsequent crosslinking. *J. Mater. Chem. B*, 3, 1479-1483.

[94] **Lin, P., Zhang, T., Wang, X., Yu, B., Zhou, F**. (2016). Freezing molecular orientation under stretch for high mechanical strength but anisotropic hydrogels. *Small*, 12, 4386-4392.

[95] **Kim, S.H., Im, S-K., Oh, S-J., Jeong, S., Yoon, E-S., Lee, C.J., Choi, N., Hur, E-M.** (2017). Anisotropically organized three-dimensional culture platform for reconstruction of a hippocampal neural network. *Nat. Commun*. 8, 14346.

[96] **Ye, D., Cheng, Q., Zhang, Q., Wang, Y., Chang, C., Li, L., Peng, H., Zhang, L.** (2017). Deformation drives alignment of nanofibers in framework for inducing anisotropic cellulose hydrogels with high toughness. *ACS Appl. Mater. Interfaces*, 9, 43154-43162.

[97] **He, X., Oishi, Y., Takahara, A., Kajiyama, K.** (1996). Higher order structure and thermo-responsive properties of polymeric gel with crystalline side chains. *Polymer J.*, 28, 452–457.

[98] **Yang, W., Furukawa, H., Gong, J.P.** (2008). Highly extensible double-network gels with self-assembling anisotropic structure. *Adv. Mater.*, 20, 4499-4503.

[99] **Wu, Z.L., Kurokawa, T., Sawada, D., Hu, J., Furukawa, H., Gong, J.P.** (2011). Anisotropic hydrogel from complexation-driven reorientation of semirigid polyanion at Ca_2^+ diffusion flux front. *Macromolecules*, 44, 3535-3541.

[100] **Wu, Z.L., Sawada, D., Kurokawa, T., Kakugo, A., Yang, W., Furukawa, H., Gong, J.P.** (2011). Strain-induced molecular reorientation and birefringence reversion of a robust, anisotropic double-network hydrogel. *Macromolecules*, 44, 3542-3547.

[101] **Khan, F., Walsh, D., Patil, A.J., Perriman, A.W., Mann, S.** (2009). Self-organized structural hierarchy in mixed polysaccharide sponges. *Soft Matter*, 5, 3081-3085.

[102] **Cui, K., Sun, T.L., Kurokaw, T., Nakajimai, T., Nonoyama, T., Chenc, L., Gong, J.P.** (2016). Stretching-induced ion complexation in physical polyampholyte hydrogels. *Soft Matter*, 12, 8833-8840.

[103] **Xie, T.** Tunable polymer multi-shape memory effect. (2010). *Nature*, 464, 267-270.

[104] **Zhao, Q. Qi, H.J. Xie, T.** (2015).Recent progress in shape memory polymer: New behavior, enabling materials, and mechanistic understanding. *Prog. Polym. Sci*. 49-50, 79-120.

[105] **Beblo, R., Weiland L.M.** (2008). Strain induced anisotropic properties of shape memory polymer. *Smart Mater. Struct.* 17, 055021.

[106] **Bilici, C., Ide, S., Okay, O.** (2017). Yielding behavior of tough semicrystalline hydrogels. *Macromolecules* 50, 3647-3654.

[107] **Wei, D., Yang, J., Zhu, L., Chen, F., Tang, Z., Qin, G., Chen, Q.** (2018). Semicrystalline hydrophobically associated hydrogels with integrated high performances. *ACS Appl. Mater. Interfaces*, 10, 2946-2956.

[108] **Miyazaki, T., Yamaoka, K., Gong, J.P., Osada, Y.** (2002) Hydrogels with crystalline or liquid crystalline structure. *Macromol. Rapid Commun.* 23, 447-455.

CURRICULUM VITAE

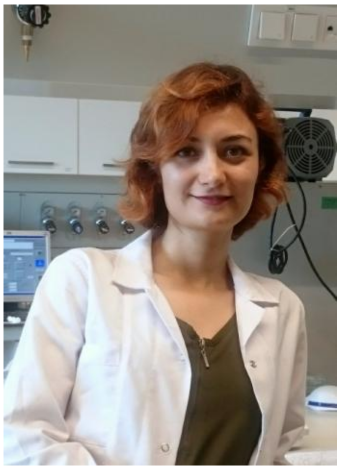

Name Surname : ÇİĞDEM BİLİCİ

Place and Date of Birth : Kadıköy, 15.12.1985

E-Mail : blc.cgdem@gmail.com

EDUCATION

- **B.Sc** : 2010, Istanbul Technical University, Faculty of Art and Science, Chemistry
- **M.Sc.** : 2014, Istanbul Technical University, Graduate School of Science Engineering and Technology, Chemistry

PUBLICATIONS

- **Bilici C.**, Karaarslan D., Ide S., Okay O., 2018, Toughness Improvement and Anisotropy in Semicrystalline Hydrogels, *Polymer*, 151, 208-217.

- **Bilici C.**, Ide S., Okay O., 2017, Yielding Behavior of Tough Semicrystalline Hydrogels, *Macromolecules*, 50, 9, 3647-3654.

- **Bilici C.**, Can V., Nochel U., Behl M., Lendlein A. and Okay O., 2016, Melt-Processable Shape-Memory Hydrogels with Self-Healing Ability of High Mechanical Strength, *Macromolecules*, 49, 19, 7442-7449.

- **Bilici C.**, Okay O., 2013, Shape Memory Hydrogels via Micellar Copolymerization of Acrylic Acid and n-Octadecyl Acrylate in Aqueous Media, *Macromolecules*, 46, 8, 3125-3131.

- **Bilici C.**, Karayel S., Demir T. and Okay O., 2010, Self-Oscillating pH-Responsive Cryogels as Possible Candidates of Soft Materials for Generating Mechanical Energy *Journal of Applied Polymer Science*, 118, 5, 2981-2988.